Alma Mater Studiorum · Università di Bologna

Scuola di Scienze
Dipartimento di Fisica e Astronomia
Corso di Laurea Magistrale in Fisica

Test of multiple sensor set-up for head motion characterization during MRI acquisition

Relatore:
Prof. Remondini Daniel

Presentata da:
Bortolotti Laura

Correlatori:
Prof. Richard Bowtell
Dott. Enrico Giampieri

Anno Accademico 2016/2017

Contents

"..study hard what interests you the most,
in the most undisciplined, irreverent
and original manner possible"
Richard P. Feynman

"..You are a wonderful creation.
You know more than you think you know,
just as you know less than you want to know."
Oscar Wilde

Abstract

L'Imaging a Risonanza Magnetica (MRI) é una tecnica di imaging medico utilizzata in questa tesi per le imaging del cervello. La ricerca in questo campo si sta focalizzando sullo studio degli scanner per risonanza magnetica a campi molto intensi, come lo scanner a 7 T utilizzato in questa tesi. La risoluzione delle immagini e l'entitá degli artefatti creati dai movimenti involontari del paziente sono proporzionali all'intensitá di campo magnetico e diventano rilevanti ad intensitá molto elevate. Le tecniche di Motion Correction, nota la cinetica dei movimenti, permettono di correggere le immagini MR. La tesi é inserita in un progetto che ha come scopo la misura indiretta dei movimenti della testa durante la scansione MRI. In particolare, mi sono concentrata sui miglioramenti da apportare al set-up e sulla caratterizzazione dei tre strumenti usati per la misura: la telecamera di campo magnetico (Clip on Camera Head, CCH) formata da 16 sonde fissate in una struttura cilindrica posizionata attorno alla testa del paziente; la telecamera ottica (Moiré Phase Tracking System, MPT) che misura i movimenti tramite l'immagine di un marker olografico supportato da un bite tenuto nella bocca del volontario; il dispositivo (Physlog) dello scanner che fornisce i parametri fisiologici (respirazione e battito cardiaco). La comunicazione hardware degli strumenti avviene grazie a un segnale di trigger, di cui ho ottimizzato la sincronizzazione. Inoltre, abbiamo acquisito dataset completi di tre volontari, a diverse condizioni. I dati sono stati sincronizzati e analizzati, tramite analisi multivariate, per caratterizzare la risposta e la stabilitá del sistema e la variabilitá individuale dei pazienti. L'analisi ha permesso di capire meglio le proprietá dello strumento e ha consentito di associare le misure del campo magnetico al di fuori del cranio ai valori fisiologici dei volontari.

Abstract

Magnetic Resonance Imaging (MRI) is an imaging technique for imaging the soft tissues of the human body, and in this thesis we focus on brain imaging in particular. Research in medical MRI is moving towards the use of ultra-high field MRI scanners, such as the 7 T scanner that was used in this thesis, since the spatial resolution of MRI increases with the strength of the magnetic field. Involuntary movements of the subject can however create artefacts in MRI that can invalidate the image, and since high resolution images are more vulnerable to motion, this effect becomes more relevant at ultra-high field. Motion artefacts can be corrected or avoided if the movements of the head during the scans are known; this is the basis of motion correction techniques.

This thesis belongs to a project to monitor head motions indirectly through measurement of extra-cranial magnetic field variations and is focused on the improvement of the set-up and the characterization of three different instruments used to perform required measurements in parallel: a field camera (Clip on Camera Head, CCH) with 16 magnetic field probes placed in a cylindrical structure inserted between the head RF coil and the head of the volunteer during an MRI scan; an optical camera (Moiré Phase Tracking System, MPT) that measures the position of a marker mounted on a bite bar held in the mouth of the volunteer; a tool of the 7 T Scanner that measures physiological parameters (Physlog), specifically respiration and peripheral pulse.

I have synchronized of the different measurements through a triggering procedure and performed an overall optimization of the hardware set-up. Moreover, data has been recorded from three volunteers, generating several time series datasets under different conditions. These data have been analysed in order to characterize the probe response and stability as a function of individual variability, through multivariate analysis techniques.

This preliminary analysis provided a better understanding of the probe properties and allowed the measured extracranial fields to be associated to physiological activity in the volunteers, including breathing and the cardiac cycle.

Chapter 1

Introduction

1.1 Magnetic Resonance

The phenomenon of Magnetic Resonance. The *Nuclear Magnetic Resonance*(NMR) experiment investigates a subatomic level phenomenon: the nuclear spin. The nuclei spins are aligned along (or opposite) to the magnetic field's direction and, if they are excited by an appropriate radio frequency, they pass to a higher energy level. When the radio frequency is stopped, the atoms give their energy back to the system.

Nuclear Magnetic Moment. The *nuclear magnetic moment* is due to the unpaired spins of the protons and neutrons in the nucleus that we investigate. The overall spin generates a magnetic dipole along the spin axis and the magnitude is the nuclear magnetic moment. The effect of many nuclei in a sample generates a macroscopic magnetization called M, which is governed by the *Boltzmann Equilibrium Law*:

$$\vec{M} = N\frac{\gamma^2 s(s+1)\hbar}{3k_B T}\vec{B_0} \quad [A/m] \tag{1.1}$$

which indicates that $\vec{M}$ depends on the number of nuclei present in the sample (N), the type of nuclei (the gyromagnetic ratio γ, $[rad/s\ T]$ is unique for each nucleus), Planck's constant ($\hbar = h/2\pi$), Boltzmann constant (k_B) and the temperature of the sample (T, $[K]$).

During magnetic resonance (MR), a constant magnetic field (B_0) aligns the $\vec{M}$ and when $\vec{M}$ is perturbed (their alignment isn't B_0), it precesses around the magnetic field and this produces an electromotive force (due to the time variation of the magnetic flux). In general, the frequency of the angular precession is described by:

$$\omega = \gamma B \quad [Hz] \tag{1.2}$$

Materials	$\chi_m \times 10^6$
Air	0.00
PVC	≈ 0.00
Fat	-7.79
Bone	-8.44
Gray Matter	-8.97
CSF	-9.04
Others Tissue	-8.47

Table 1.1: Magnetic Susceptibility of some materials. [19]

So, the electromotive force is proportional to the strength of the B field and so are the ω and the sensitivity of the NMR experiment. For fields from 1 to 23 Tesla, the frequency of precession of hydrogen nuclei varies from 42 MHz to 1 GHz [14].

The presence of the patient causes magnetic field variations that depend on the magnetic susceptibility of the tissue: The equation 1.2 becomes: $\omega = \gamma(B + \Delta B)$, where $\Delta B = \chi_m B$. Hence, the frequency of precession depends slightly on the anatomy.

1.2 Magnetic Resonance Imaging (MRI)

Magnetic Resonance Imaging (MRI) is a technique that can produce very clear images of the inner parts of the human body, without damaging the tissues. Sir Peter Mansfield won the Nobel Prize in Physiology and Medicine in 2003 for his work in conceiving and developing MRI.

70% of the human body is composed of water. A water molecule is made of hydrogen and oxygen atoms: the spins of the hydrogen nuclei are influenced by the magnetic field applied.

MRI uses radio frequency to stimulate the magnetization of the nuclear spin of hydrogen nuclei in water molecules in the body. The signals originating from this magnetization are measured and processed to produce a detailed picture of the human body. The major advantage of this technique is that it is non-invasive for the patient because it does not use any radiation. Moreover, MRI provides a contrast of the soft tissues better than other medical imaging techniques such as X-Ray computed tomography.

To acquire an image of the human body, three different electromagnetic fields are required:

- **Static Magnetic Field**: common name is B_0 field. This is necessary to align the proton spins to generate the net magnetization vector ($\vec{M}$) in the Hydrogen nuclei of human body.
- **Gradient Magnetic Field**: commonly named G_X, G_Y, G_Z, depending on the direction of the gradient. These are necessary for the spatial localization of the

signal. The gradient changes the value of the magnetic field, so the resonant frequencies of the protons depend on their position in the space.

- **Radio Frequency**: common name is RF. This is the most important electromagnetic field for generating the MR signal. It is usually centred at the proton resonant frequency (equation 1.2) and it rotates the net magnetization vector away from the direction of static magnetic field. Its frequency is generally in the range from 10 MHz to 400 MHz [17]. It is possible to change the duration or the intensity of the applied RF pulse to change the flip angle: the most common RF pulses produce magnetization which angles are 90° and 180°, the transverse or the opposite direction of $\vec{M}$. After the perturbation, the net magnetization vector recovers its direction to the original static magnetic field, the time of the process depends on the tissue and is characterized using two parameters. The first is the *spinlattice relaxation time* (T_1) [1], which describes the recovery of thermodynamic equilibrium, and the second is the *spin-spin relaxation time* (T_2) [2], which depends on the loss of phase coherence of the spins: the general relation between these parameters is $T_2 < T_1$.

The images obtained by MRI represent the spatial distribution of the magnetization, the appearance depends on the physical proprieties of the tissue and on the RF pulse sequence applied, as show in Figure 1.1.

k-Space

The MRI is based on encoding the spatial information in the NMR signal produced by the nuclei spins of the sample. It is possible to produce one dimensional, two dimensional, or three dimensional information. Considering the 2D space, the NMR signal has two coordinates: frequency and phase that characterise the k-space (Figure 1.2). To produce that signal in a way to be decoded, it is necessary to use spatially varying magnetic fields to produce a unique couple of coordinates, called $k_x,\ k_y$, in each point of the k-space that matching the $x,\ y$ coordinates in the real space. This process is called *spatial encoding*:

Frequency Encoding: A magnetic field gradient produces a linear variation of magnetic field with the position, the equation 1.2 in the presence of field gradient

[1] The **Spin-lattice relaxation time** (T_1) represents the interaction between the nuclei and experimental environment and corresponds to the recovering of the component of the $\vec{M}$ along the static field (the recovery of the longitudinal magnetization). It is a process slower than T_2, but T_1 and T_2 are large compared to the precession time. For hydrogen in water, the precession period is $\approx 10^{-9} s$ and the $T_1 \approx 1\, s$.

[2] The **Spin-spin relaxation time** (T_2) represents the interaction between the nuclear spin and corresponds to the decay of the component of $\vec{M}$ transverse of the static field (the decay of the transverse magnetization).

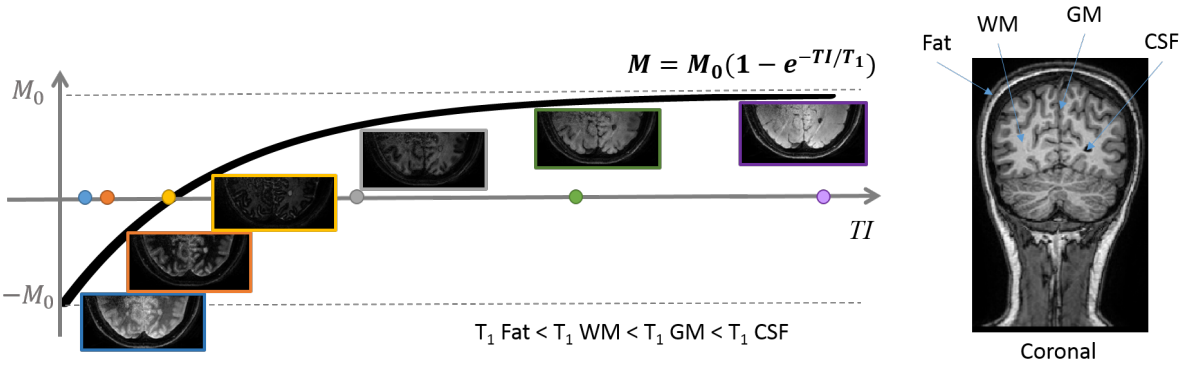

Figure 1.1: *T_1. Using inversion recovery techniques (IR), it is possible to acquire images with enhanced T_1 contrast. After a single inversion RF pulse, the magnetization of each different tissues recovers at different rate, RF is related to the T1-value. Images are acquired at different inversion times (TI), and the contrast at each inversion type depends on the recovery of the tissue magnetization at that time. The Figure shows the inversion recovery curve for grey matter (GM) and images of the brain at different TIs, there are visible different type of tissue: the fat around the skull, the white matter (WM), the grey matter (GM) and the cerebrospinal fluid (CSF). The images are acquired at different TI. The first (blue point) is acquired too early, so the magnetization of the nuclei is close to the opposite of equilibrium value ($-M_0$) and the tissue that has a really short T_1, hence tissue with short T_1 (as the fat) are bright. It is possible set the TI to as suppress the signal from the GM (yellow point), this is called the null point. At the null point for GM the CSF is brighter than the other signals because its T_1 is the longest and it magnetization is still negative. After the null point, the GM becomes brighter as the magnetization recovers, while at longer TIs the CSF become darker as TI approaches the null point for CSF. [Picture of the brain cortex, made by: Rosa Sanchez, University of Nottingham, 2017] [Picture of the brain on coronal projection, made by: Daisie Pakenham, University of Nottingham, 2017]*

$(B = B_0 + \Delta G = B_0 + G \times x)$ becomes: $\omega = \gamma B = \omega_0 + \gamma G x \quad [Hz]$. The frequency of the signal indicates the position, usually along the x-axis, in the presence of an x-gradient. The frequency encodes one dimensional information.

Phase Encoding: To have two, three or more dimensional information it is necessary to use other gradients to change the phase of the signal. In 2D space, as the x position is encoded in frequency, the y position could be encoded in phase. The phase is related to the gradient by: $\phi = \gamma G_y y \tau$ where G_y and τ are the intensity and the duration of the gradient.

Selective Excitation: For 2D and 3D imaging it is necessary to select the slice of the sample to scan. The equation 1.2 becomes: $\partial\omega = \gamma G \partial s$, so to select the slice ∂s it is sufficient to send a gradient G centred on the frequency $\omega_a = \frac{\omega}{2}$

It is clear that the movements of the patient introduce encoding errors. Changing the

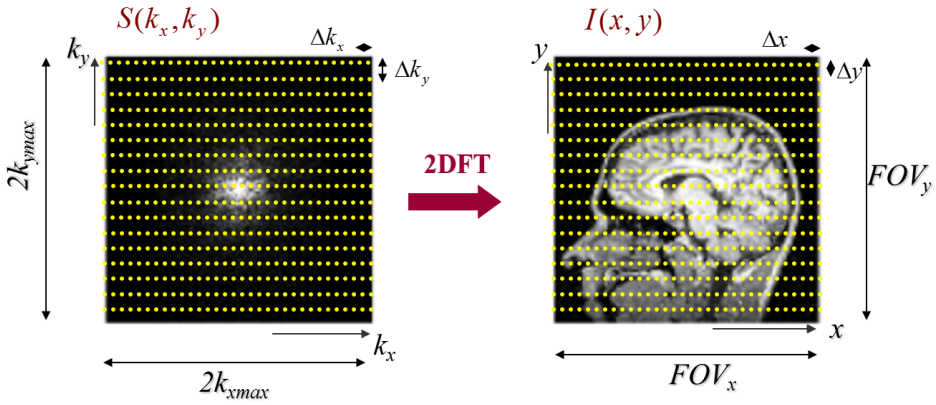

Figure 1.2: ***k-space and 2D space.*** *The k-space representation on the left is the signal acquired during MRI scanning, it is processed by the two dimensional Fourier Transform to obtain the image. They are two different representations (in two different space) of the same object. The important relation between the k-space and real world is that the field of view (FOV) of the image is inverse proportional to the amplitude and the duration of the phase encoding gradient:* $FOV \propto \frac{1}{\Delta k} = \frac{1}{\Delta G t}$ *and the spatial resolution also* $\delta s \propto = \frac{1}{k_{max}} = \frac{1}{Gt}$, *where* G *and* t *are the intensity and the duration of the gradient. Hence, to have large FOV it needs a small k-space steps and to have a high spatial resolution it needs a large* $G \cdot t$ *product. [Picture made by: Bowtell Richard, University of Nottingham, MR classes, 2016].*

order of application of the gradients for k-space scanning is the way to diversify the MR sequences.

Artefacts

MRI is a powerful technique for medical imaging, but like all the techniques, it is subject to errors. These errors are called image artefacts because they produce information (structure) on the image that is not anatomically present and can mimic pathologies and lead to improper diagnosis. The artefacts emerge for different reasons. For example, the interference between MRI unit and other electronic devices could create an interference pattern on the image (e.g. Zipper artefacts), but usually the MRI scanner is housed in a RF screened room which reduces these effects. There are inherent physical artefacts, like chemical shift artefacts due to the frequency oscillation of different tissues or magnetic susceptibility artefacts due to variations in magnetic proprieties of the tissue or anatomical MR compatible implants. These artefacts could be reduced by changing the MR sequence.

The problem of the motion of the patient during MRI is a complex problem. To reduce the effects of breathing, heartbeat and blood flow, the patient is advised to remain still or sometimes breathold for a few seconds. Also, it is possible choose a sequence

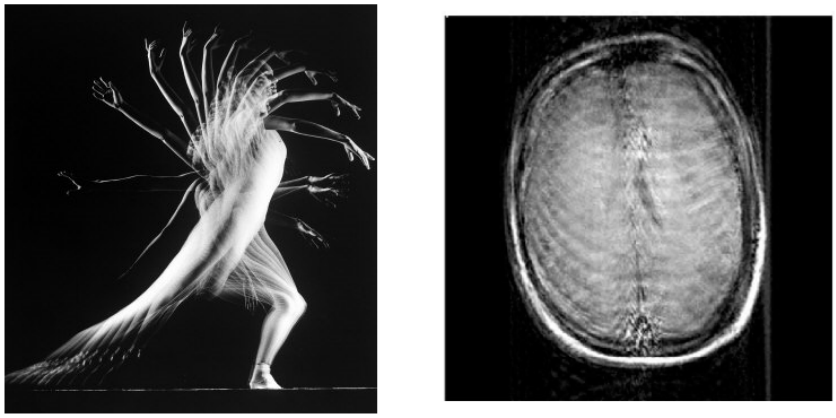

Figure 1.3: ***Motion****. The difference between movement in real world and the effect of the movement in MRI [Zaitsev et al, Neuroimage, 2006].*

that synchronizes the time repetition (TR) [3] period with the respiration. In Figure 1.3, is possible to see the effect of movement during image acquisition on MR image of the human head. It is clear that patient involuntary movements is a fundamental problem in MRI that causes image artefacts due to erroneous positional encoding of the k-space data. The utility of MRI is limited by motions artefacts in young and elderly patients, where premature diagnosis is much important. The movements are classified as *rotation*($R_X,\ R_Y,\ R_Z$) and *translation* ($T_X,\ T_Y,\ T_Z$), as usual. The typical artefacts (Figure 1.4, Figure 1.5) due to the movements are called *blurring* and *ghosting*. Blurring means that the edges aren't sharp as they could be. Ghosting is an effect that produces shape repetition.

Motion Correction

If we assume that the magnetic field and the applied gradients are constant, the movement of the patient produces a shift of the region of interest (ROI) of the scanner. As explained on page 3, if the ROI shifts, the same region could be excited with different values of gradients and reconstructed at two different locations in the image. The same effect emerges if the B field and gradient aren't uniform.

The idea of *Motion Correction* is to correct the k-space based on the pose (position and orientation) of the patient during the acquisition. The Method is divided into *Prospective Motion Correction*, that is a real time correction, and *Retrospective Motion Correction*, that is a post-processing correction. Both methods improve image quality.

Prospective Motion correction: The aim to prevent image artefacts due to movement of the patient. Updating the scanner coordinates during image acquisition

[3] **Time Repetition**. To allow recovery of longitudinal magnetization it is necessary wait before send the next sequence. This time is called *time repetition* or TR and depend on the TR/T_1 ratio.

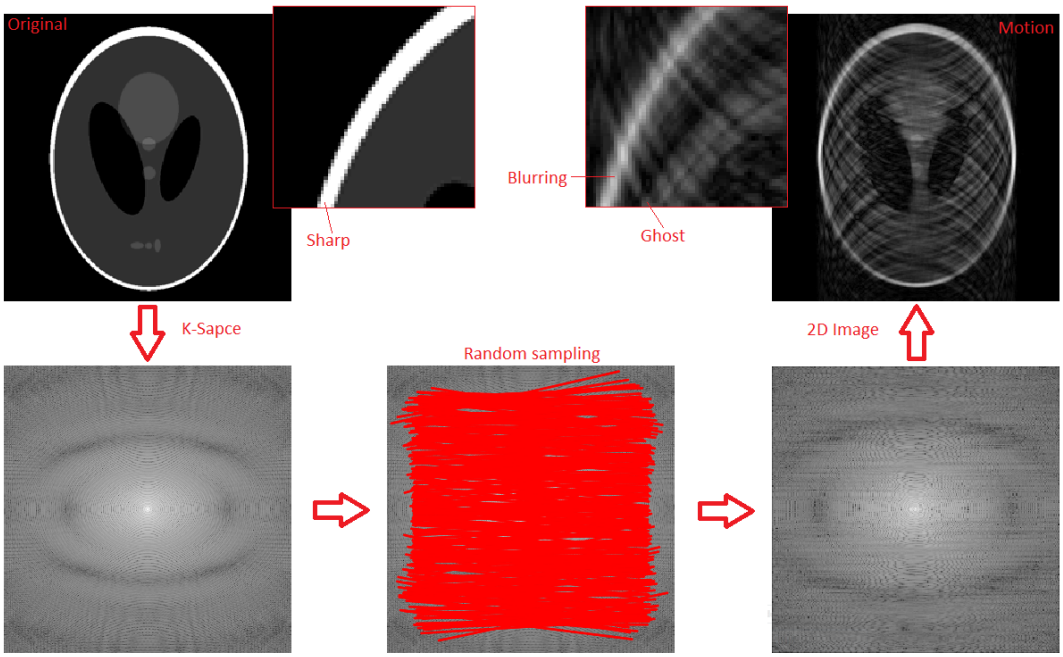

Figure 1.4: ***Blurring and Ghosting***. *These pictures shows simulations of motion effect [Code written by: Smith James, SPMIC, University of Nottingham, 2016]. The simulations modify the k-space of original picture to product the artefacts, in this case it represents artefacts due to a pure rotation. The k-space of the image affected by motion looks quite similar to the k-space of original image, but it has a hole (missing data) and overlap information. The motion image present blurring (the effect is more visible on the sharp white line) and ghosting (the white oval is repeated several time on the 2D space).*

to maintain the consistency of the data.

Retrospective Motion correction: The aim to reduce image artefacts due to the movement of the patient, and to correct the k-space information after the acquisition.

- *Translation*: The effects of translation in the real world is to produce a phase change in k-space. To correct it, it is sufficient to multiply each line in the k-space by an appropriate spatially varying phase.
- *Rotation*: The effects of rotation in the real world is to produce a rotation of k-space lines. To correct it, it is sufficient to rotate each line in the k-space.

The two techniques produce different results and it is possible to use both methods (prospective motion correction during the acquisition and then retrospective motion correction) for better results. Prospective motion correction provides more flexibility than retrospective motion correction because it can be applied in most sequences and

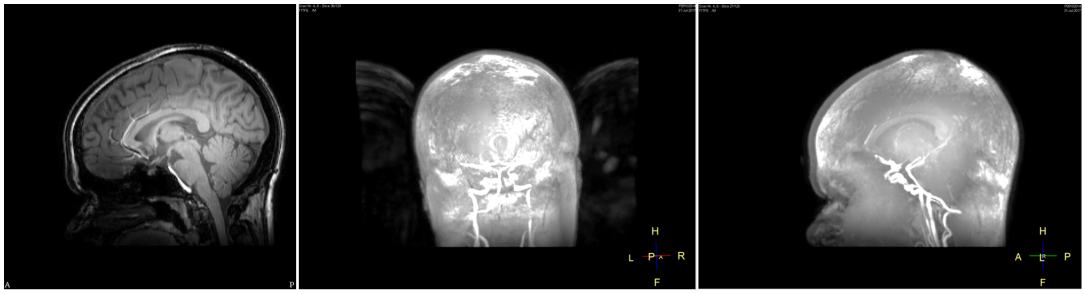

Figure 1.5: ***Example of ghost motion artefact.*** *These pictures show clearly the ghost problem during MRI scans. The sequence used to obtain this structural brain image is called Magnetization-Prepared RApid Gradient-Echo imaging (MP RAGE) and it is used to enhance the contrast between different brain tissues (on the left). On the other figures, the same sequence is used in a 3D reconstruction that highlights brain vessels. On the 3D coronal section you can see the artefacts on the left and on the right of the head. In the 3D sagittal section the artefact is the grey border around the forehead and the nose of the subject. [Picture of coronal and sagittal section of the head, made by: Lucrezia Liuzzi, University of Nottingham, 2017]*

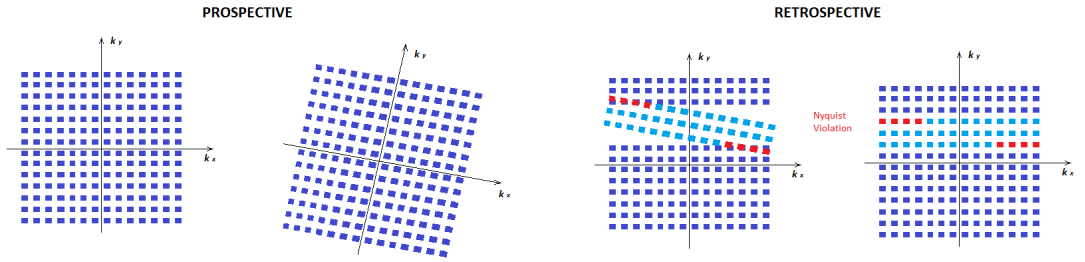

Figure 1.6: ***Motion correction.*** *Only in prospective motion correction the ROI of the image follows the patient.*

avoids the local Nyquist violation [4] (Figure 1.6). Also, the prospective motion correction compensates the spin-history effect (the consequence of the patient movements is that tissues move through the slice). The most important advantage of the real time correction is that the image is ready immediately.

The aim of the project where my thesis is included is to find better regression methods to predict the movement of the patient by the perturbation of the magnetic field. In the future, this method will be used in retrospective motion correction and ultimately in prospective motion correction. My thesis is focused on improving and charactering the

[4] **Nyquist Theorem** (or the sampling theorem). The sampling frequency must be at minimum twice the maximum frequency component of the signal. This theorem defines the main condition of signal sampling to avoid the aliasing imperfections during the acquisition: if f_{sample} is the maximum frequency of the sample, the $f_{sampling} > 2 \cdot f_{sample}$. Aliasing imperfections are due to acquisition undersampling.

current set-up of the experiment to obtain more suitable datasets to begin the regression analysis and qualify the relation between the movements and the changing in the magnetic field.

Chapter 2

Instruments and Set-Up

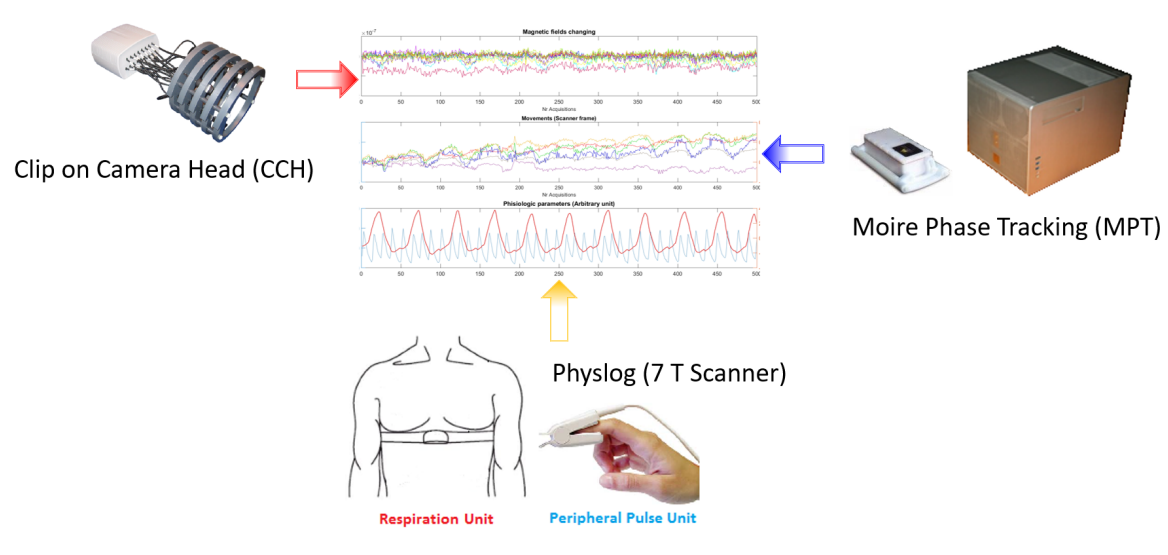

Figure 2.1: ***Idea of the experiments set-up.***

The set-up of the experiments was developed in the previous work [1]. It is basically formed by three instruments (Figure 2.1) placed into the magnet bore to quantify the magnetic field perturbations and to relate these to the movements. The instruments are:

Field Camera: The *Clip on Camera Head* (CCH) field camera is used to measure the perturbations of magnetic field around the head of the patient. It is described on page 22;

Optical Camera: The optical camera *Moiré Phase Tracking* (MPT) that is used for recognize the movements. It carries out a pattern recognition on the image of a

passive holographic marker that is fixed to the mouth of the patient. It is described on page 30;

MR Scanner's Physiological Monitoring: The MR scanner's physiological monitoring (*Physlog*) consists of a chest belt to measure breathing of the subject (RESP parameter) and a finger sensor for the peripheral pulse (PPU parameter). It is described on page 19;

These instruments are managed by different computers, each instrument produces its own log file. Hence, we have to correlate in time the measurements using various TTL trigger pulses. To help the correlation in time of the data stream, we created a simple OR gate using an integrated circuit that couples the instruments during the experiment.

2.1 Set-up description and improvement

This section describes the new set-up and talks about the improvements done on the set-up of the experiments and on the datasets line-up. Currently, the instruments dialogue through a built-in OR gate we have designed with the help of the electronic engineer and the laboratory technician of the Sir Peter Mansfield Imaging Center. Thanks to the OR gate, the way to locate the data stream of the measurement on the log file is improved, as will be described on page 57.

2.1.1 Scheme

The scheme of the connections between the instruments is reported in Figure 2.2. Each instrument is managed by a different computer that produces its own log file. The CCH and Physlog send different triggers to mark the measurements on their log file. The MPT camera has only one TTL input gate and it cannot identify the TTL received. The 7 T Scanner manages the physiological measurements (PPU, RESP) and the imaging (MRI, B field Map). Its TTL signal is sent to the field probes (CCH) and to the MPT camera through the OR gate. The field probes are active instruments connected with their own computational unit, that saves the measurements of each probe during the scans. For each dynamic value of the scans, the computational unit sends the TTL signal to MPT camera through the OR gate. It is clear that the OR gate was built to have a clear TTL tag on the log file of the MPT camera in order to have an automatic acquisition during the experiments. That log file is the connection in time that is used to synchronize the data stream and will be described in Figure 2.3.

In conclusion, the instruments dialogue through an OR gate, that was designed and built-in with the help of the electronic engineer and the laboratory technician of the Sir Peter Mansfield Imaging Center. Thanks to the OR gate, the operation became easier in the lab and also it avoids the irrelevant spikes on the log file. The way to locate the data

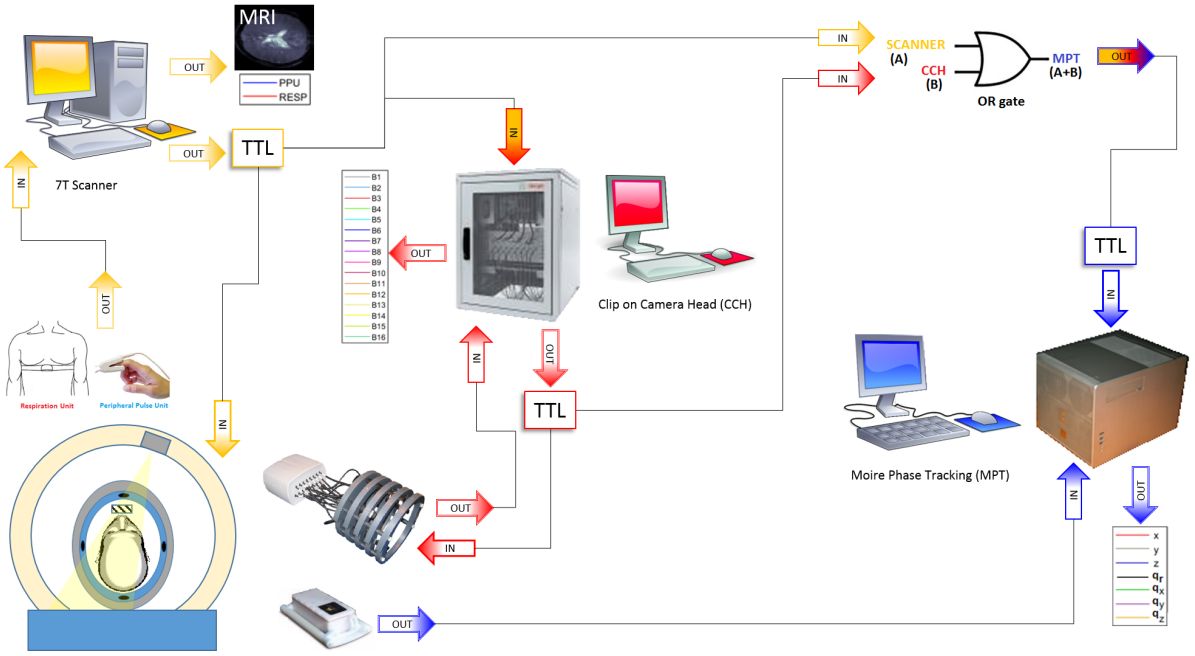

Figure 2.2: ***Scheme of connection.*** *The scheme of the instruments inside the bore is at the bottom left of the Figure. From them, the input/output signals for the active instruments (CCH) and only the output for the passive instruments connect them with the respective computer and computational unit. The TTL signal is underlined and on the top right of the picture there is the symbol of the OR gate built to match the instruments. Also, each instrument gives us a different type of data.*

stream of the measurement on the log file is improved an now it uses the time string (as will be described on page 57).

OR gate

In order to combine the trigger signal from 7 T Scanner and Kineticor into one single trigger read in by Skope, we built an OR gate. We used an integrated circuit *74F00*: this integrated circuit belongs to a family of TTL (Transistor Transistor Logic) integrate circuits that contains a base logic gate, in this case it contains four NAND gate. The NAND is an universal gate that can be used to construct any logical system. It is economic and easy to fabricate. Furthermore, we used a 9 Volt alkaline battery (550 mAh) and a voltage regulation system based on *LM 7805*. The *LM 78xx* family is a family of voltage regulators based on diode characteristic.

Circuit Scheme. The circuit is composed on three part (Figure 2.4):

- *Power Supply Circuit*: The *IC 74F00* required a 5 volt supply to work. The 9 volt

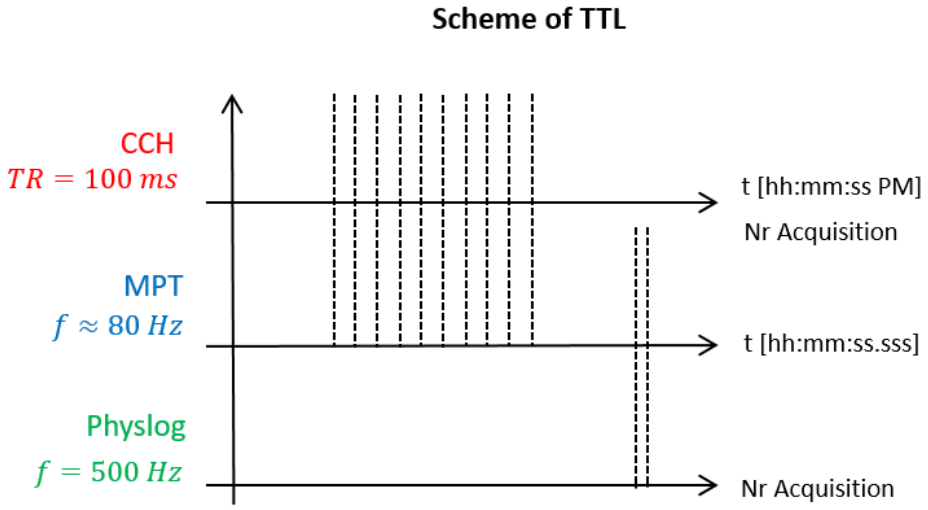

Figure 2.3: ***Scheme of TTL signal****. Intuitive scheme about the TTL signal sent from the scanner and from CCH (black dashed line). The CCH is connected with the MPT and the MPT is connected with the Physlog. The MPT log file is used to the line-up of the data stream.*

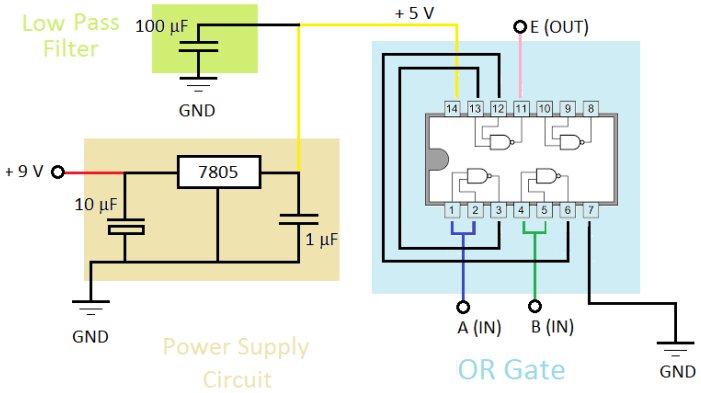

Figure 2.4: ***OR****. Circuit scheme*

alkaline battery is too high a voltage for the IC. So, it is necessary to step down the tension. This is achieved by using a linear voltage regulator, *LM 7805*. Decoupling capacitors (list) are used to ensure a clean power supply.

- *OR Gate*: The OR gate is implemented using only NAND gates from *IC 74F00*. The truth table of the logic gate is verified in Figure 2.6.b.

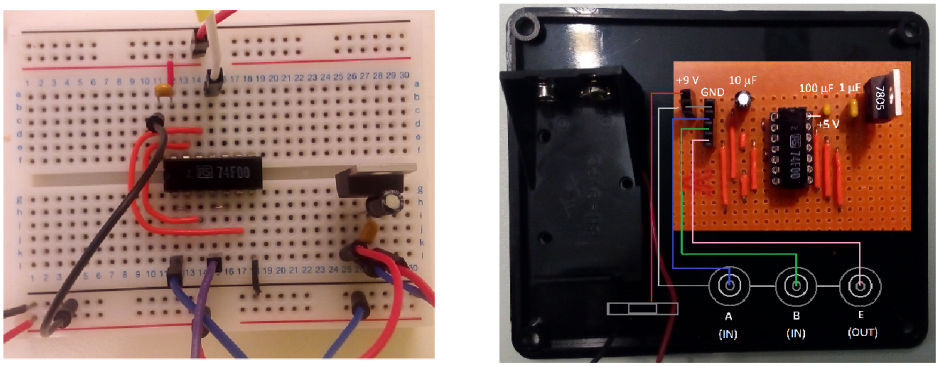

(a) (b)

Figure 2.5: ***OR****. (a) Breadboard, (b) Black Box.*

A [V]	B [V]	E [V]
5.01	5.01	4.30
5.01	0.00	4.29
0.00	5.01	4.29
0.00	0.00	0.18

Table 2.1: ***Measurement of truth table of OR gate.*** *The error is considered on the last digit:* ± 0.01 *Volt. The column names correspond to the nodes identified in Figure 2.4*

Check the IC 74F00. In order to check the functionality of the IC 74F00, we assembled the circuit on the breadboard (Figure 2.5, a). We used a digital multimeter set on 20 V scale and assumed that the error is on the last digit (± 0.01 Volt). The results are reported in table 2.1 and clearly show that the system behaves like an OR operation; when a high signal is received by all the inputs (A or B), high output is given.

Check in the lab Before mounting the circuit on the copper board and fixing it on the black plastic box, we checked the behaviour of the circuit in the laboratory. The input A will be the Scanner signal, the input B will be the Skope signal and the output of OR gate will be the input of Kineticor. The measurement is on table 2.2. The output is measured between low state of A gate and high state of B gate, so it has got the same duration of B signal. We soldered the circuit components on a copper board, that is low cost, quick and easy to use. At the end the copper board with the circuit is fixed on the cover of the black box, near the battery. Also, we put three BNC sockets for the input and output gate and a switch to turn on or off the circuit.

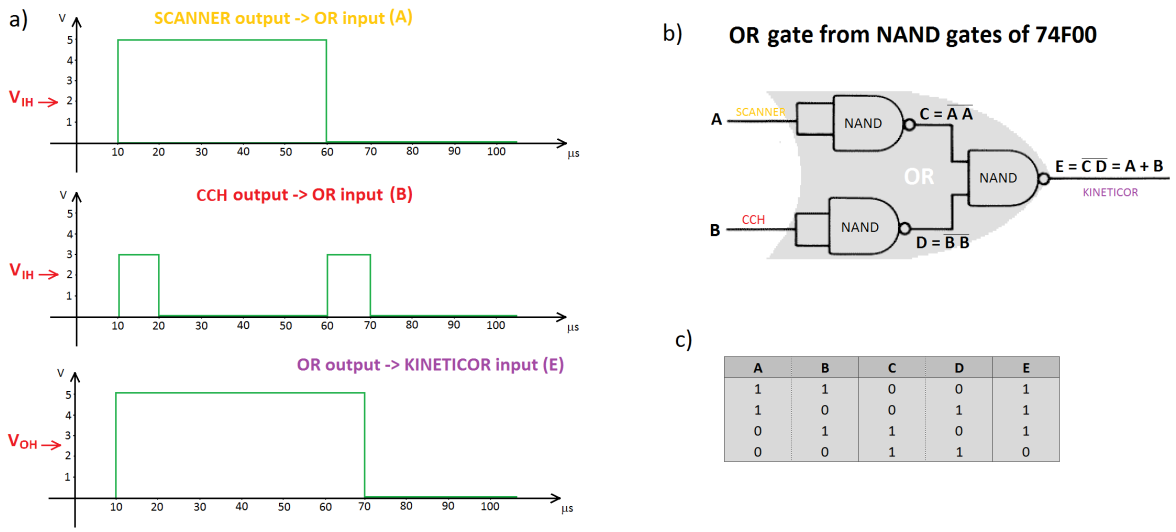

A	B	C	D	E
1	1	0	0	1
1	0	0	1	1
0	1	1	0	1
0	0	1	1	0

Figure 2.6: ***Scheme of OR gate signals.*** *(a) Signal sent to check the truth table of OR gate. (b) OR gate scheme inside the IC 74F00. (c) Table of truth of OR gate.*

	A	B	E
Voltage [V]	5	3	$5 \div 4$
Time [μs]	50	10	10

Table 2.2: ***Measurement of TTL signal of Instruments.*** *The error is considered on the last digit:* ± 0.01 *Volt.*

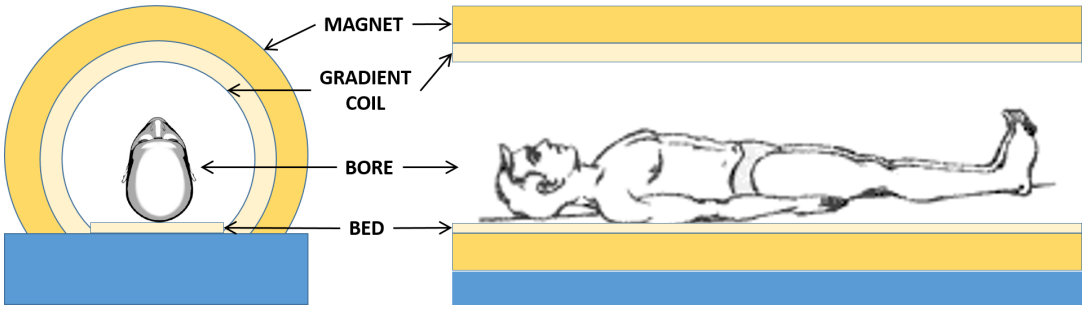

Figure 2.7: ***MRI 7 T scanner cutaway, closed tunnel style.*** *The MRI scanner is made up of several parts, the principal components are indicated in the picture. The* magnet *provides the constant magnetic field, it is really constant only in the center of the bore, where the subject is positioned. The* bore *is the tunnel where the bed scrolls during the MRI: the* bed *is mobile to permits the correct positioning of the part of the body of the subject to scan. The* gradient coils *produce the gradient used during the imaging sequences.*

2.2 Scanner 7 T

The scanner is a *7 T Philips Ingenia Magnetic Resonance Imaging Scanner*. It can produce cross-sectional images, spectroscopic images and/or spectra in any orientation

of the internal structure of the body[5]. It is formed mainly by the magnet and magnet bore where the subject is positioned during the scan.

Why do we use 7 T? The typical value of magnetic field used in hospital scanners is 1.5 Tesla or 3 Tesla (called *High-Field*). 7 Tesla (called *Ultra High-Field*) scanners are used mainly for research. The quality of the image increases with the strength of the magnetic field: there are some lesions (mainly in the brain) that are visible only at 7 T. For low magnetic field, spatial resolution is lower and the involuntary movement of the subject can be tolerated. This isn't true for high field.

Perturbations. The 7 T magnetic field in the Magnetic Resonance Scanner is highly stable, but even variations of the field at level of parts per million can produce artefacts in MRI [6]. There are several sources of such perturbations. These include *reproducible perturbations*, such as the imperfection of system behaviour (hardware properties, finite bandwidth, non ideal pass-band response of gradient, shim coil, eddy current, ...) or external sources of noise (temperature, pressure, traffic, elevator, power line, ...), which are fixed by the calibration of the instrument. We have analyzed the *non-reproducible perturbations* due to the movements of the head of the patient. These movements are *voluntary movements* or *involuntary movements* (like those due to breathing).

The reason for the perturbations on the high magnetic field due to head movement is that the head is composed of 78% of water. The magnetic susceptibility of water is around -9 ppm, so the magnetisation of the water in high magnetic field is enough to produce a significant field perturbation [2].

In previous experiments [1], it was head movements of different types of head movements were analysed (shake, nod, feet, "eight") and it was found that there is a correlation between the measurement of the magnetic field and the movements.

Safety. The 7 Tesla scanner doesn't have an active shield around it, the intensity of the B field decreases slowly with distance from the magnet instead having a exponential decrease. It is necessary to remove all the magnetic objects before going into the magnetic room: any loose ferromagnetic object may cause damage or injury if it gets pulled toward the magnet. Also, the eddy current creates a B field in all the conductive materials that move into magnetic field. The safety concerns are about implanted medical devices that contain metal (pacemakers, artificial limb, ...) which can malfunction around the magnet. Furthermore, tattoos and make-up can cause skin irritation or burn when exposed to RF.

RF Coil. The coils are designed to measure the specific part of the body. In general, they are an hardware component of MRI scanner used to create the magnetic field (ideal coils produce an uniform magnetic field) and detect the signal. The static magnetic

field B_0 is generated with gradient coils: this type of coils also generates a gradient of magnetic field to localize the signal. The RF is generated by radio frequency coils: that type of coils transmits and receives (T/R) the signal. To compensate the inhomogeneities of the magnetic field, another magnetic field is generated by using shim coils. The coils used in this thesis to acquire B field map measurements are MRI head coils. The coil looks like a helmet, and has got 32 channels. Between the head coil and the patient, we fixed the probes of the field camera (Figure 2.13).

2.2.1 Strength of magnetic field

First, we are always inside a weak magnetic field: the Earth's magnetic field is approximately half of a Gauss ($\approx 0.5\,Gauss$, so order of magnitude 10^{-5} Tesla). It isn't constant in time and it isn't homogeneous in all the part of the world. The magnetic field used for MR experiment and clinical investigations goes from less then 1 Tesla [1] up to 20 Tesla for animals: it highly stable in time and doesn't change during the MR experiment.

To improve the strength of magnetic field, it is necessary to solve technological, physiological/biological limit issues.

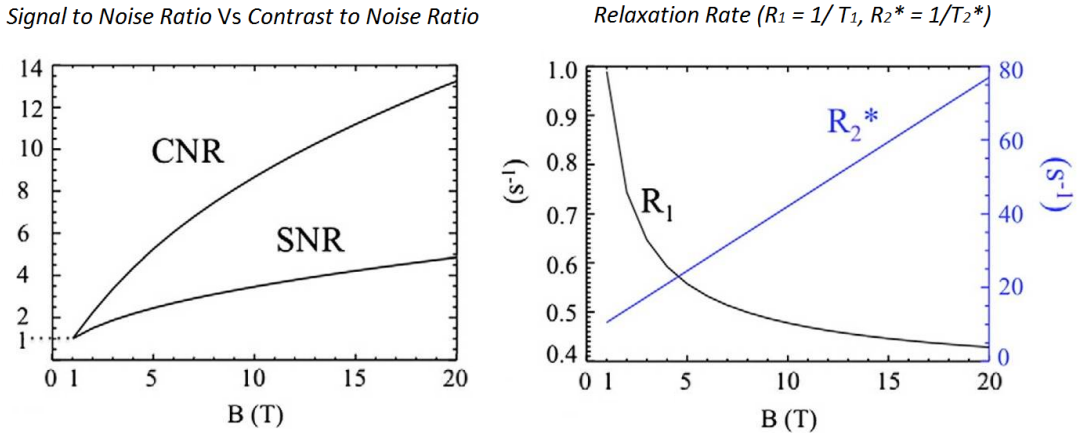

Figure 2.8: ***Image quality***. *Pictures of relaxation rate ($R_1 = \frac{1}{T_1}$, $R_{2*} = \frac{1}{T_{2*}}$) and the SNR ($SNR \propto \sqrt{B}$) and CNR ($CNR \propto \frac{\Delta R_{2*}}{R_{2*}}$ until 10 T, after $CNR \propto \sqrt{B}$) versus the B field, normalised to the value of 1 Tesla. To obtain that relation, we are assuming the optimal scanning conditions: the repetition time of the sequence is less than T_1 of the tissue and the acquisition of the signal has a duration that scales with T_{2*} of the tissue, and that the noise is only thermal noise [15].*

[1] $1\,T = 10000\,Gauss$

Difference between low magnetic field and high magnetic field. As written in equation 1.2, the sensitivity, contrast and resolution of the NMR experiment increase with the strength of B field. Signals (resolution and contrast) and also the noise, increase. The stronger magnetic fields (from 7 to 9 T) are able to acquire images of the small anatomical structure of the brain. The price of increasing the strength of magnetic field is cost, reduction of versatility and increase of system complexity. The goals that are obtained on preliminary studies are on critical disease, like Multiple Sclerosis, Alzheimer's disease, Epilepsy, Movement disorder, Angiography, Schizophrenia and brain tumors. Also, for example, it is possible to discriminate arteries and veins by the concentration of the haemoglobin [15].

A limit of spatial resolution in human application of high magnetic field is that the tolerance of the motion of the patient decreases, the magnetic susceptibility effect on the interface of different material (most important is air-tissue) increases and the scanning time increases. For example, the order of magnitude of the movement due to breathing is one tenth of a degree for rotation and one tenth of a millimetre for the translation.

The spatial resolution in human brain imaging is fundamental because it is a heterogeneous organ, with complex structure and functions. For anatomical imaging the spatial resolution is approximate $0.5 \times 0.5 \times 0.5\, mm^3$ [15]. The signal to noise ratio (SNR) and the contrast to noise ratio (CNR) are a function of the magnetic field as is shown in Figure 2.8. SNR scales with the voxel volume and increase linearly with field strength. CNR decreases with the voxel volume and scales with field strength. Therefore, the CNR increases more than SNR: at high magnetic field it is possible to recognize microstructures difficult to see at low magnetic field [15].

2.2.2 Biological Effect

MRI is considered a safe technology: it does not require a ionizing radiation and it isn't able to change the structure or composition of the tissue inside human body [17].

The three fields of MRI (static and gradient magnetic field and RF) interact with the electromagnetic proprieties of the tissue. The human body is considered a conductive dielectric, whose proprieties are determined by the electrical interaction of polar molecules and ions. Furthermore, the majority of human tissue has got diamagnetic or weakly paramagnetic proprieties [16].

The most statistically relevant side effects due to the static magnetic field that affect the patient are nausea, vertigo and metallic taste. Also, the non statistically relevant effects are due to the gradient of the magnetic field that causes peripheral nerve stimulations when switched on or off rapidly. The effects of the RF are divided into thermal and non thermal. The main problems are the thermal effects that cause heating of the tissue (depending on the shape and the intrinsic tissue proprieties) usually less than 1° for scanning period less then 30 minutes in 7 T scanner[17]. It is necessary to adjust the parameters of the scan to minimize these effects. Furthermore, the tattoos and metal-

based pigments applies on the skin could cause first (or second) degree burns on the skin. All the effects are reversible. My personal experience is that I usually fall asleep inside the 7 T scanner.

The specific absorption rate (SAR) is the maximum value of power per kilogram applied to the patient; usually the value is 2 W/kg for human head and 4 W/kg for human body.

The most of the health incidents related to MR experiments are due to the presence of ferromagnetic devices left in the scanner or inside the patient (like medical devices). The effect is called the "projectile effect" because the ferromagnetic object is susceptible to attraction an rotational force proportional to the distance from the bore entrance and their mass. Furthermore, there are some thermal effects due to the eddy currents inside metallic closed loop.

Until now, there haven't been side effects associated with the strength of magnetic field used for clinical investigations.

2.2.3 Physiological measurements

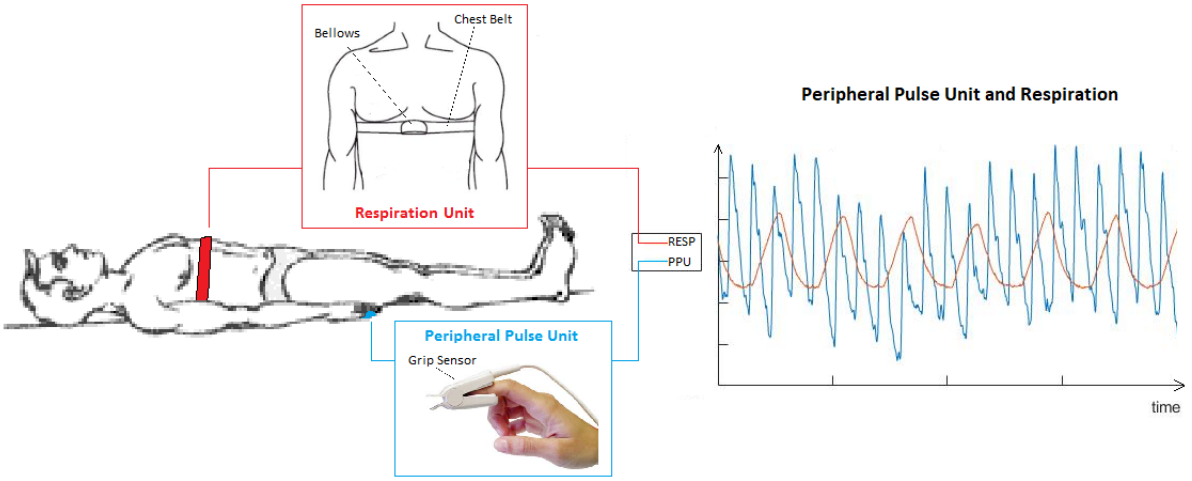

Figure 2.9: ***Physiology Measurements***. *Probes that we used to measure respiration and the heart beat.*

The MRI system uses additional peripheral devices for synchronizing the acquisition process with the subject's breathing or cardiac cycle. The synchronization allows to acquire the signal at the same point in the respiration cycle to avoid a big portion of the motion artefacts on the image. We use it only to obtain the signals of cardiac cycle and respiration (Figure 2.9). The sampling rate of the instrument is 500 Hz, it is constant and cannot be customized. It isn't possible to use it for medical investigation because the absolute value is distorted by the magnetic field, hence it measures the

relative changing of the parameters and it doesn't need a calibration. The log file of MRI system's physiological logging unit is used in this thesis to analyse the frequency of respiration and the breathing cycle.

The set up consists of one chest belt and a finger clip (Figure 2.9), fixed on the body of the patient:

PPU: The *Peripheral Pulse Sensor* acquires the cardiac cycle by the measurement of the changes of blood flow in the capillary of the index finger (plethysmography) and transmits the signal via fiber optics. In synchronized MRI sequence, it is used to suppress the artefacts caused by the flow of the blood or cerebrospinal fluid in the spine;

RESP: The *Respiratory Sensor* is a chest belt that measures the breathing of the patient. It is fixed on the lower chest, the part that most expands during inspiration, by a velcro strap. The respiratory signal is used to reduce the motion artefacts due to the breathing during synchronization of MRI sequence. The mechanism of the measurement is described in Figure 2.10. The belt is fixed around the top of the subject's chest. During the inhalation, the bellow inside the belt is squeezed and the opposite occurs during exhalation.

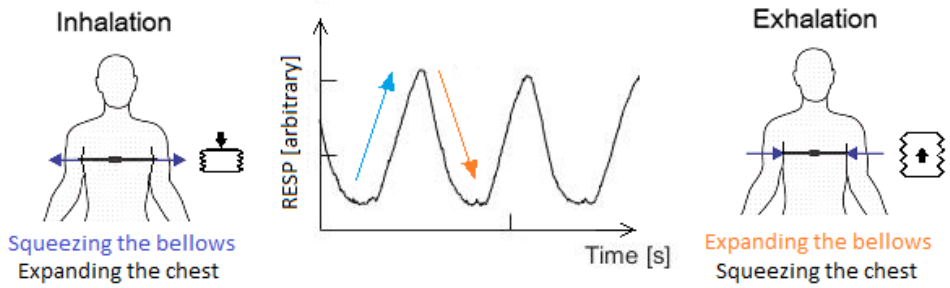

Figure 2.10: ***Physlog****. Mechanism of respiration measurement. The bellow is squeezed during the inhalation, so the signal increases and becomes free to expand again during the exhalation.*

2.2.4 B Field Map

It is possible to do a preliminary measurement of the changing of the magnetic field inside the head with Echo Planar Imaging (EPI) scan. When the nuclei are perturbed, the signal measured is ideally: $S(t) = M(t) \cdot exp(i\varphi(t))$. It is composed of two parts: the magnitude ($M(t)$) and the phase ($\varphi(t)$). The changing of the magnetic field inside the head is correlated with the changing of the phase of the signal, instead the magnitude is used to produce the MR image as usual.

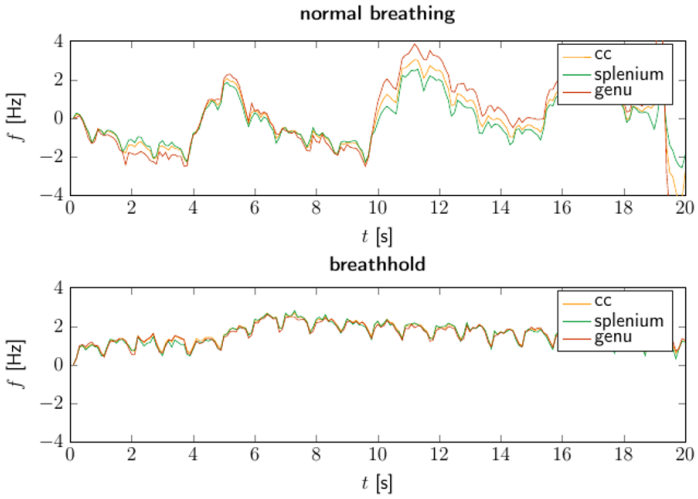

Figure 2.11: ***B field map***. *An example of the frequency changing within corpus callosum (cc) due to the breathing [Elena Kaleban, University of Nottingham, 2017]. The plot shows also the signal that came form the posterior and anterior part of the cc, called respectively splenium and genu. In two separate EPI (Echo Planar Imaging) scans, was asked to the subject to breath normally and hold the breath for 20 seconds. The plot shows the frequency changing calculated for 1000 EPI dynamics. It is related to the magnetic field variations inside the brain. Hence, in that measurement the magnetic field variation is* $\pm 9.4 \cdot 10^{-4}$ $[T]$.

The phase contains the information about all the sources of the perturbations of the magnetic field, e.g. hardware imperfections, gradient imperfection (eddy current), ... and the perturbations due to the physiological movements. If we assume that all the sources have a constant behaviour, except the physiological related field perturbations, it is possible obtain the trend of the phase related to it. The changing of the phase ($\Delta\varphi$) could be extrapolated from the ratio of the referred signal (S_n) and each signal (S_t). The changing of the phase is related to the echo time (TE) of the sequence [2] and the frequency of angular precession (page 1, as usual ω $[rad\ s^{-1}] = 2\pi\Delta f$) as: $\Delta\varphi = \omega TE$, hence $\omega = \frac{\Delta\varphi}{TE}$. As is written on equation 1.2, ω depends on the gyromagnetic ratio of the proton ($2.6750 \times 10^{-8}\ s^{-1}T^{-1}$) and the value of magnetic field (ΔB). The result of the process is the frequency of the signal, evaluated as: $\Delta f = \frac{\gamma \Delta B}{2\pi}$ as it is shown in Figure 2.11. To calculate the corresponding magnetic field variations:

$$\Delta B = \frac{2\pi\Delta f}{\gamma} \tag{2.1}$$

In the picture 2.12 it is clear that the magnetic field inside the head follows the breathing cycle of the subject.

[2] **Echo Time**. The echo time is the time between the application of RF pulse and the peak of the signal induced in the coil, measured in milliseconds.

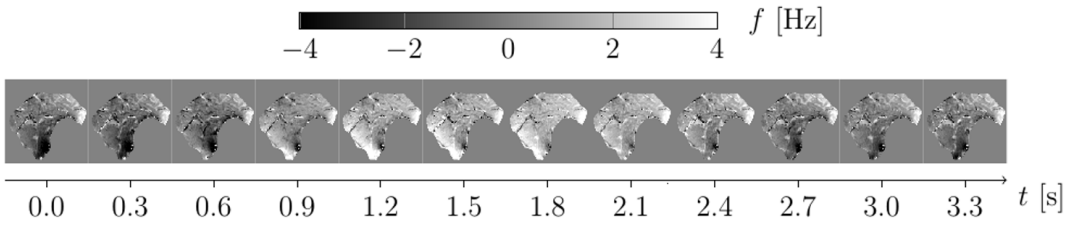

Figure 2.12: ***Anatomically B field map of Figure 2.11****. Anatomic picture that shows in gray scale the frequency variation within the brain during one breathing cycle [Elena Kaleban, University of Nottingham, 2017].*

2.3 Magnetic field Probes

Any kind of physical measurement needs a sensor to qualify the phenomenon, our task is to measure the perturbation of the magnetic field. The MRI technique uses three electromagnetic fields (static and homogeneous, static with gradient and RF pulse) to obtain the images. These fields are ideally perfect, but there are several sources of perturbations (like manufacturing variability of magnets, magnet drift, heating effect, gradient chain delay, eddy current effects, ...) that produce imperfections on the fields. Also, the presence of the patient or the phantom can produce field variations. To measure that behaviour it is possible use different types of magnetic field sensors: the NMR probes of the instrument used are liquid state probes made with ^{19}F. The sensor needs to be fast to reveal the dynamics of the gradient field, and small size to be compatible with the spatial inhomogeneity of magnetic field. Usually, the probes measure FID (Free Induction Decay) of the material the probes are made of (in that case, the probes measure the FID of ^{19}F): the FID has to be long enough to be measured and depend only on the perturbations of the magnetic field, hence the order of magnitude of the sensitivity should be at least 10^{-9} T. The shape of the probe is ellipsoidal to limit the effect of the inhomogeneity due to the magnetic susceptibility of the container of the probes. The container is closed to prevent the entering of gas bubbles. In these conditions, the only source of random noise is the thermal noise (the dominant contributions came from solenoid and the circuitry) that is proportional to the SNR and the square of the acquisition bandwidth: $\epsilon = SNR\sqrt{BW}$ [18].

2.3.1 Clip-on Camera Head (CCH)

The *Clip-on Camera Head* (CCH) is produced by Skope. It is a field camera used to measure the perturbations of B field around the head of the subject.

The maximum magnetic field supported is 12 T and the instrument is allowed only with RF pulse at the ^1H Larmor frequency. The frequency of acquisition is 1/TR (Repetition Time, usually is 0,175 ms). The 16 field probes are NMR sensors made with ^{19}F,

they are flexible to operate and we place them on the head-coil array support. The acquisition data is managed by computer. The software libraries is under the MIT licence (LUFA Library. Copyright (C) Dean Camera, 2013.) [3].

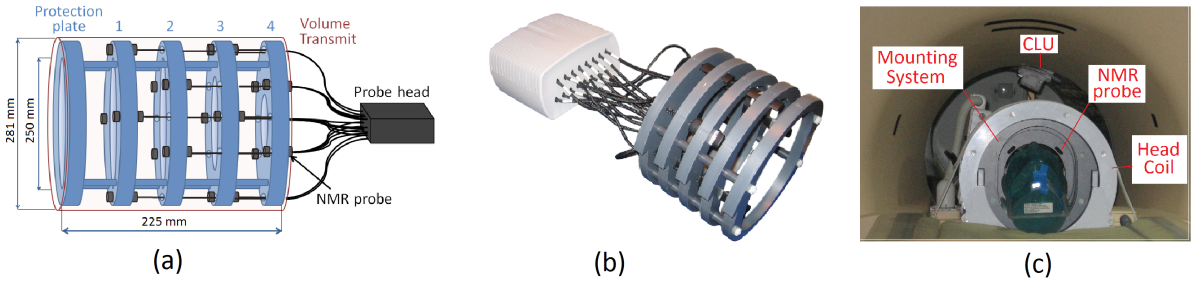

Figure 2.13: ***Mounting System****. (a) Schematic diagram of the mounting system. The protection ring is plotted only in this scheme. (b) Photo of the mounting system. (c) Photo of the mounting system put inside the head coil. On the top of the scanner it is visible the optical camera (CLU) whose description is in the next section. Inside on the mounting system there is Victor, the anthropological phantom used for developed the mounting system.[1]*

Mounting system. We used a portable mounting system that was developed in the previous work [1]. The system is custom built and it is fabricated with PVC to be MR compatible and also its has got a magnetic susceptibility close to the air value (table 2.4). The probes inside the scanner must be oriented along the axis of the static magnetic field. The 16 probes are fixed on 4 rings, the fifth ring is built as a protection and it won't be considered in the next sections. For each ring, 4 probes are arranged at angles of 90°, the rings are parallel and rotated at angles of 45°. The rings are connected by rods. The rings are oval, the internal measures are minor axes equal to 190 mm and major axes 250 mm: it was modelled to be inserted in the empty space between the patient and the head coil and to stay as close as possible to the head (the vicinity depends on the dimension of the head of the patient, except for the part where the head rests on). The mounting system is represented in Figure 2.13, that set up has been removed and replaced for each experiment inside the head coil. The probes are really sensitive to the position, for the last experiments we decided to stick them with adhesive tape on the mounting system. The positions of the probes are obtained during the calibrations process, an example is visible in Figure 2.14.

Parameters

The system is formed mainly by two parts. One goes into the magnetic field: that part includes the field probes array of the CCH and the wire for T/R signals. The other is the Acquisition System that consists of the booster unit, that manages the CCH

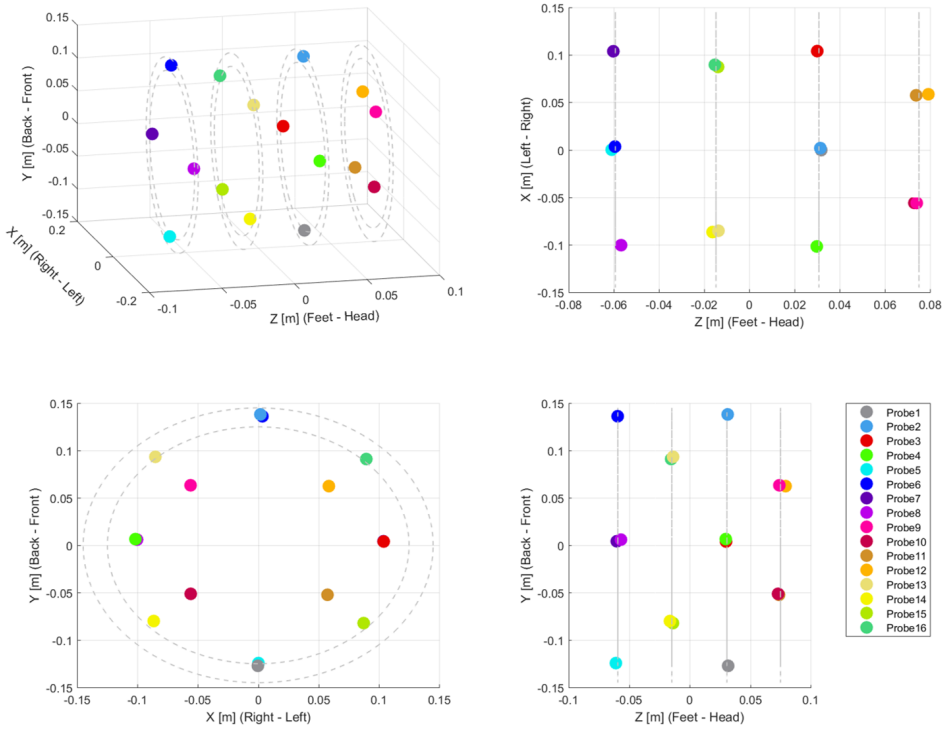

Figure 2.14: ***Position of the probes***. *Position of the probes with the set-up described in Figure 2.13 (without the protection ring) for subject 192 inside the bore. Each probe is represented by one filled circle in three projection and on 3D view, that correspond to the Figure 2.13.(a). The alignment of the probes on each plane is good (the deviation is less than 1 cm), except for the probe 12.*

trough the application on computer desktop and receives the external trigger from the 7 T Scanner.

There are several parameters to set up, which are schematically described in the table 2.3:

CCH Acquisition. The scheme of the acquisition is shown in Figure 2.15. On the top of the figure there is the external trigger signal from the 7 T scanner to CCH, that indicates the beginning of the measure. After that, a RF pulse is generated by the CCH system to excite the probes. After the system has acquired the measurement, there is a delay between the end of RF pulse and the measurement [3]. Between the RF pulses there is the so-called Dynamic. It is possible to acquire more than one measurement for each dynamic, each measurement is called an acquisition. The Interval is the time between two acquisitions. In this experiment the choice is to acquire one Interval for each Dynamic, so the duration of acquisition coincides with the duration of the intervals and the number of acquisitions coincides with the number of dynamic (that became the

Scan Parameters	Description	Value
Nr Acquisition	(Nr Dynamics × Nr Intervals)	$30 \div 4000$
Aq Duration	(Interleave TR × Nr Intervals)	$150\,[ms]$
Nr Dynamic	The number of acquired dynamics.	$30 \div 4000$
Dynamic TR	The repetition time between each dynamic.	Variable
Nr Interleave	The number of intervals for each Dynamic.	1
Interleave TR	The repetition time between each Interval.	$80\,[ms]$
Aq Delay	Delay of acquisition start	$0.5\,[ms]$
Aq Frequency	Acquisition center frequency.	$\ldots\,[Hz]$

Table 2.3: ***The usual values of the scan parameters for CCH acquisition.*** *For this experiment, CCH is coupled with the external trigger, so the Dynamic TR is the same of TR of scanning sequence.*

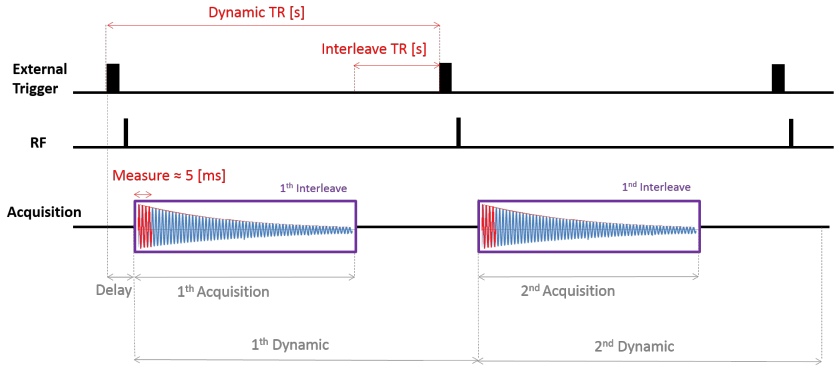

Figure 2.15: ***Time scheme of the parameters for the acquisition.*** *Note that each acquisition is preceded by an RF pulse for field probe excitation.*

number of data points in the log file). The measurement of the magnetic field is taken at the start of the the FID of the probes, so in the first 5 ms after the start of the acquisition. The frequency of the signal is sensitive to the local magnetic field. The duration of each dynamic is managed by the external trigger, so the Dynamic TR is the same of TR of scanning sequence: for an imaging sequence, Dynamic TR is 175 ms. To have a rapid measurement and low resolution imaging, we could use 100 ms. The frequency of acquisition of the signal is the inverse of Dynamic TR, so it is approx 5 Hz for TR equal to 175 ms, and 10 Hz for TR equal to 100 ms [3]. The TR values used during the measurements are reported on page 26.

Sampling rate

The parameters set for the acquisition are already described on table 2.3 (page 25) and on the time scheme (Figure 2.15). The number of acquisitions parameter changes for each measurement and determines the duration of the acquisition. The TR (repetition

Day of experiment	**TR [ms]**	**f [Hz]**
23 November 2016, Old	175	5.7
24 May 2017, Dataset	100	10.0
19 June 2017, Resting state	100	10.0

Table 2.4: ***Repetition Time used in the different experiments.*** The dataset of 23th November is an example of the datasets acquired during previous work [1]. The dataset of 24th May and 19th June are the datasets taken for that thesis.

time) determines the frequency of the measurement. On the dataset of 23th November (tagged "Old" because it is taken in a previous work) the choice was using the TR suitable for the imaging sequences. For the datasets of this thesis, we chose to have a rapid measurement and using 100 ms. The sampling rates of acquisition of the signal are reported on table 2.4.

2.3.2 Calibration

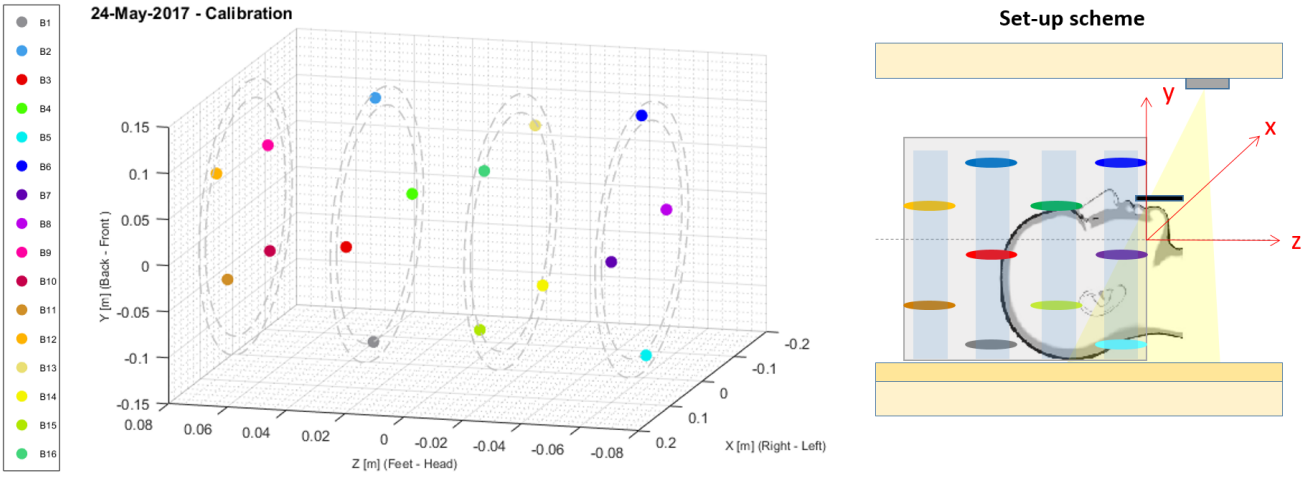

Figure 2.16: ***Results of calibration process (24 May 2017).*** *The 3D plot on the right shows the position of the probes (the protection ring isn't included). The 2D scheme on the left shows the position of the probes around the head. The rings are enumerated from the neck to the top part of the head, the protection ring isn't represented.*

The calibration described below is robust against eddy currents, gradient oscillations, gradient delays, ... but obviously it isn't robust as well against field fluctuations and drifts during the field measures that depend on the stability of the MR system, thet usually are very small. Other effects that can influence the precision of the measurements are mechanical vibration or drift of the mounting surface (scanner bed or plastic rings). The

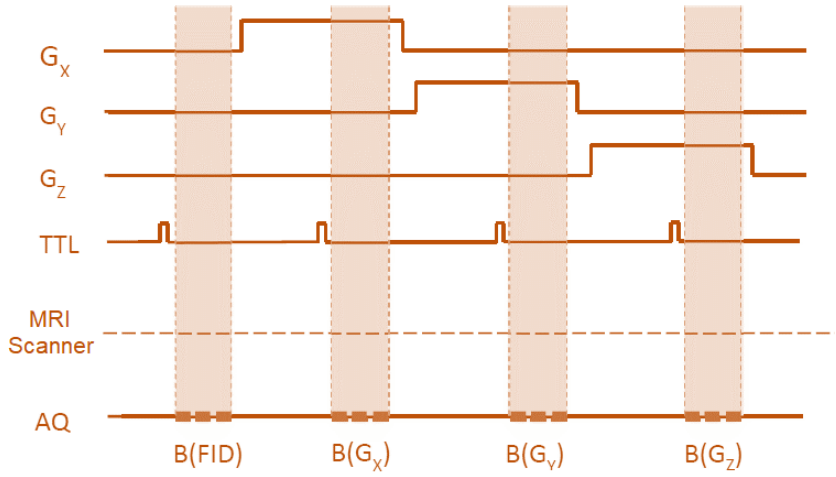

Figure 2.17: ***Sequence of Skope Calibration.*** *The sequence plays in the scanner consists of four types of probe FIDs. During the 2nd to the 4th FID only, the scanner applies an external field gradient to the X, Y and Z axes with the recommended field force (*$2.5mT\ m^{-1}$*). The positions of the probes are extrapolated from the field values that the gradients create in each probe and from the nominal gradient strength. The TTL signal is an external trigger to manage the field camera acquisitions. The FID is acquired after a certain time from the beginning of the gradient to avoid the error due to eddy currents or mechanical gradient vibration. [3]*

field camera calibration consists of the measurements of the off-resonance FIDs (free induction decay) values of the field probes and field probes positions evaluated on the scanner camera frame. The off-resonance calibration process is necessary to compensate for the inhomogeneity of the static magnetic field present in the actual scan set up. It is relevant for the accuracy of phase data, k-space data, and field data. Calibration of the position is necessary to know the position of the probes and to calculate the k-space data. After the calibration, the position of the probes is given in the scanner reference frame.[3] We perform both before measurement and to perform is necessary that the scanner executes the sequence described in Figure 2.17.

The precision of the calibration process is fundamental for the accuracy of the measurements of field and k-space data. The field measurement could be more precise than the stability of the field during the calibration measurement.

Shifting issue

The process described on page 26 is computed at the beginning of the experiments or before each measurements. In the first case, we use a phantom. In the second case, the measurement happens while the volunteer is inside the bore.

The system is moved and reseated each time to permit the swap of the subjects. This procedure produces a little shift of the probes inside the plastic rings, we noticed this after

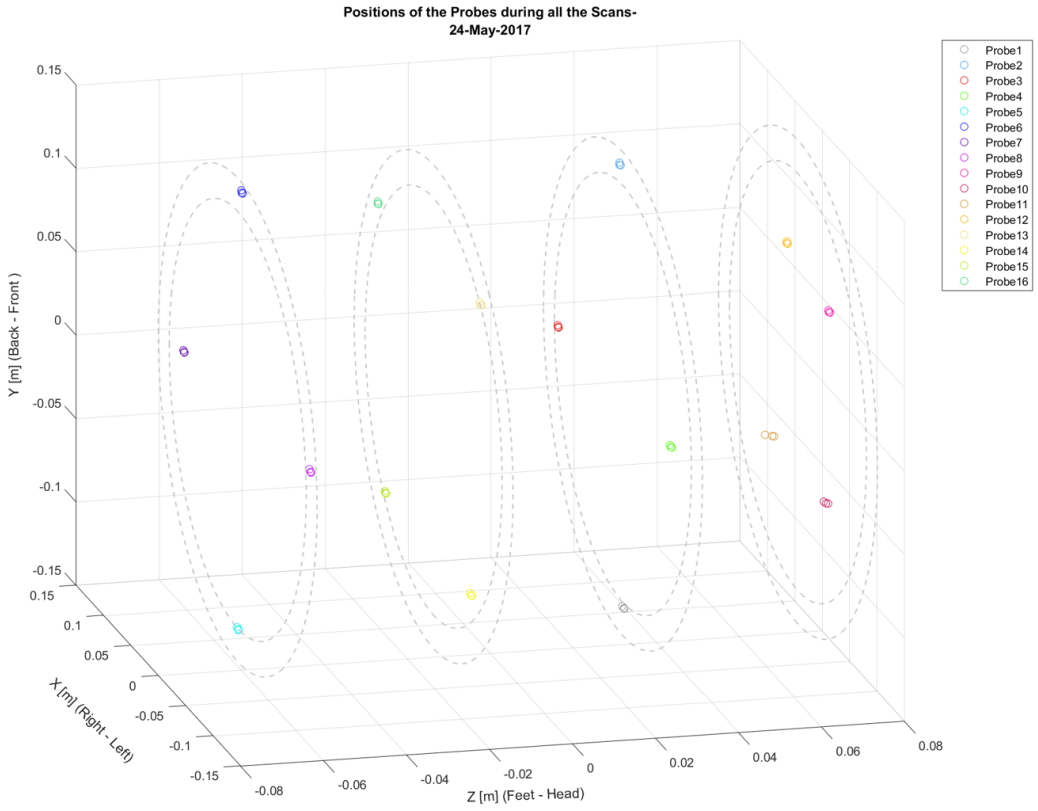

Figure 2.18: ***3D plot of the shift of the positions of the probes during three different scans.*** *The system is moved and reseating each time to permit the swap of the volunteers. Each position is represented by one circle on the plot. The deviation of the probes during the different scans is less than 1 cm, except for the probes 10 and 12. The probes 10 and 12 are close to the box that connects the probes to the computer, so they are the most unstable.*

the first day of measurement (24th May 2017) and we used a tape to stick the probes on the plastic rings for the second experiment (19th June 2017). The measurements strictly depended on that procedure to compare the measurements between the subjects. An example of the shifting problem is reported in Figure 2.18.

2.4 Tracking system

Tracking System. The methods to measure the head pose for motion correction are divided by the phenomenon used and the dependence on the sequence, interaction with the patient and the accuracy and precision of the image. Methods can be roughly

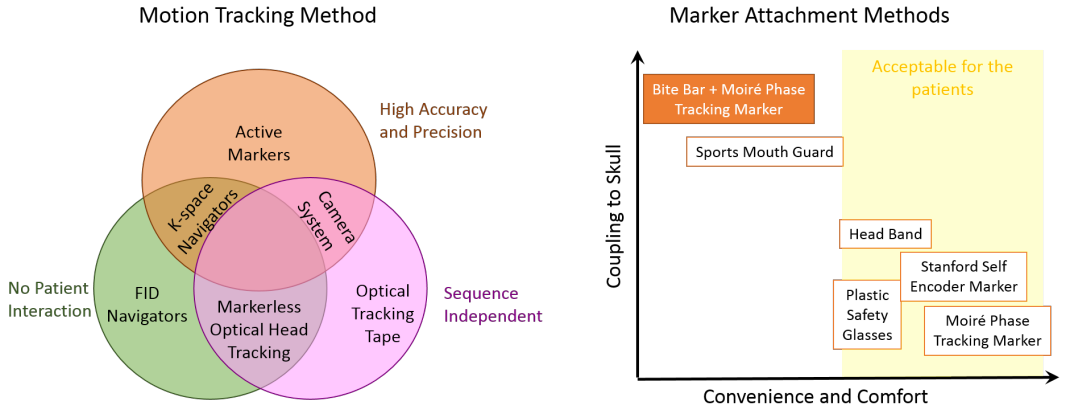

Figure 2.19: ***Tracking System****. The best choice is dependent on the specific case. On the left, the tracking systems are divided by the physics phenomena used and the precision of the measurement, interaction with the patient and the dependence of the MR sequence. On the right, the plot correlates the solution analysed by the best of the measurements and the comfort of the patient. The choice is always a compromise between the comfort for the patient and the measurement accuracy. The "coupling chain" means that the brain is coupling with the skull and the marker is coupled with the brain because this is in turn coupled with the skull. Hence, the best choice for the measurement is the one that is better coupling with the skull. Unfortunately, it is usually the less comfortable for the patient. The coupling on the skin solution is the most comfortable, but the skin isn't rigidly coupled with the skull, so the marker is vulnerable to the facial expressions. The skin solution is the worst choice for the measurement.[8].*

classified as field detection, navigator and optical method. The field detection can be used for prospective motion correction by detecting the scanner gradient and rearrange the direction of the gradient by the pose of the head in the scanner. It needs probes (MR probes or three or more active marker connected rigidly, positioned on the head of the subject on non-collinearly pose) to evaluate the position and the orientation. The navigator method is also used on prospective motion correction and uses the position of the image in the FOV of MRI like a navigator. For example, the Fat Navigator (FatNav) methods are based on the image registration of the fat that covers the skull. The advantage of the navigator technique is that it doesn't need additional hardware or marker bound on the head of the patient, it is a very comfortable "markerless" solution for the patient. The last method, also the method that is used for the measurements of this work, is the optical tracking and includes a laser system, bend-sensitive optical fibres and an optical camera system.

The optical methods are divided into in-bore and out-bore: we used an optical in-bore single camera system fixed inside the scanner. The advantage of optical methods is that it is independent from the MR sequence timing and, in our case, it uses a passive marker to recognize the pose. The camera is MR compatibile and oriented in the direction of

the subject. The marker must be rigidly attached to the head: in our case, it is fixed on a bite bar placed into the mouth of the patient, fixed to upper teeth and hence coupled with the skull ([**?**]). The relative position of the marker on the subject is a reproducible set-up (the relative position of the marker to the camera depends on the position of the patient inside the bore). One source of error could be the fixing system of the camera inside the scanner and of the marker on the bite. The pose data is computed using an external computer that gives us the pose in the reference frame of the camera and then, in post processing, they can be transformed into the coordinate of the MR scanner [8].

Quality of tracking data. The quality of tracking data is defined by three parameters [8]:

1. *Precision:* The precision describes the level of jitter or the level of noise;
2. *Accuracy:* The accuracy describes the discrepancy between the true pose and the measurement pose;
3. *Latency:* The latency is the delay between the measurement and the arrival of the data on the computer or, in prospective motion correction, on the scanner.

Accuracy and precision for high precision tracking systems, are less than $50\,\mu m$ for prospective motion correction [8]. For the in-bore tracking system, the precision is influenced by the vibrations of the scanner during the image acquisition. Latency is due to the physical transmission of the data and to the analysis data method used to reconstruct the pose (depending on the magnitude of the subject motion).

2.4.1 Moiré Phase Tracking system (MPT)

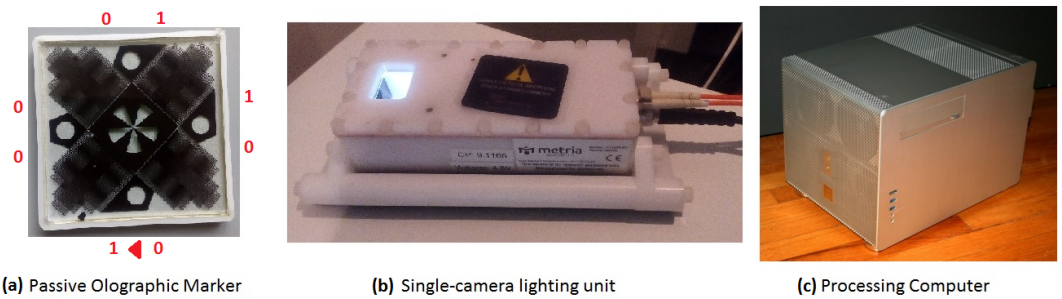

(a) Passive Olographic Marker **(b)** Single-camera lighting unit **(c)** Processing Computer

Figure 2.20: ***Moiré Phase Tracking System.*** *(a) The holographic marker has got a printed coded to distinguish it. The black triangle contains the code: corner black means 1, corner white means 0, read clockwise. The marker's code in that case is: 1001100. (b) is the CLU insert on a plastic tilted support, outside the bore of the scanner. (c) is the computer dedicated to the optical system. [4, 8-9].*

We use the "Moiré Phase Tracking System", Model MT 384ib, produced by Metria Innovation [4].

The Moiré Phase Tracking (MPT) is the optical camera that uses Moiré fringe patterns to determine the pose. It is a real-time 3D motion tracking that operates by (Figure 2.20):

- **Passive holographic markers**. The marker has got three different parts: a central star burst, four circle on the edges, an holographic cross that forms a moiré patterns. It is passive because is doesn't transmit data: the camera records its image and, in post processing, reconstructs the position of the marker by a pattern recognitions process. Each marker has a different ID number that is identified by a binary code on the marker. The patient uses a bite bar with the holographic marker, designed to be visible to the camera when the subject is in the scanner. The markers that we used are of two sizes. The bigger one is used during the calibration process and it is a square $65 \times 65\,mm$. The smaller ones are squares $15 \times 15\,mm$ and they are used for the subjects bite bar.

- **Single-camera lighting unit** (CLU): The CLU is in-bore camera and it is fixed in a plastic support. That support is fixed inside the bore (Figure 2.21: it is a movable system that we fixed (and removed) inside the bore for each session. Furthermore, the plastic support isn't rigid, it has a tilt regulation to choose the best inclination to spot the markers. Therefore, one source of noise is the vibration of the scanner during the scan. Furthermore, the cable for the transmission of the signal passes on the back of the bore and goes outside of the room. The power and signal wires are MR compatible as they are built to annihilate the magnetic field effects.

- **Processing Computer**: It is an external computer used for pose determination. The pattern recognition of the image is a fast process: it uses the last known position as an estimation of the position. If the marker goes out of the ROI, the process may be longer and the latency increases. This is the reason why the frequency may vary: it should be 80 Hz, we can set it lower to avoid the latency problem. An example of the output screen during MPT camera acquisition is in Figure 2.22.

The data acquisition of MPT camera is independent of the scanner and it begins and ends with the proper computer. It creates a log file for each using. The method used to extrapolate the data from the log file is an improvement in this thesis and will be described on page 57.

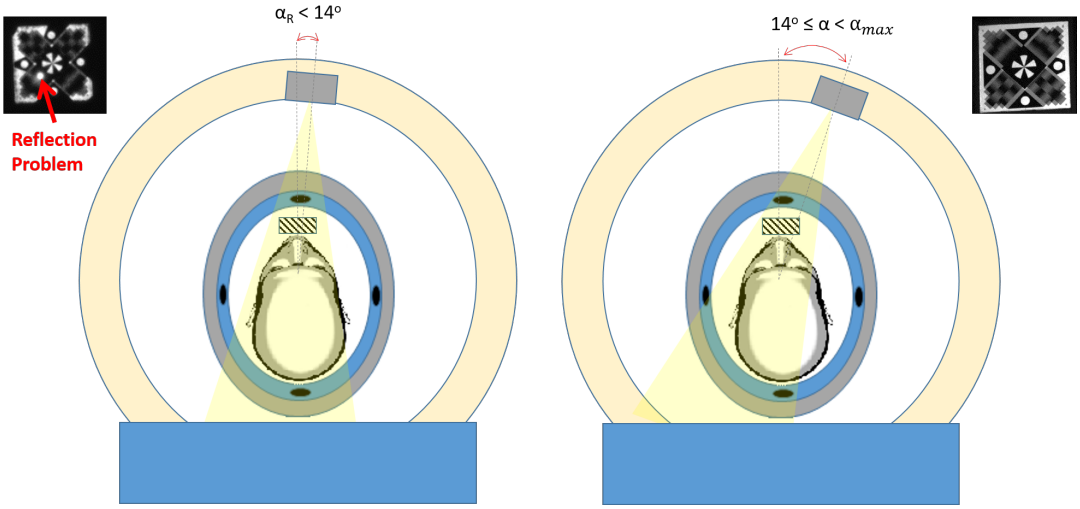

Figure 2.21: ***The CLU plastic box position in the scanner bore.*** *On the right, the actual set-up. The plastic support is rotated with respect to the vertical position, the lower (14°) and upper (α_{max}) limits of the rotation are defined by the set up of the experiment. The α_{max} angle is linked with the FOV of the camera. On the left, the wrong set-up: the light is reflected in the optical camera and prevents tracking. $\alpha_R < 14°$ are the angles of the CLU that produce the reflection problem.*

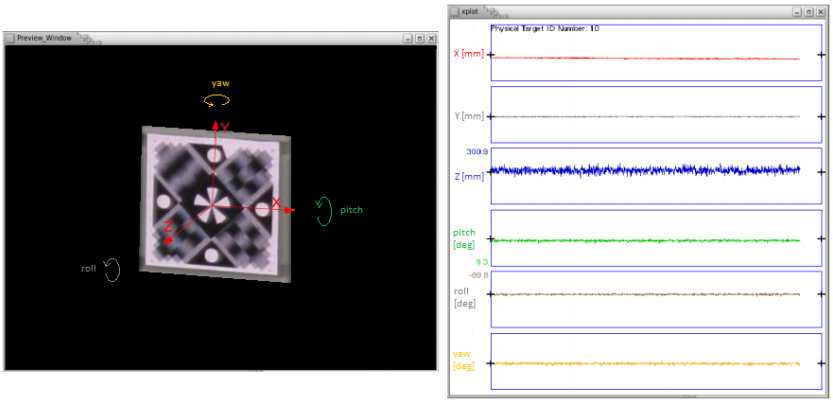

Figure 2.22: ***Example of the output screen during MPT acquisition.*** *On the left, it is visible the marker and its system of reference. On the right, there is the plot of a translation (in camera reference frame) and rotation (on marker frame). In particular, it shows an example of pure translation along z axis. [4, 27].*

Sampling rate

It is possible to set the average acquisition frequency of the MPT camera ($f\,[Hz]$); the acceptable range was evaluated experimentally and it is $75 \div 85\,[Hz]$. Anyhow, the real frequency of acquisition depends on the pattern recognition process (page 30), hence

Day of experiment	f [Hz]	Time between two measurements [ms]
23 November 2016, Old	85	≈ 12
24 May 2017, Dataset	80	≈ 13
19 June 2017, Resting state	80	≈ 13

Table 2.5: ***Frequency set for three different experiments and related time interval between two measurements.***

it isn't constant during the measurement. The range was evaluated in post processing and it is $\div 85\,[Hz]$ Our choices for the the experiments are reported on table 2.5 (the dataset of November 23rd is tagged "Old" because it was taken during previous work).

2.4.2 Calibration

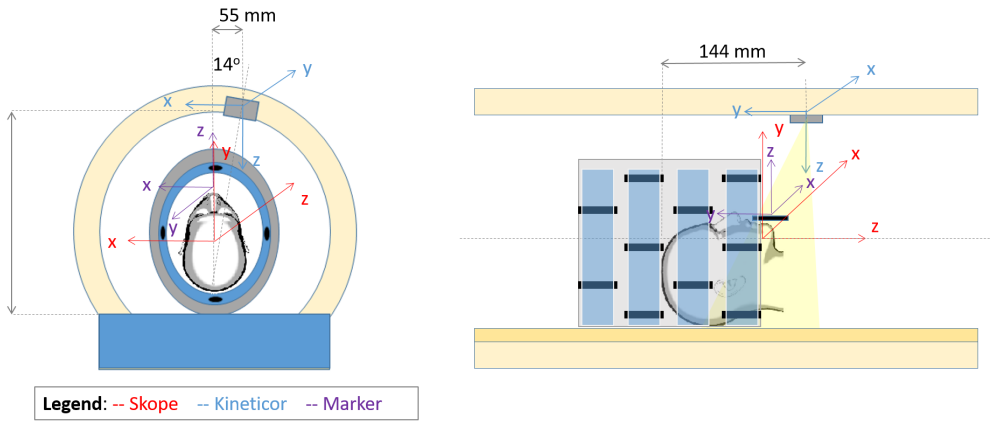

Figure 2.23: ***System of reference.*** *Relative position between the system of reference of CLU (MPT), Marker and CCH. The CLU is integrated with the magnet bore. The CCH is integrated with the bed, but the bed isn't strictly jointed with the magnet bore to permit the roll out and in of the patient.*

The calibration of the camera is a long process. The approach is called *cross-calibration process*. The cross-calibration approach involves collecting poses in camera and magnet frame, using a non symmetric phantom (Figure 2.24), and finding the best function that fits the data. This process is a non-iterative approach: the phantom is moved in eight different positions (Figure 2.24) to collect enough datasets to solve the fitting problem between the image of the camera and the measurement of the pose. During the experiment, the camera is attached to a fixed support in the magnet, so we assume that the system of reference of Kineticor is fixed and parallel to the system of reference of Skope (Figure 2.23).

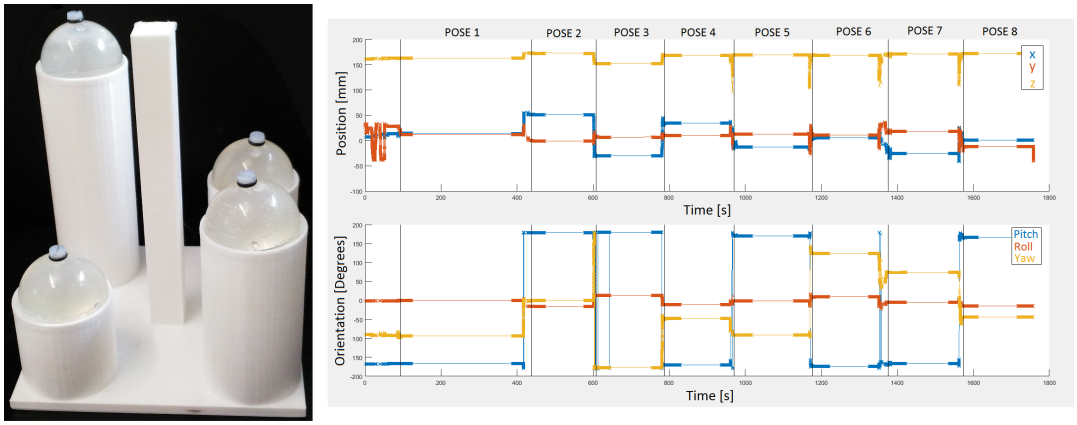

Figure 2.24: ***Phantom used for the calibration.*** *The phantom is completely antisymmetric in order to recognize the different positions of the water ball fixed on the top of the plastic tube. On the left, the eight different positions of the phantom are plotted. It is clear that the phantom is left in each position enough time to acquire the MR image.*

The aim of this thesis is a qualitative analysis between the changing in magnetic field and subject movement. Hence, no MPT camera calibration was needed. Further, determining the MPT camera calibration is a very long process in time and mainly it is an additional massive source of error on the measurement. Hence, it wasn't carried out before each experiment and the conversion of the measurement in the scanner frame is approximated (the approximation will be explained on page 60).

2.4.3 Field of View (FOV)

The optical properties of the lens determine the *Field of View* (FOV) of the camera. The field of view is the angular extent of the camera that defines the sizes of the scene that is imaged. We measured it directly using the big and the small markers. The camera was left on the ground with the CLU unit directed to the ceiling, so it is possible to measure the length of movement of the marker in front of the CLU. The big marker was shifted on the edge of an imaginary rectangle ($\Delta X \times \Delta Y$) at the minimum height at which the camera could see the marker (Z), the movements are checked directly on the computer screen. An analogue measurement was carried out with the small marker ($\Delta x \times \Delta y$, z). The vertical and horizontal FOVs are calculated for both measurements, as shown in Figure 2.25. The results are given as the mean of the two values.

Before taking the measurement it is important to check on the computer screen that the marker is on the center of the FOV and that the movements of the marker don't go out of FOV. Otherwise, the measurements are invalidated.

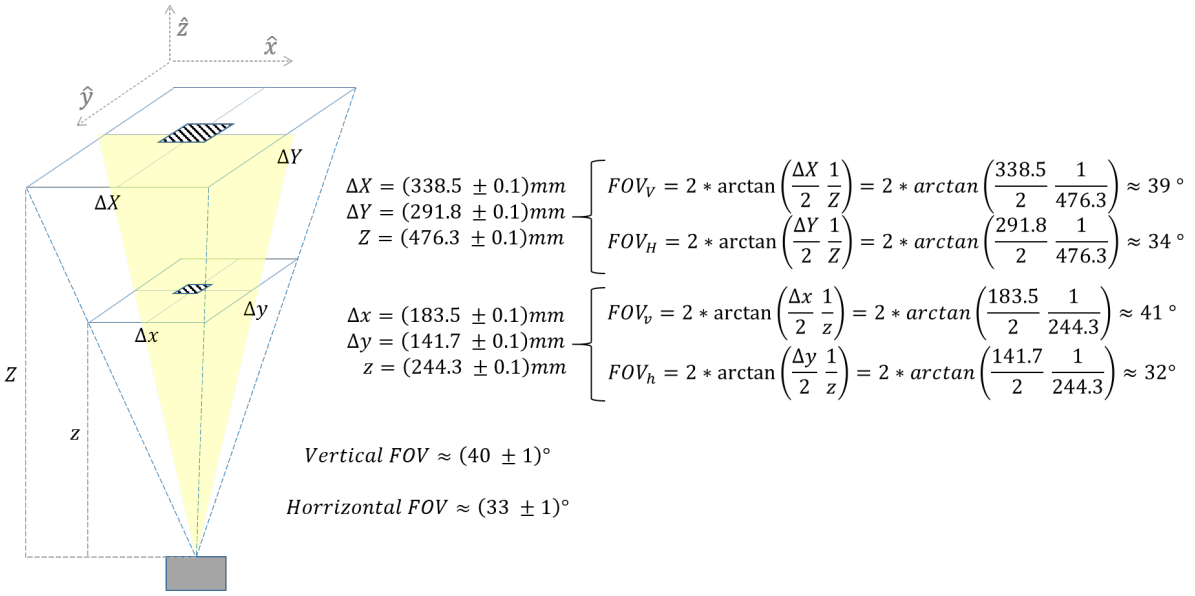

Figure 2.25: ***Field of View****. Scheme of the measurement, measurements and values of the vertical and horizontal FOV.*

Resolution. The resolution of the camera is of the order of magnitude of $10^{-2}\, mm/pixel$. The maximum range for the measurement is defined by the focus and the depth of the FOV for the translation and the minimum radius of the ellipse that encloses the central starburst for the rotation. For the translations, a blur effect on 4 or 5 pixel compromises the measurement. For the rotation, the radius is maximum when the marker is normally oriented to the camera and decreases with the tilt of the marker. The minimum radius seen is 11 pixel. [4, p.25].

2.4.4 Marker

During the experiment we use a passive holographic external marker (MPT) mounted on a bite bar (Figure 2.26) coupled with the skull of the patient. We assumed that the system formed by head and the bite-bar can be modelled as rigid body. Individual bite bars were made for each subject using thermal-setting dental plastic. On the top of dental arcade there is a plane extension to fix the holographic marker.

Pattern Recognition. The mechanism of pattern recognition methods exploits Moiré Pattern fringe formed on the marker. [3] The sequence of the method is:

1. **Starburst**: The central target is used to determine the position of the marker in x,y of the FOV (Field Of View) of the camera;

[3] Moiré patterns are interference patterns produced by the overlapping of similar patterns.

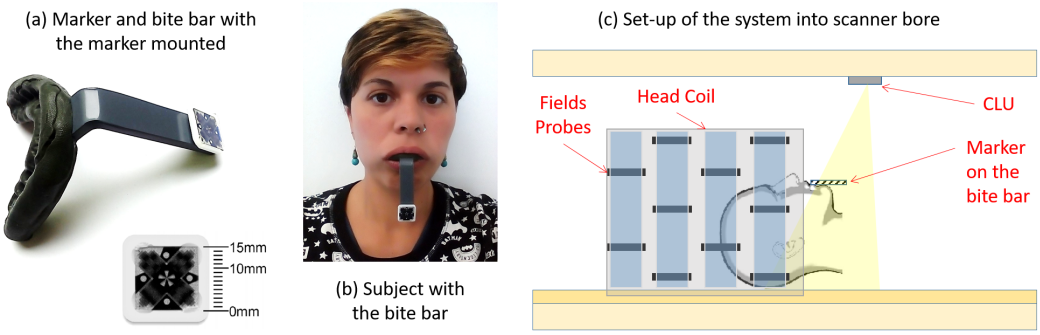

Figure 2.26: ***Marker set-up.*** *(a) The marker is* $15 \times 15mm$ *plastic square that is fixed on the end of a bite bar. (b) The bite bar is held in the mouth of the subject during the measurement. (c) The scheme of the set-up shows the relative positions of the marker and the CLU.*

2. **Corner Circle**: The corner circles are used to determine the translation along the z axis (away from/towards the camera) - because the separations of the circles in pixels change depending on distance;

3. **Holographic Cross**: The holographic cross is used to recognize the rotation - because the brightness of the cross and phase of the holographic lines change according to the orientation.

4. **Prediction**: The position of the marker is predicted using the last known position as an estimation for the future position.

Single and double marker measurement

The measurement of the movements of the markers is described from page 30. The MPT camera permits to record the movements of a single marker or for more than one marker. The configuration of the CLU and markers is described in Figure 2.27. The *single marker configuration* is sufficient to evaluate the movements of the head of the volunteer. The marker used is one of the small markers (called 192, 193, 195). The main problem of this configuration is the reflection problem, described on page 32. The *double markers configuration* is used in this thesis to evaluate the movements of the volunteer and of the scanner bed simultaneously. The differences between the single marker configuration are that we fixed the big marker (called 206) on the bore bed and that the plastic support is tilted. The main problem of this configuration is that the bed marker could be covered by the shoulder of the volunteer, it is different for each volunteer.

It is clear that if we didn't compute the calibration process, the values of the measurement with different configurations couldn't be compared, nevertheless the approxi-

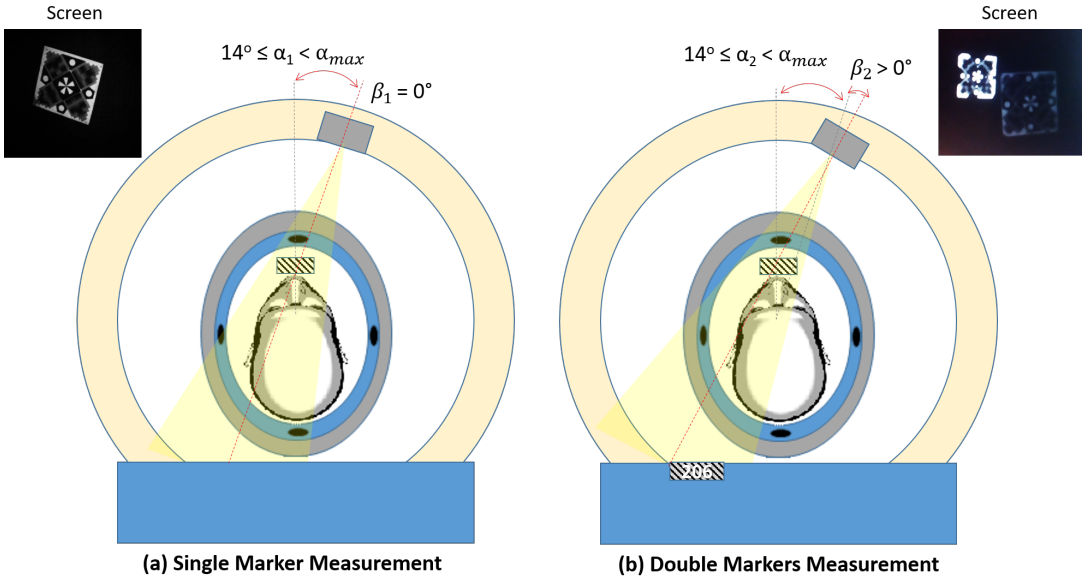

Figure 2.27: ***Single and double markers measurements****. The picture shows the set up used to take the single marker (a) and the double marker (b) measurement. The plastic box that contains the CLU is rotated with respect to the vertical position (α_n angle), as described on 32. The $\alpha_2 > \alpha_1$ to avoid that the shadow of the head of the volunteer covers the bed marker. The tilted angle (β_n) of the plastic support depends on the FOV of the camera. In (a) measurement, it isn't necessary to tilt the plastic support to spot the marker on the bite bar. In (b) measurement, it is. The angles aren't measured, but the best solution is evaluated for each experiment by the picture of the markers on the screen connected to the processing computer of the MPT camera.*

mations are described on page 62. The inclination of the CLU in the bore is different, hence the values of the movements recorded.

2.4.5 Error

The total error in the MPT camera measurement has several factors. As it is explained on page 35, the MPT camera uses the marker to recognize the movements of the head and each section of the marker is built to measure a specific parameters. Also, the relative orientation between the camera and the marker is important and the marker must be coupled the most rigidly as possible with the skull. If all the process is consid-

ered, the error in the final dataset is given by different terms:

$$\begin{aligned}\text{Total Error} = &\Big(\Delta\text{Coupling between bite bar and the skull}\Big)\cup \\ &\cup\Big(\wr\Delta\text{Calibration}, \wr\Delta\text{Measure}\Big)\cup\Big(\Delta\text{Missing Value}, \Delta\text{Down Sample}\Big)\end{aligned}$$

1. The first term is a huge practical problem because it can't be evaluated: it is strictly dependent on the vigour of the patient in holding the bite. In Figure 3.2 on page 43, it is reported an excluded measurement where the patient didn't hold the bite very well.

2. The second term considers the mechanism to obtain the measurement during the calibration process and during the measurement. The symbol $\wr\Delta$ means that there aren't constants for each single measurement and also for each translation and rotation values:

   - The translation along x and y axes on the camera frame (so along x and z axes on scanner frame, Figure page 33) are evaluated by the center of the starburst. The accuracy of the evaluation depends on the tilt angle of the marker.
   - The translation along z axes on the camera frame (then along y axes on scanner frame) is evaluated by the separation of the corner circle. There is an error on each identification of the circle (that depend on the tilt angle of the marker) and an added error in the evaluation of the separation between these. Hence, the error on the translation along z is higher than the error on the translation along x and y axes in the camera frame.
   - The mechanism behind the measurement of the rotation angle is more complicated because it depends on the fringe pattern and on the relative orientation between the camera and the marker. Also, we use the dual quaternion algebra to extract the rotation angle from the quaternion given directly to MPT camera.

   The error carried for each consideration increased for the calibration process, hence we decided not to do the calibration until now and to not consider that error: $\wr\Delta\text{Calibration} \equiv \oslash$.

3. The last term is due to the preprocessing of the data, as the process to fill the missing value (it will be described on page 61) and to down sample the dataset (it will be described on page 60) to match the measurements in time. The down sample process consists on taking the average between the data points that are

around the moment where the magnetic field is measured by the CCH. That error could be easily evaluated as the mid-range between the taken data points.

Overall, the total error is quite complicated to evaluate precisely, so we decided to consider it as ± 0.1 $[mm]$ for the translation and the ± 0.1 $[^\circ]$ for the rotation.

Chapter 3

Measurements

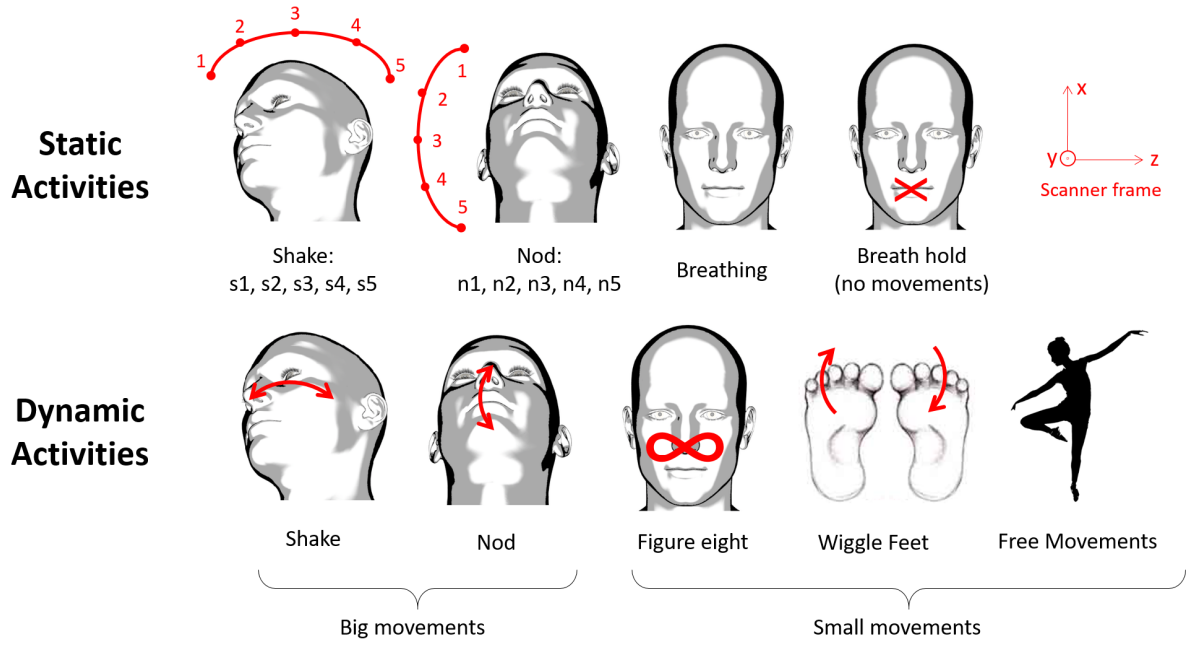

Figure 3.1: ***Activities.*** The figure shows the activities carried out during the experiments. They are referred to the scanner frame of reference. We decided to call the voluntary movements *activities*. During all the activities, except for the breath-hold, the volunteer breaths. Hence, the "Breathing" activity is the resting state. The activities are also divided into static and dynamic. The latter category includes big and small movements.

The future aim of the project is to qualify the relation between head movements (voluntary or not) and the changes in the magnetic field. Hence, to verify the improvement of the set-up of the experiment and characterize it, we have acquired a reasonable number of measurements. We asked the volunteers to make certain voluntary movements,

that we decided to call *activities* (Figure 3.1): it is clear that the activities aren't pure rotations or translations, but they are always a mix between rotations and translations. The activities are divided in *small movements* and *big movements* based on the range of the movement. The first group is the most realistic during a typical MRI experiment, the second is used to record the extreme situations. The *shake* dynamic activities are rotations around the z axis in the scanner reference frame (y axis on MPT camera reference frame). The shake poses involve holding shake activities in 5 steps called *s1, s2, s3, s4, s5*. Likewise, the *nod* dynamic activities are rotations around x axis on scanner and MPT camera reference frame, the nod poses are holding nod activities in 5 steps called *n1, n2, n3, n4, n5*. The last two static activities are influenced only by the breathing, they represent the most common situation during MRI acquisition. The first one is called *breathing* and the volunteer rests in the scanner. The second is called *breath-hold* and theoretically the patient rests: during the measurement we notice that the chest of the patient is still, but the trend of the head is a small nod movement (from n5 to n3). The last group of small dynamic activities includes head movements and head movements influenced by other parts of the body. The *figure eight* activity involved in drawing in the air a figure of eight with the nose. The *wiggle feet* activity produces a small movement of the head of the volunteer. The *free movements* activity is a series of random movements that the volunteer decides.

The experiments, done on different days of acquisition, include a group of the activities described below and a set composed of all the activities chosen, called the *Motion set*. Furthermore, some measurements were acquired more than once, they are tagged with the suffix *rep*.

3.1 Dataset

A brief description of the measurements is reported on table 3.1. Each activity of each dataset contains: the magnetic field values as a matrix of "$16 - by - NrAcquisition$" data points; the movements measurements as a matrix of "$6 - by - NrAcquisition \times 8$"[1] data points. For the longest datasets we acquired the physiological parameters, the data are a matrix of "$2 - by - NrAcquisition \times 50$"[2] data points. The final datasets analysed does not contain all the activities acquired, as will be clarified later.

Date	Description	Marker	Activities
23 November 2016	Old	1	s1, s2, s3, s4, s5, n1, n2, n3, n4, n5, Breathing (Rest), Motion set, Motion set rep, Wiggle feet, Wiggle feet rep, Breath hold
24 May 2017	Dataset	1	Motion set, Wiggle feet, Free movements, Pose1 (s1), Pose1rep, Pose2 (n1), Pose2rep, Pose3 (n5), Pose3rep
19 June 2017	Background	2	Breathing (Rest), Breath hold

Table 3.1: ***Brief description of the dataset.*** *The dataset of 23rd Novemeber is an example of a dataset acquired during previous work [1]. The dataset of 24th May and 19th June are the dataset taken after the improvement of the set-up. The differences between the old and the other datasets are the span of the activities chosen and the parameters of the instruments. They are described in the next subsections.*

Static Activities	**Pose1 (s1)**	**Pose1rep (s1)**	**Pose2 (n1)**	**Pose2rep (n1)**	**Pose3 (n5)**	**Pose3rep (n5)**
Volunteer 1 (M192)		X	X		X	
Volunteer 2 (M193)	X	X	X	X	X	X
Volunteer 3 (M195)	X	X	X	X	X	X
Nr Acquisitions						
Volunteer 1 (M192)	100	100	100	100	100	100
Volunteer 2 (M193)	100	100	100	100	100	100
Volunteer 3 (M195)	100	100	100	100	100	100

Dynamic Activities	**Motion set**	**Wiggle feet**	**Free movements**
Volunteer 1 (M192)	X P	X P	
Volunteer 2 (M193)	X P	X P	X P
Volunteer 3 (M195)	X P	X P	
Nr Acquisitions			
Volunteer 1 (M192)	4000	1000	
Volunteer 2 (M193)	2500	1000	600
Volunteer 3 (M195)	2500	1000	

Table 3.2: ***Dataset of 24 May 2017.*** *The Nr Acquisition parameter of CCH changes for each dynamic activity and it is 100 for all the static activities. The TR (repetition time) parameter of CHH is 100 ms. The average frequency of acquisition of MPT camera is 80 Hz. A cross indicates a good dataset, formed by magnetic field variations and movements measurements, and a P indicates the physiological measurements has been acquired. It is a single marker experiment.*

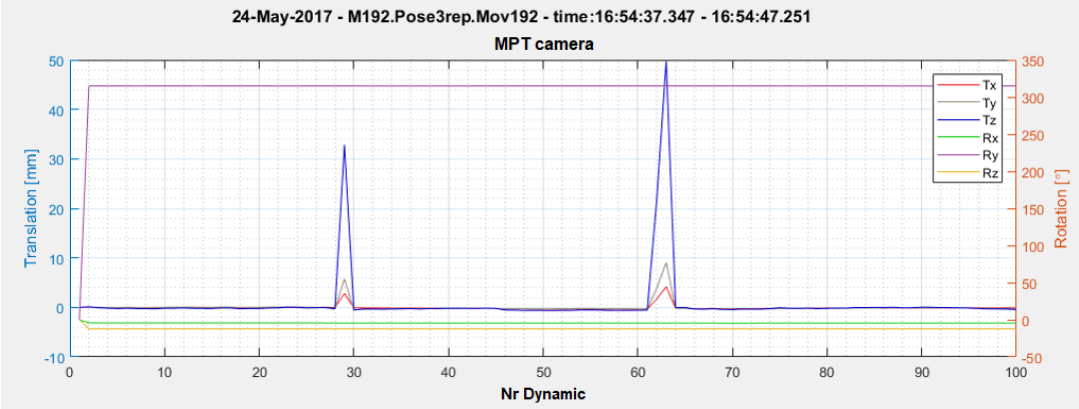

Figure 3.2: ***Example of discarded measurements for coupling problem and wrong conversion.*** *The plot shows an example of measurement of the movements by the MPT camera. The data are already down sampled by the CCH sampling rate and they are elaborated in order to have a centred distributions around zero. Furthermore, they are converted to the system of reference of the scanner: the big rotations at the beginning of the rotations value aren't real. The coupling between the bite bar and the skull strictly depend on the vigour of the volunteer to hold the bite. In this case, we know that the patient fell asleep during the measure and released the bite at least twice (that corresponds to the peaks on the translation measure). We can't use this dataset because we don't know if the problems are only at the times of two peaks or on during all the whole acquisition.*

3.1.1 24th May 2017 dataset

The Table 3.2 describes the dataset acquired on 24th May 2017. It is a single marker experiment, the set-up of the MPT camera is described in Figure 2.27, page 37. The dataset includes static and dynamic activities. We chose the activities by the analysis of the past work [1]. The *motion set* is the longest acquisition because it is composed of all the activities chosen. The *wiggle feet* is a small movement activity, so the acquisition is longer than the static activity. The *free movements* activity is failed for two of three volunteers because the marker often went out of the FOV of the camera: we decided that this is not a good activity for the future experiments. The static activity, as *Pose N* and *Pose N rep* are taken before and after the B field map measurement, so we are sure that the volunteers didn't change the pose. Unfortunately, volunteer 1 fell asleep during the measurements of Pose 1, 2 rep and 3 rep and release the bite bar, it is clear on the MPT measure (Figure 3.2). We discarded all of this dataset. First, we weren't sure about the coupling between the bite bar and the skull. Second, when the marker isn't spotted for several time, the pattern recognition process computed to the MPT unit failed because it

[1] "8" is the ratio between the sampling rate of the optical camera and of the magnetic field probes : $80\,Hz/10\,Hz = 8$.

[2] "50" is the ratio between the sampling rate of Physlog tool of the 7 T Scanner and of the magnetic field probes : $500\,Hz/10\,Hz = 50$.

Static Activities	Vibe Measurement		Breathing (resting state)		Breath Hold	
Marker	192	206	19X	206	19X	206
M666 (Phantom)	X	X				
Volunteer 1 (M192)			X P	X	X P	X
Volunteer 2 (M193)			X P	X	X P	X
Volunteer 3 (M195)			X P		X P	
Nr Acquisitions						
M666 (Phantom)	2000					
Volunteer 1 (M192)			2000		100	
Volunteer 2 (M193)			2000		100	
Volunteer 3 (M195)			2000		100	

Table 3.3: ***Dataset of 19 June 2017.*** *It is a double marker experiment, so the number of the markers on the bed (206) and on the volunteers (called 19X except for the phantom where the marker 192 is used) are used to distinguish the datasets. A cross indicates a good datasets, formed by magnetic field variations and movements measurements, and a P indicates the physiological measurements has been acquired. The phantom is the anthropology one. The TR (repetition time) parameter of CCH is 100 ms. The average frequency of acquisition of MPT camera is 80 Hz.*

is based on the position recorded on the previous image that, in this case, doesn't exist. Considering the CCH fields probes, we observed during the measurement that the probe B10 isn't reliable: that probe isn't well fixed into the ring, probably it moved during the exchange of the volunteers.

3.1.2 19th June 2017 dataset

The Table 3.3 describes the dataset acquired on 19th June 2017. It is a double marker experiment, the set-up of the MPT camera is described in Figure 2.27. We use a configuration with two markers to evaluate the movements of the volunteer and of the scanner's bed simultaneously. The marker on the bed (number 206) is located near the right shoulder of the volunteer, it is the only position available to be sure that both markers are in the FOV of the MPT camera. Unfortunately, for the volunteer 3 we had to discard the data of the bed marker because the right shoulder of the volunteer covered the marker on the bed. Considering the CCH field probes, we fixed all the probes to the plastic rings to avoid probe movements during the exchange of the volunteers.

3.2 Subjects

The subjects of the experiments are one anthropological phantom and three volunteers. The magnetic field variations depend on the movements of the volunteer, hence

the phantom doesn't influence it.

Tag of the subjects issue. The only instrument that diversifies the subjects automatically is the MPT camera. It uses the ID of the marker to tag the log file. Hence, we decided to adopt that convention to distinguish the subject. The numbers of the markers uses for the volunteers are 192, 193, 195. The subjects are tagged by the marker used with "M" at the beginning of the number as "MXXX', e.g. "M192" is the volunteer that used the marker 192. During the calibration of the MPT camera, measurement of the FOV and during the measurement with two markers it was necessary to use the bigger marker, because at distances up to $\approx 30\,cm$ the small marker became not clearly visible on MPT camera frame. The tag of the bigger marker is 206. The tags of the phantoms are chosen manually because we stick on its neck the marker 192. To avoid misunderstanding, we choose 666 for anatomic phantom and 616 for the water ball phantom, these are three figures numbers that hadn't other meaning for this experiment.

3.2.1 Phantoms

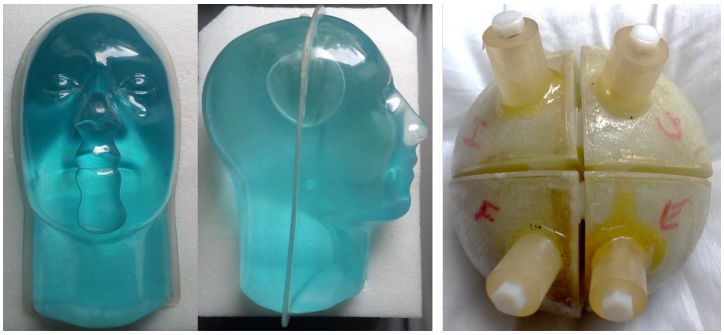

(a) 666 - Victor (b) 616

Figure 3.3: ***Phantom.*** *The figure (a) is the anthropological phantom used for developed the mounting system, the name assigned in the dataset is M666. The figure (b) is water ball divided in 4 parts with different concetration of doped agar. The name assigned is M616, but it used only the occasional calibration process between the day of the experiments.*

Figure 3.3 shows a picture of the anthropological phantom. It is designed to be similar to a human head and it is filled with a doped water that simulates the soft tissue. During the experiment, we give it the nickname of "Victor", but to have a consistent name with the other volunteer, it is identified as M666 in the dataset (a three digit number that doesn't correspond to the markers).

3.2.2 Volunteers

Head dimension

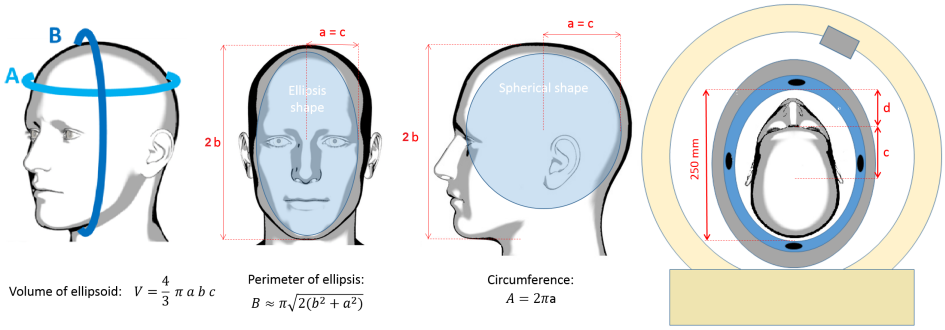

Figure 3.4: ***Head****. We can approximate the head as an ellipsoid. We measured the circumference of the head (A) and the circumference of the face (B) to obtain the ellipsoid parameters (a, b, c). On the right, the head is shown inside the mounting system indicates how to calculate the distance of the head to the upper part of the ring.*

Each movement, voluntary or not, of the volunteer inside the scanner produced a magnetic field perturbation, that depends also on the distance of the object from the field probes. Each head is different in shape, volume and by the distance of the probes. Usually, the head is modelled as a water-like sphere in the upper part of the head (where the brain is, usually). The measurement suggests that the most of the magnetic field variations are due to the bottom part of the head. The hypotheses are that the model of the head shape is incomplete and the magnetic field variations are more influenced by the chest movements that move the bottom part of the head. These hypotheses will be verified by theoretical simulations in the future.

Head shape

The proposal is that the head is a water-like ellipsoid formed by the rotation of an ellipse (figure 3.4). Hence, most of the water is on the upper part of the head, but there is a small volume of water in the bottom part also.

We had measured the head of the volunteer to start to verify this hypothesis. The measurements taken are the circumference of the head (A) and the circumference of the face (B). The first (A) is modelled as circumference and the second (B) is modelled as an ellipse. To obtain the volume of the ellipsoid ($V = \frac{4}{3}\pi abc$) it is necessary to know the radius of the sphere ($a = \frac{A}{2\pi}$), the major axis ($b = \sqrt{\frac{B^2}{2\pi^2} - a^2}$) and the minor axis (we approximate $c = a$). The average distance from the front of the head to the upper part of the field probes could easily be evaluated by the diameter of the plastic rings ($25.0\,[cm]$, Figure 2.13) minus the double of the minor axis: $d = 25.0 - 2 \times a\,[cm]$. The distance

volunteer (Weight [kg])	$A \pm 0.1$ $[cm]$	$B \pm 0.1$ $[cm]$	a $[cm]$	b $[cm]$	V $[cm^3]$	d $[cm]$
Volunteer 1 (M192) [≈ 55]	55.4	57.4	8.8	9.5	≈ 3100	≈ 7.4
Volunteer 2 (M193) [≈ 67]	58.0	62.0	9.2	10.5	≈ 3800	≈ 6.5
Volunteer 3 (M195) [≈ 90]	57.0	67.3	9.1	12.1	≈ 4200	≈ 6.9

Table 3.4: ***Measure of the heads and qualitative values of equivalent water volume and distances to the upper fields probes.***

between the last ring and the top of the head depends on the comfort of the volunteer. It couldn't be estimated in the same way, but using the MRI (it will be describe on the next subsection). On the Table 3.4 there are the volume and the distance to the upper field probes for the three different volunteers to have an estimate of the volume (the error of this measure isn't evaluated): The conclusions of the measurements of the shape of the head and the position of the head inside the ring set are that volunteer 1 (M192) has got a quasi-spherical head (A and B are similar), volunteer 3 (M195) has got an oval head, volunteer 2 (M193) is in between. The volume of the heads of volunteer 3 (M195) and 2 (M193) are bigger than the volume of volunteer 1 (M192). The distance from the upper part of the head to the probes situated in the upper part of the ring directly depends on the circumference of the head.

Head placement: MRI and B field map

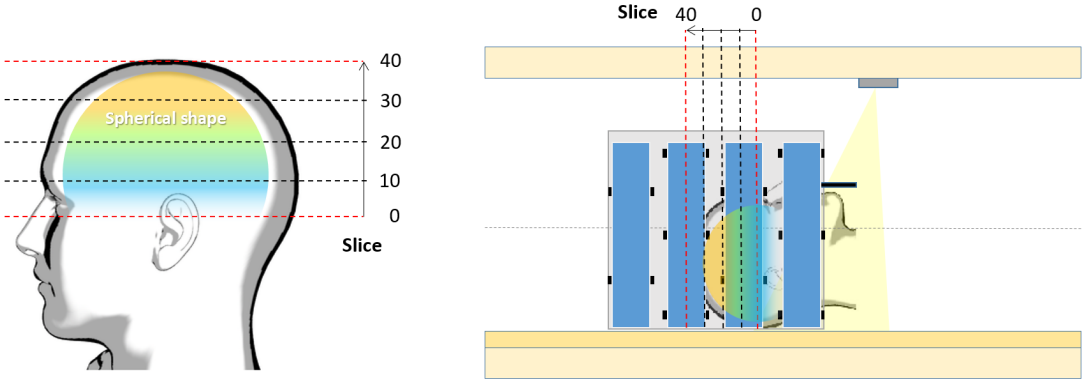

Figure 3.5: ***Slices acquired during MRI and B field map measurements.*** *The 40 slices are acquired from the axial planes, the picture shows the position of the slices on the head with the plastic rings of CCH. The head in the left of the picture is showing a sagittal plane to visualize the positions of the axial slice.*

We acquired MRI and *B field map* measurements to analyse the differences between volunteers with the same set-up configuration. The MRI is a representation of the magnitude of the signal, the B field map is the pattern of the changing of the magnetic

field inside the head. This type of measurements is always referred to scanner reference frame. The resolution of the pictures is low ($64 \times 64\, pixel$). We acquired 40 axial slices of the head, approximately from the plane that intercepts the ears to the top of the head, that corresponds approximately to the second and the third rings of the plastic support (Figure 3.5). The head RF coil is used to acquire the B field map, the CCH field probes support is inserted inside the head coil as is described in Figure 2.13, page 23. The head coil is fixed to the bed. The head goes inside the coil: the anatomical part visible on MRI depends on the dimensions of the head and on the activities because we didn't change the FOV of the scanner, therefore the field changes are visible on B field map. In general, we know that the magnetic field changes inside the head are bigger than the changes that we measured outside.

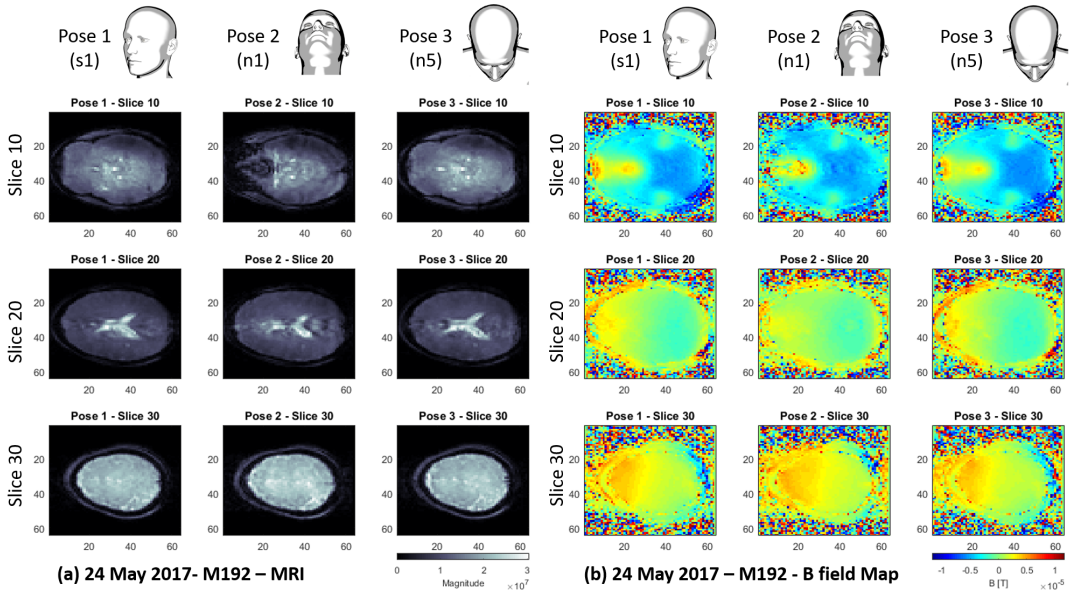

Figure 3.6: ***MRI (a) and B field map (b) measurements of volunteer 1 (M192).***

The results for the volunteers are shown in Figures 3.6, 3.7, 3.8 that are organized into two matrix $Slice \times Activity$, for three static activities (Pose 1, Pose 2, Pose 3) times three slices (10, 20, 30). The overall order of magnitude of the magnetic field value inside the head is $10^{-5}\, T$, the external part of the head couldn't be evaluated well, it is the reason why we use the CCH field probes camera. The CCH reveals that the order of magnitude of the magnetic field value outside the head is $10^{-5}\, T$ as well, but the order of magnitude of the magnetic field variation is $10^{-7}\, T$, hence in the pictures the B field map of the space outside the head is noise.
The pictures of slice 10 represent the middle part of the head. The anatomical information of that slice changes too much by dimension of the head of the volunteers. For example, the eyes on the front part of the head are visible only for the volunteer M193

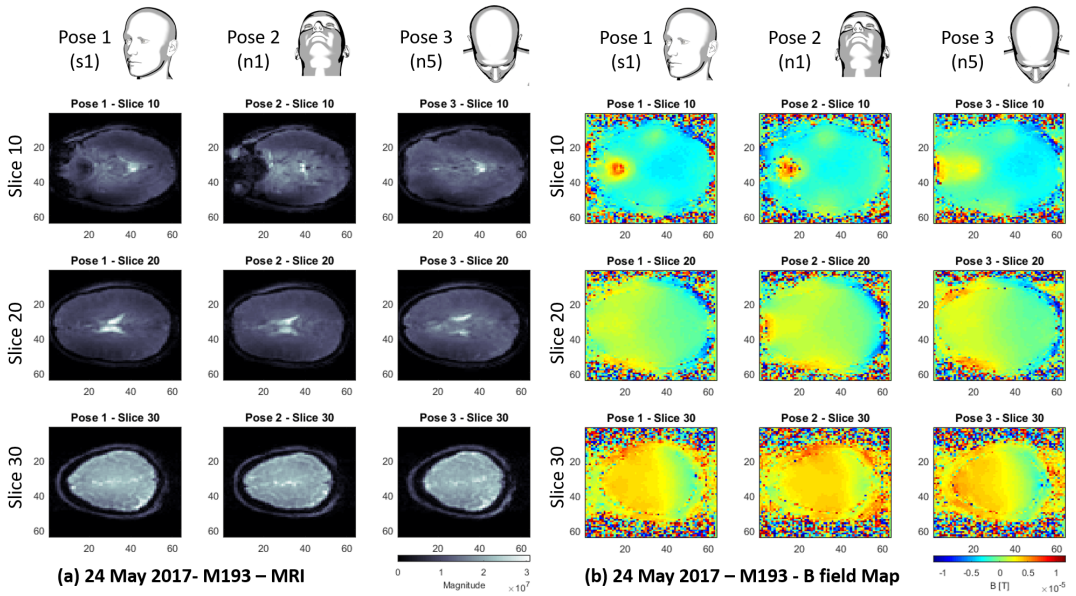

Figure 3.7: ***MRI (a) and B field map (b) measurements of volunteer 2 (M193).***

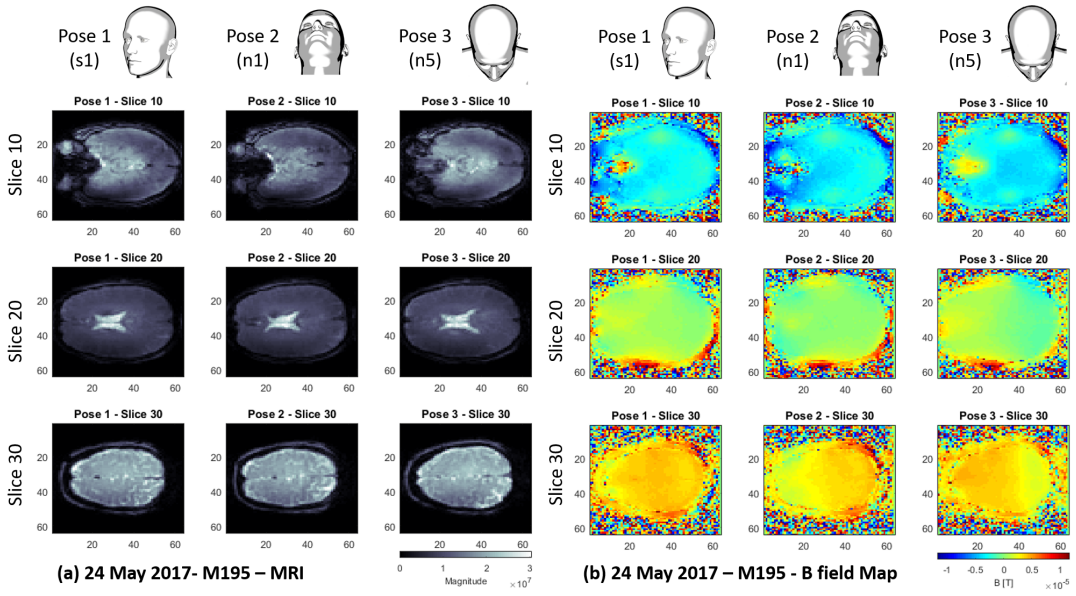

Figure 3.8: ***MRI (a) and B field map (b) measurements of volunteer 3 (M195).***

and M195. It means that the B field changes inside and outside the head depend on different parts of the head by the volunteers. In fact, the B field map pattern is really different for different volunteers, but the pattern is clearly separated on the front and the back sides of the head.

The pictures of slice 20 represent the middle part of the brain. The cerebrospinal fluid (CSF) is the only anatomical part clearly identifiable and its shape is slightly different for each volunteer. That slice was approximately between the second and the third ring, so there aren't field probes around it.

The pictures of slice 30 represent the upper part of the head and correspond approximately to the probes on the third ring. The magnetic field inside the head doesn't change as the slice 10 because the upper part of the brain is homogeneous, as is shown on MRI picture. It changes between the front and the back part of the head.

Hence, it is clear that the anatomical information by slices changes by the static activities, because the pose of the head changes. The magnetic field changing is different on the front and on the back of the head. The changes on the back of the head is approximately zero for all the volunteers, for all the activities, for all the slices. It means that we don't expect a big change of the external magnetic field measured by the probes around the back side of the head. In conclusion, it is possible that the probes on the second plastic ring carrier more information than the third due to the anatomical structure of the head.

3.2.3 Frequency of physiological parameters

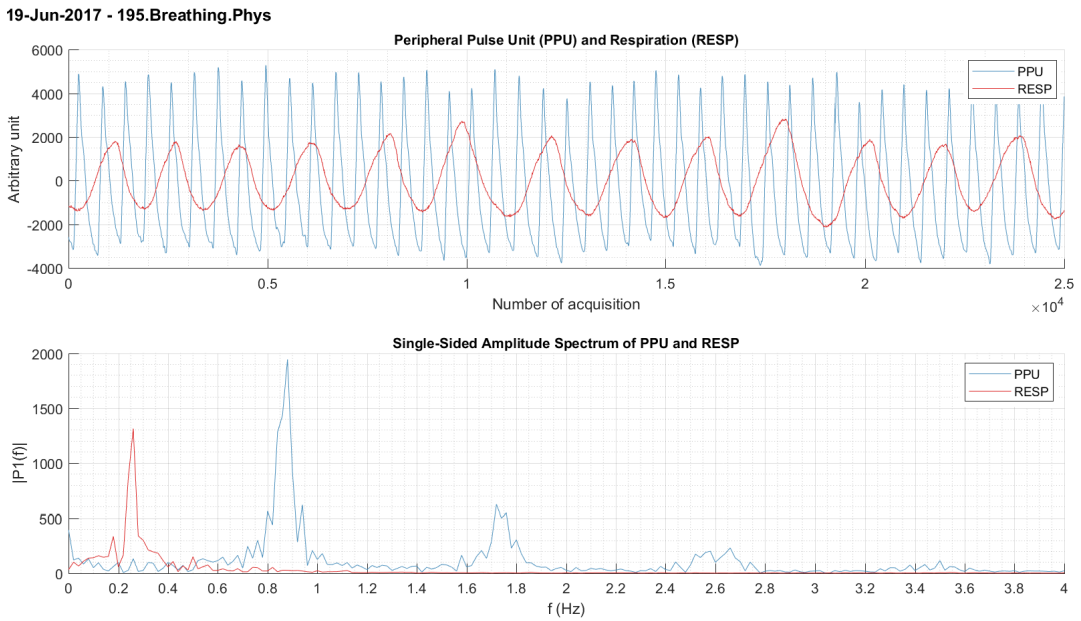

Figure 3.9: ***Example of Fourier analysis of the PPU and RESP measurements.*** *The picture shows the Fourier Analysis of the signal of the volunteer 3 (M195) during the Breathing activity on 19th Jun 2017. The dataset is cut on 25000 data point (plot on top). The frequency spectrum limit is set to 4 Hz to observe the low frequency.*

	Volunteer 1 (M192) (Hz)		**Volunteer 2 (M193)** (Hz)		**Volunteer 3 (M195)** (Hz)	
Measurement	PPU	RESP	PPU	RESP	PPU	RESP
Motion set	0.98	0.32	1.18	0.26	0.86	0.36
Wiggle feet	0.94	0.32	1.28	0.26	0.94	0.38
Breathing	0.82	0.20	1.12	0.18	0.88	0.26
Average Frequency	0.91	0.22	1.20	0.23	0.89	0.33

Table 3.5: ***Measurement of the frequencies of the peripheral pulse and respiration.*** *The errors in the peak are evaluated as* $\pm 0.02\,Hz$.

The idea of the project is that the involuntary movements of the volunteer, due mainly to the breath, produce a part of the magnetic field changing. Hence, to better identify that component in the Fourier analysis of magnetic field changes and the movement signal for each volunteer, we compute the Fourier analysis of the physiological measurement (PPU and RESP) described on page 19.

As explained on page 65, the bandwidth ($\mathbb{F}$) and the resolution frequency (Δf) of the spectrum are related to the sampling frequency (F_s) and the number of data points (N). The sampling frequency (F_s) of the instruments is $500\,Hz$ and it is constant. To have a large number of data points, we chose the longest datasets (Motion set, Wiggle feet, Breathing) and fixed $N = 25000$, to have a comparable resolution frequency. The datasets are acquired on different date, but we assume that the physiological values of the volunteer don't change by day. An example of the Fourier analysis computed is in Figure **??**. The bandwidth ($\mathbb{F}$) and the resolution frequency (Δf) are evaluated as equation 4.1.1 (page 66):

$$\mathbb{F} = \left[0; \frac{500}{2} - \frac{500}{25000}\right] = [0; 250]\,Hz \qquad \Delta f = \frac{500}{25000} = 0.02\,Hz$$

On Table 3.5 there are the values of the frequency that correspond to the cardiac cycle (PPU) and the breath (RESP) for each volunteer, for each activity. In general, the cardiac cycle frequency is around $1\,Hz$ and the frequency of the breathing is around $0.3\,Hz$. The frequencies that correspond to the Breathing dataset are less than the other activities. The reason isn't the different day of the measurement, but the type of activity undertaken. The Motion set and the Wiggle feet are dynamic activities, instead the Breathing is a static activity. Hence, the volunteer moved some part of the body and did a soft aerobic activity, probably this is the reason of the slight increment of the parameters compared to the resting state. The last row of the table is the average of the physiological parameters of the volunteer. That value will be considered during the Fourier analysis of the measurements of magnetic field changes and the movements.

3.3 Preprocessing Data

To carry out the data analysis, it is necessary to obtain three synchronized datasets. To summarize the information written so far:

- The experiment is based on three datasets acquired by using three different instruments (Figure 2.1) placed into the magnet bore to quantify the magnetic field perturbations and to relate these to movements and physiological parameters. These instruments are managed by different computers and each instrument produces its own log file. The methods used to sample the data are completely different for the three instruments, as will be described in the next subsection. Also, the reference frames of the CCH and MPT are different: the CCH data are in the 7 T scanner (or magnet) frame, the MPT data must be converted according to the appropriate approximations (this process is described on page 60);

- The instruments aren't built to work together: it is impossible to synchronize the start of the acquisitions, their sampling rate is different, neither customizable nor constant, and they don't acquire the data in the same reference frame. The sampling frequency of the CCH magnetic field probes depends on the repetition time (TR) chosen. The frequency of the MPT camera (f_{MPT}) is approximately constant, the latency depends on the pattern recognition process. The frequency of Physlog tool (f_{Phys}) is constant. Their values for the dataset of 24th May and 19th June are: $TR = 100[ms]$, $f_{MPT} \approx 80[Hz]$ and $f_{Phys}500[Hz]$. The data must be down sampled to be compared (it will be described on page 60);

- The only way to connect the measurements is to send a common TTL signal. We built an OR gate to couple the instruments automatically, to make the operation easily in the lab and to avoid the production of irrelevant spikes in the log file. The result is that the CCH and MPT measurements are aligned by the beginning of the measurements, the MPT and Physlog are aligned by the end. Thanks to the OR gate (described on page 12), the way to locate the data stream of the measurement on the log file is improved, and now the time string (described on page 57) is used. The time line-up process is managed by comparing the time strings and the variable that records the trigger on the MPT camera. This process is more complicated than the protocol used before, but the synchronization is better (now the precision of the alignment is $\pm 6\, ms$.) and the algorithm works automatically;

3.3.1 Log file

Each instrument creates a proper log files, each file contains the data point and additional information. The main differences that complicate the lining up of the data

sets are: the length of the stream of data points recorded, the presence or not of an associated time string and its time resolution.

Clip on Camera Head (CCH)

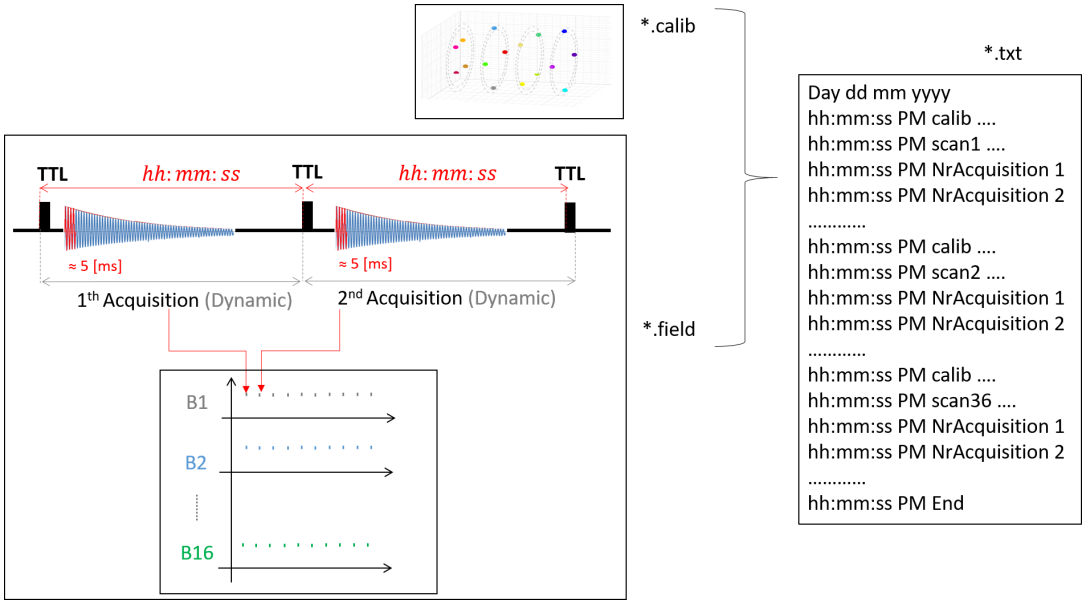

Figure 3.10: ***Log file created by CCH acquisition system.*** *The picture shows the scheme of the file created. One* $^*.calib$ *and* $^*.field$ *files are created for each scan. The* $^*.txt$ *contains the list of the operations done from the turn-on of the CCH to the last scan.*

The CCH system is turned on independently. The first log file that is written is a $^*.txt$ file (Figure 3.10), which contains the time register of the operation computed. The time string is read directly from the operation system of the computer, the time string is recorded in AM/PM format $hour : minutes : second\, PM/AM$ (hh:mm:ss PM). For these instruments only, the experiment is divided in to scans: we associate the scans to the subjects and to the activity. Each scan produced several files, we use $^*.field$ that contains the value of the magnetic field measurements at the probes, and $^*.calib$ that contain the position of the probes in the scanner reference frame. The data points in $^*.field$ are divided in to Dynamics and each dynamic is divided in to Acquisitions: we set the number of Acquisitions as number of Dynamics, so we simply call it "Nr Acquisition". This file contains a lot of information, we also used the value of the repetition time used (TR).

As described on page 24, TR is less than one second: it is clear that the time string recorded in $^*.txt$ isn't precise enough to associate the time to the data point and to associate the data point with the data of the other instruments. The way to solve this problem was [1] building the time vector according to the instructions written on the

manual. The improvements since that thesis is that we don't need to do this any more, it is explained in the next section.

The name of *.*field* and *.*calib* files are encoded and report the name of the scans: the built-in function to automatically read all the files for each scan is written in MatLab language. The name of the *.*txt* log file contains the date-string: '24-May-2017' for the experiment of 24th May 2017 and '19-Jun-2017' for the experiment of 19th June 2017.

Moiré Phase Tracking (MPT)

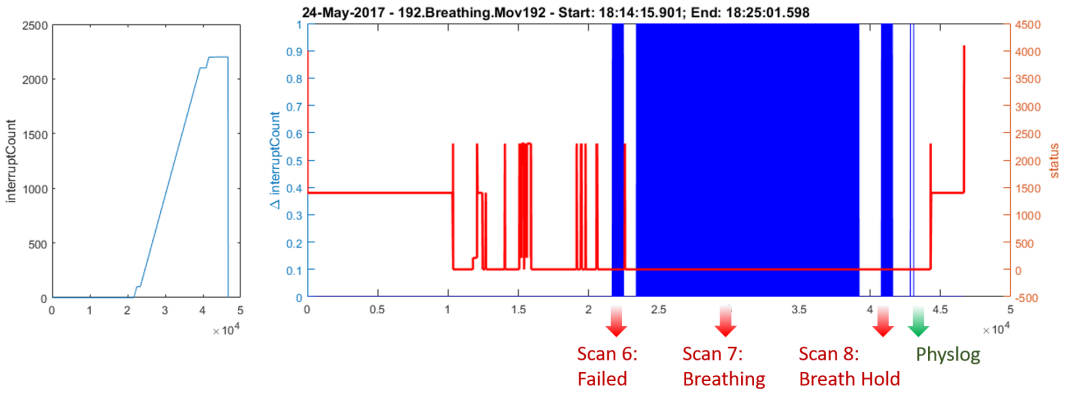

Figure 3.11: ***Variables interruptCount and status of MPT camera.*** *The plot on the right represents the variable InterruptCount: it is an integer and increases by one unit for each TTL pulse received. The plot on the left shows the incrementing of InterruptCount to enhance the moment when the TTL signal is received: due to the under sampling of the figure, the series of peaks looks like a solid rectangle. The red line represent the status variable used for discriminating valid data points.*

The MPT camera processing computer produces two log files (one for the measurement and one for diagnostic/engineering purposes) containing text information [4, 24, 54].

The used informations in "measurement log file" are is:

- *InterruptCount*: This is the TTL counter of the MPT camera. It counts each TTL signals sent to the MPT computer, an example is shown in Figure 3.11. The series of peaks on the right plot corresponds to the TTL signal, each group corresponds to the TTL pulses during the scan on the CCH log file. The last two spikes correspond to the TTL signals of the scanner that appears also into the Physlog log file. These are the reasons why the MPT is the key instrument to synchronize the instruments and down-sample the MPT and Physlog data.

- *Status*: This variable tags the data point with a value which indicate the valid measurements (Figure 3.11). It distinguish between five different situations: (I)

the marker is spotted and the pose is reconstructed well, *status* = 0; (II) the marker is spotted, but the pose isn't reconstructed well, *status* = 1500; (III) the marker isn't spotted, *status* >> 2300. In case of a measurement with two markers, all the conditions before are valid and (IV) it indicates the condition when only one marker is spotted, *status* = 2300. The status variable is used to evaluate the goodness of the data and fill the missing data (the process will be described below). One of the improvements is using this variable also to evaluate the percent of the missing value, that is less than 1% for all the datasets.

- *Frame Time*: This is a string that records the time of acquisition of all the data points, from the turn on to the turn off of the computer. This time string, combined with the interrupt count variable, gives us the time string of each TTL signal. This information is used to match the measurements in time. The time string format is 24 hours, it is directly read from the operation system of the computer with millisecond the precision (as 'hh:mm:ss.sss'). During the thesis, we discovered a bug on that reading process. The bug concerns the milliseconds part of that string. Our hypothesis is that when the trigger is near to the end of the second, the string 'hh:mm:ss.000' is interpreted as 'hh:mm:ss' and a signed byte for the millisecond interpreted as 'hh:mm:ss.-01'. We have sent an advisory to the manufacturer and are still waiting for the reply. Meanwhile, the missed time strings are filled with the time in between the previous and the next data point.

- *Position and Quaternion*: These variables are made up of float numbers determined by the pattern recognition process of the marker. The positions (x, y, z) represent the translation in millimetres, while rotations are represented by quaternions (qr, qx, qy, qz). [3] The function to convert the quaternion into the pose value will be described on page 3.3.3. It was developed for the previous work and improved in this thesis.

The name of the file is encoded and reports several information, among which the ID of the marker spotted as 'MXXX' (where 'XXX' could be '192', '193, '195', '206'). We switched on and off the computer during the swap of the subjects to create different log files.

Physlog

The instrument is a device included in the scanner, so the only trigger that it records on the log file is the Scanner trigger. The log file includes information about the peripheral pulse (PPU) and respiration (RESP) and the scanner trigger (mark). The Physlog doesn't record any time string. The gradient waveforms to are represented in Figure

[3] The use of quaternions is the method used to represent pose and rotation together in computer graphics. [4, 67]

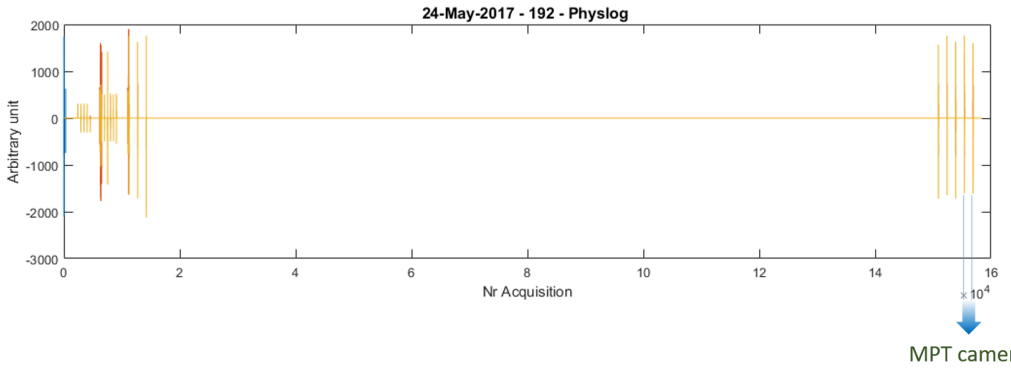

Figure 3.12: ***Physlog mark variable on its log File.*** *The plot represents the gradient of the 7 T scanner sent. The last two spikes correspond to the TTL signal also, that is detected by the MPT camera.*

3.12, the last two spikes correspond to the TTL pulse used to correlate the measurement with the MPT camera, they are the spikes visible also in Figure 3.11.

Physlog creates one file for each turn-on and turn-off of the tool. The name of the file is encoded and reports several process information, but we changed it to add the information to the CCH and MPT.

Description

Scan	MarkerID	Activity	NrAcquisitions	Physio
1	NaN	Calibration	NaN	0
2	NaN	Calibration	NaN	0
3	666	VibeMeasure	2000	0
4	193	Breathing	2000	1
5	193	Breathold	100	1
6	NaN	NaN	NaN	0
7	192	Breathing	2000	0
8	192	Breathold	100	0
9	195	Breathing	2000	0
10	195	Breathold	100	0

Figure 3.13: ***Scheme of the log file handwritten.*** *The scheme reported in the figure represents the double markers experiments done on June 19th. The name of the columns are the variables of the log file of each instrument, the last one is added to tag the scans where we measure the physiological parameters. The marker IDs on the description file are the markers of the subject, the marker stick on the bed was the always '206'. The calibration is done only at the beginning of the experiment because the field probes were stuck on the plastic rings. The scan number six failed.*

Before the beginning of the reading phase of the log file of the instruments, the files

are organized in different folders and renamed. In the past work the matching between the activity done and the scan was made by hand. The improvement of this thesis is doing the process automatically using a handwritten log file called *description*(Figure 3.13). This file summarizes the main information of the instruments and matches the measurements with the activity. The day of the measurement is defined in the program similarly to the string used on the CCH log file name: '24-May-2017' for the experiment of 24th May 2017 and '19-Jun-2017' for the experiment of 19th June 2017.

The first column (Scan) reports the numbers of the scans made by CCH during the experiment: the data aren't in all of that scan. The second column (MarkerID) has a double aim: the rows tagged with 'NaN' represent the scans that aren't good acquisitions (without the subjects inside the bore or the failed scans); the rows tagged with the numbers of the markers tell which subject is into the bore during the scan. The phantom's marker is the '192' as well, hence in that file it is represented as '666': that detail is corrected during the reading of description file. In case of double markers experiment, the marker on the bed is always the '206', hence it isn't written on the description file. The single and the double marker experiments are recognized by the day of the measurement. The third column is the sequence of the activity done: the tag 'Nan' means that the acquisition has failed. The first three columns are used to select automatically the $^*.field$ and $^*.calib$ files of CCH, the MPT log file and, after the time line up, to assign the activity to the data stream. The fourth column is used to double check the number of data points selected during the reading of the data stream. The last column is Boolean: it set to a value of one in case the physiological parameters are acquired.

3.3.2 Time line-up

To summarise the information given until now:

- The data stream in the log file of the instruments is different. The CCH produces one file for each scan (we match it with the activity), the other instruments record all the data streams, from the turn on to the turn off of the instruments, and in a single file we manually turn on and off between scans. We wrote an added log file to match the information of the instruments.

- The instruments use different sampling rates and these are not customizable or constant at all. Their values for the dataset of May 24th and June 19th are: $f_{CCH} = 1/TR = 10[Hz]$, $f_{MPT} \approx 80[Hz]$ and $f_{Phys}500[Hz]$;

- The CCH and the MPT camera record the time strings, but with two different standards, the AM/PM and the 24 hours standard respectively, and with different precisions, the second and the millisecond respectively. In the first case, the time

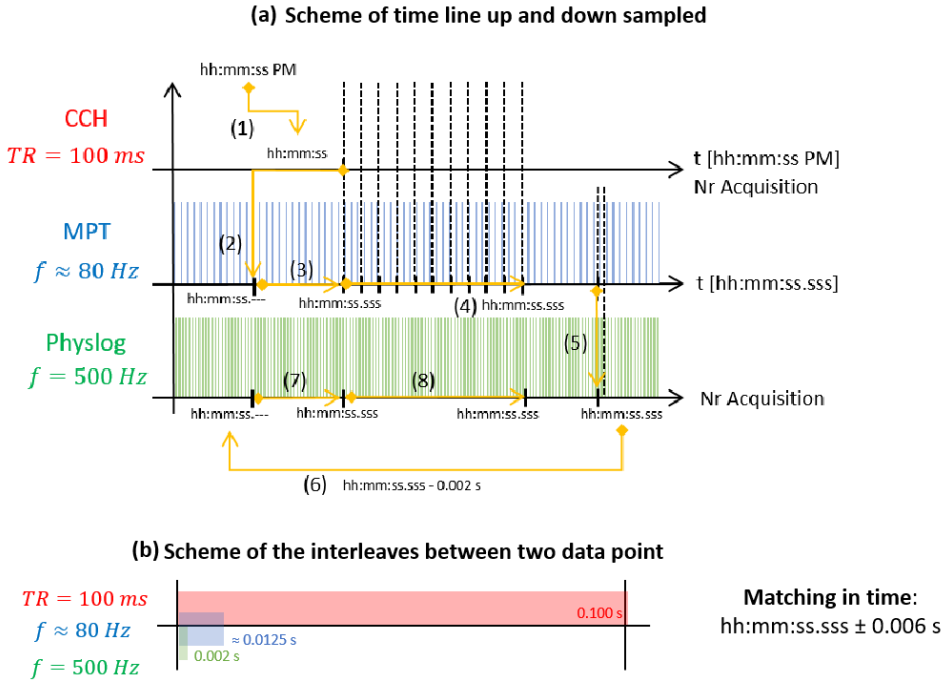

Figure 3.14: ***Scheme of the time line-up.*** *(a) The picture shows the TTL signal (black dashes lines) overlap with a representation of the sampling frequencies (continuous lines, except for CCH that corresponds to the black dashed line) of the instruments. The orange arrow indicates the pathway to match the stream data of the instruments. The idea is correlating the CCH and MPT data streams (arrows: 1, 2, 3, 4) and then the physiological data stream (5, 6, 7, 8, 9). (b) The scheme shows the relative duration (not in scale) of the times between two data points of the instruments (CCH in red, MPT in blue, Physlog in green). They are aligned in the scheme, but in reality the small ranges could be switched on the big ones. The errors committed in the alignment of the data stream is evaluated as half of the average time interval of MPT.*

string isn't written in the same file of the data, whereas in the second case it is. Physlog does not record any time string.

- The data streams of the instruments are connected by using the TTL signal, the scheme is reported in Figure 2.3, page 13. The CCH is connected with the MPT and the MPT is connected with the Physlog. The OR gate permits to have a clean TTL signal recorded into the variable interruptCount of the log file of MPT.

The automatic time line-up is a complicated process managed by the handwritten file description. The log files are imported in to MatLab program and the code to process the line-up is written in MatLab language. The process requires that the CCH and MPT computers times are synchronized at the beginning of the experiments. The scheme of the process is shown in Figure 3.14.b and it involves in eight steps:

1. **Time string conversion:** The first operation is to open the $*.txt$ file of CCH and find the time string that corresponds to the first valid scan. The time string is converted from the AM/PM format to the 24 hours format. If the CCH and MPT computers weren't synchronized at the beginning of the experiment, the time difference would be added in that step to shift to the time strings in the time frame of the MPT camera;

2. **Time string finding:** The second step reads the time string of the MPT and markers with an imaginary cursor the data that correspond to the string '(1)hh:mm:ss'. It isn't implicit that it corresponds to the first scan acquisition, hence the imaginary cursor is wound back by one second: 'hh:mm:ss.—';

3. **Beginning of the scan:** The beginning of the CCH scans is easy to find using the variable interruptCount. That variable increases by one unit each trigger, in the case of CCH. Hence, its increment is zero from the imaginary cursor to the first trigger (the first acquisition of the scan). The imaginary cursor is moved forward to find the first time strings of the acquisition '(3)hh:mm:ss.sss'.

4. **End of the scan:** The acquisitions of the scans ends when the interruptCount variable stops increasing. The ending time string is '(4)hh:mm:ss.sss'. The data stream of the MPT is extracted: the quaternions, scans, interrupt count and time string are saved. They are used during the down-sampled process (it will be described on page 60). The line-up between the CCH and MPT is concluded. The imaginary cursor is at the end of the scan in MPT log file.

5. **Scanner trigger finding:** The last issue is the line-up of the MPT and Physlog data streams. The way chosen to assign the time strings read on the MPT log file to the corresponding data point in Physlog file. To find that string, the imaginary cursor is moved forward until the next increment of the interruptCount variable is found;

6. **Time string definition:** The time string in the Physlog file is defined backwards, from the last time string found '(4)hh:mm:ss.sss' to the time string read on the CCH file ('(1)hh:mm:ss'). The reason is similar to the one explained in step two: the sampling frequency of the MPT and Physlog are different and the first isn't constant, so it isn't implicit that the calculated time string matches with the time string of the beginning of the acquisition ('(3)hh:mm:ss.sss');

7. **Beginning of the scan:** To find the beginning of the scan on the Physlog time string, the string defined are compared with the '(3)hh:mm:ss.sss': the comparison process stops when the time string is greater than the reference string. The compared process is repeated during the down-sampling process and in the next step.

8. **End of the scan:** The last data point is found in the comparison process. The data stream of Physlog is extracted: the PPU, RESP and the time string are saved.

The precision of the alignment is evaluated as the half of the time interval of the MPT camera $\pm 6ms$ (Figure 3.14.c). The reasons are the line-up process and that the instruments aren't synchronized.

An example of the line-up of the three datasets is shown in Figure 4.20 page 87. The plot shows the effect on the magnetic field variations due to the respiration and the related movements of the subject.

Down sample movements dataset.

The datasets extracted in the line-up process are not sampled at the same frequency, it is therefore necessary to down sample the dataset of the MPT and Physlog to obtain three datasets to compare. The process is best managed using the time string as is done in step 3 and 4 of the time line-up process.

The down sampled datasets of the MPT and Physlog contain the mean value of the data point in a definite interval around the trigger point. The reason is that the magnetic field value is measured in the first 5 ms after each trigger, the next value is taken after the TR time (on this thesis is 100 ms for each experiments). The data of the MPT camera and the Physlog during the remain 95 ms aren't correlated with the measurements of the magnetic field. On the other hand, the MPT average time interval between the data points is $\approx 12\,ms$, but the camera datasets are too noisy to take the instant value to represent the pose measured. Hence, the other reason for taking the average value is smoothing out the noise of the data. The interval taken for the MPT data is 4 data points ($\approx 48\,ms$): the data point that corresponds to the acquisition, one data point before and two data points after the trigger point. The Physlog dataset isn't extremely noisy and the time interval between the data points is $2\,ms$: the interval taken is 3 data points ($6\,ms$), the data point that corresponds to the acquisition and the subsequent two.

3.3.3 Frames issue

The CCH acquires the data of the magnetic field around the head, the changing of the magnetic field is related to the movements of the head that are measured by the MPT camera. The frames of the measurement are different, as it is shown in Figure 2.23 on page 33. The CCH acquires the data on the magnet frame, the MPT camera in camera frame. To use the MPT measurement it is necessary to convert the data from the camera frame to the magnet frame (or 7 T scanner, seen on page 33)). The MatLab function to do this ('cam2mag.m') was written in the previous work [1]. It uses dual quaternion algebra to compute the conversion and transform the quaternions into the corresponding

translation and rotation values. The improvement is in the way the missing values are handled (tagged by $status \neq 0$). Now, the function 'cam2magMean.m' filling the missing values taking the mean of the previous and the subsequent data points and gives the percentage of missing values of the dataset analysed.

Furthermore, the CCH and the MPT aren't integrated, hence also their frames aren't. We know that the pump of the magnet vibrates to generate the magnetic fields, in our set-up the CCH is integrated with the magnet bore. The CCH is integrated with the bed, but the bed isn't strictly jointed with the magnet bore to permit the roll out and in of the patient. We will check if the vibrations produce any effects on the measurements of the movements of the head with a background measurement (page 81).

Reference frame approximation

The MPT camera gives us the measurements of translation and rotation in the system of reference of the camera. The translations (x, y, z,) are given in millimetres and the rotations are coded in a quaternion (containing three-dimensional complex numbers q_r, q_x, q_y, q_z,). The function "cam2magMean.m" uses the MPT camera calibration (where it is available, otherwise it uses the identity dual quaternion matrix) to convert the measurement into the scanner's reference frame. We decided to call them T_x, T_y, T_z and R_x, R_y, R_z. Using the identity dual quaternion means to compute an approximation on the relative position of the reference frame. The scheme of the pose of the volunteer inside the magnet bore is shown in Figure 3.15. The scheme in the center represents the situation considered in this thesis, where we didn't compute the calibration before each measurement and we considered that the marker is rigidly coupled with the skull and represents perfectly the movements of the head referred to the isocenter of the magnet bore. That situation is computed considering the transformation matrix between the camera frame to the scanner frame as an identity dual quaternion. The consequences are that we can compare the measurements taken in different set-ups if we ignore the subsequent considerations. The set-up is defined by:

- The position of the camera inside the bore, that is fixed using dual-lock tape. The camera must be positioned and removed for each experiment and positioned by hand approximately in the same place. Furthermore, we consider that the systems of reference of the MPT camera and scanner are aligned (as you can see in Figure 2.23, page 33) but in reality they are not because this causes a reflection problem (page 32).

- The relative orientation between the marker and the camera could be the same for each acquisition.

- The position of the marker along the y axis of the MPT frame (z axis on scanner frame) depends on the translation of the bed, so of the volunteer, inside the bore.

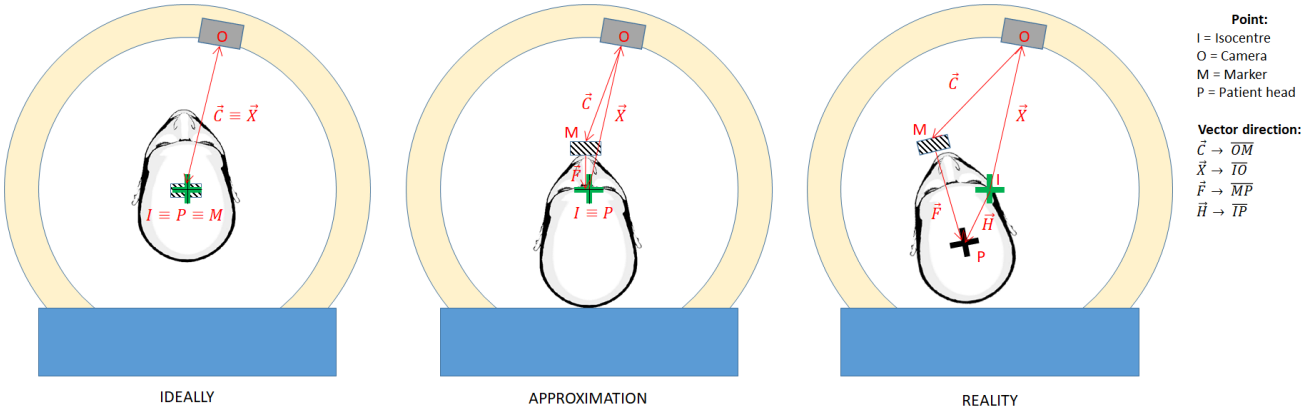

Figure 3.15: ***Approximation***. *This is a schematic representation of the position of the patient inside the magnet bore. Ideally, the marker directly represents the movements of the head which is at the isocentre of the bore. As you can see on the left figure, the point that represents the center of the head (P) and the center of the marker (M) are coincident with the isocentre of the magnet (I),or scanner frame, and the camera (O) measures directly the movements of the head. This situation can't be real for many obvious reasons, first of all that it is impossible to place and reveal an optical marker inside the head of the volunteer. The reality, figure on the right, is more complicated. The optical camera views the marker ($\vec{C}$) on the bite bar. The bite bar is fixed to the upper teeth of the volunteer, ideally rigidly coupled with the skull ($\vec{F}$) depending on the dental fit of the bite bar. The calibration process gives us the transformation to convert the measurement from the frame of MPT camera to the scanner frame ($\vec{X}$). For motion correction, it is necessary to know movements of the head relative to the isocenter of the magnet ($\vec{H}$). Until now, we consider the valid approximation, figure on the centre, due to the choice to not compute the calibration process before the measurement ($I \equiv P$) and to consider as rigid the coupling between the marker and the skull of the volunteer ($\vec{F} = const$).*

That position is managed by hand or fixed at the center of the length of the magnet bore.

- The position of the marker along the z axis of the MPT frame (y axis on scanner frame) depends on the dimension of the head of the patient: the bigger the head, the closer is the marker to the camera.

- The position of the marker along the x axis of the MPT frame (x axis on scanner frame) depends on the most comfortable position of the volunteer inside the coil, that is fixed on the bed.

The only way to bypass these experimental set-up problems is to consider not the absolute value of the measurement, but instead its variation.

An example of the conversion is in Figure 4.19 page 86.

Chapter 4

Analysis

To summarize the analyses presented so far, the anatomical part of the head that corresponds to the ring changes by the volunteer and the slice that corresponds to the second ring shows the major magnetic field changes and the respiratory frequency is a property of the volunteers. This could be one of the reasons why the model that will be developed in the future part of the project could be customized for each volunteer. The aim of the analysis of this thesis is the characterization of the signal of the CCH (Clip on Camera Head) field probes based on the actual set-up. The methodology used for the data analysis is PCA (Pricipal Component Analysis) validated by HCA (Hierarchical Cluster Analysis), they are described in section 4.1.

This is a preliminary analysis of the set-up that will be used in the fitting problems that concern the next part of the project in which this thesis is included. It is necessary to characterize the behaviour of the magnetic field probes to better describe the phenomenon.

We are interested in characterizing the changing in the magnetic field due to the movements of the head of the volunteer. The order of magnitude of the value of the magnetic field around the head is $\approx 10^{-5}\,T$. The changes on the magnetic fields are of the order of magnitude $10^{-8}\,T$ without the volunteers and $10^{-7}\,T$ with the volunteers. To visualize the changing, the datasets used for the plot shown in the analysis chapter are preprocessed to visualize the variations with respect to the first data point. The same process is done on the movements, the absolute value of the measurements depends on the definition of the reference frame. All the measurements, of the magnetic field and of the movements, are referred to the scanner frame. The instruments sampled the phenomenon at three different frequencies, but the analysis is referred to the magnetic fields measurement. Hence, the dataset of the MPT camera and the physiological measurement are down sampled, but the down sampled datasets are used only for the analysis that required a cross control of the phenomenon.

The analysis is divided in three parts:

1. **Preliminary Analysis.** The first part concerned the development of a protocol to

divide the field probes in clusters based on the measurements of May 24th 2017 (it is a single marker experiment). The methods used are the PCA (principal component analysis) and HCA (hierarchical cluster analysis) on series. The datasets utilized are the magnetic field changing of the activities "Pose 1 rep", "Pose 2" and "Pose 3" of the volunteer 1, M192. The only parameter of the phenomenon that changes is the relative position between the head and the probes. The data are shown in Figure 4.7, 4.8, 4.9 respectively. The number of acquisitions is 100 for each datasets, that corresponds to 10 seconds for the time repetition chosen ($TR = 100\,ms$). The magnetic field change is on the order of magnitude of $\pm 1.5 \times 10^{-}7\,T$. The plots of the movements are also present to allow the matching of the changing with the movements of the head, the data are down sampled. The range of the translations and rotations depend strictly on the activity, the maximum values are $\pm 1.2\,mm$ for the translations and $\pm 0.5°$ for the rotations, the errors are $\pm 0.1\,mm$ and $\pm 0.1°$ respectively.

2. **Background.** The second part concerned the test of the protocol on the measurements of the June 19th 2017 and the evaluation of the noise due to the vibration of the pump. Firstly, we are looking for a background cluster of the probes based on the measurement done with the phantom, subject M666, dataset "Vibe Measure" (Figure 4.14). The phantom doesn't move (as shown on the movements plot), therefore it doesn't produce changing in the magnetic field; the range is around $\pm 0.5 \times 10^{-}7\,T$. The last part concerns the characterization of the vibrations of the bed, that is the mobile part of the 7 T scanner, by the movements measurements. The experiment was a double marker experiment: the marker 206 was stick on the bed, up the the right shoulder of the subject. Unfortunately, the measurements are good only for three subjects out of four: "Vibe Measure" dataset of the phantom (M666), "Breathing" datasets of the volunteer 1 (M192) and the volunteer 2 (M193). The dataset length of the down sampled dataset is 2000 (number of acquisition of the CCH instrument), hence the length of the not down sampled dataset is ≈ 15000 data point for the MPT camera (in time $\approx 3\,min$): only the first 500 acquisitions are reported on Figure 4.17, the rotations measurement are reported for further informations, but their range are ten times less than the error of the instrument. The first 1000 data points of the not down sampled dataset are used for the Fourier analysis, the Figure 4.18 shows the low part of the spectrum, because they are enough to have a resolution frequency less than $0.1\,Hz$.

3. **Resting State.** The last part are the conclusive analysis. The datasets used are the resting state ("Breathing") of all the volunteers (Figure 4.19, 4.21, 4.23). The only parameter of the phenomenon that changes is the relative position between the head and the probes, due to the involuntary movements and the shape of the head. Those datasets are analysed with the protocol developed in the first part. To

explain the clusters obtained, we compare all the information that we have about the volunteer's head. The latest information is about the characteristic of the breathing movements, it is extrapolated from the PCA analysis of the movements of the head. The resting state analysis reveals a common cluster subdivision, in spite of the different anatomic characteristics and movements.

The clusters are visualized as the right Figure 2.16 (page 26) where only the probes of the cluster are filled. The ring visualized are the rings that contain the probes and they are called as explained in Figure 2.13.

4.1 Methodology

The methodology used are: Fourier Analysis (the relative algorithm is the Fast Fourier Transform, FFT), Principal Component Analysis (PCA) and Hierarchical Clustering Analysis (HCA).

4.1.1 Fourier Analysis

The *Fast Fourier Transform* (FFT) algorithm is used to compute the *Fourier analysis* of the signal. It converts the data from the original domain (usually time-domain or space-domain) to the frequency domain. This analysis reveals the frequency components of the signal. The main idea is that each signal is formed by sine wave components, each one with its own amplitude, frequency and phase. The goal of this analysis is to decompose the signal into its components to extract useful information from it. For example, the FFT and its inverse (*Inverse Fast Fourier Transform*) are used during the frequency encoding process (Figure 1.2, page 5) to obtain an MR image. In that case, the useful information are the phase and the magnitude of the NMR signal. In MRI these values are matched with spatial information to produce the images of the body. About the analysis of the signals, the Fourier analysis is widely used. For example, it is used to identify the frequency of the signal that corresponds to the noise and cleaning the signal in post processing.

Consider a time-domain signal $s(t)$. The frequency domain representation ($S(f)$) is the Fourier transform of $s(t)$:

$$S(f) = \int_{-\infty}^{+\infty} s(t) e^{-ift} dt \tag{4.1}$$

As usual, "acquiring a signal" means sampling a continuous-time signal into discrete-time signal $s(t)$. Hence, $S(f)$ is a discrete-frequency signal. $s(t)$ is characterized by the number of data point acquired (N) and the sampling rate (F_s). These characteristics

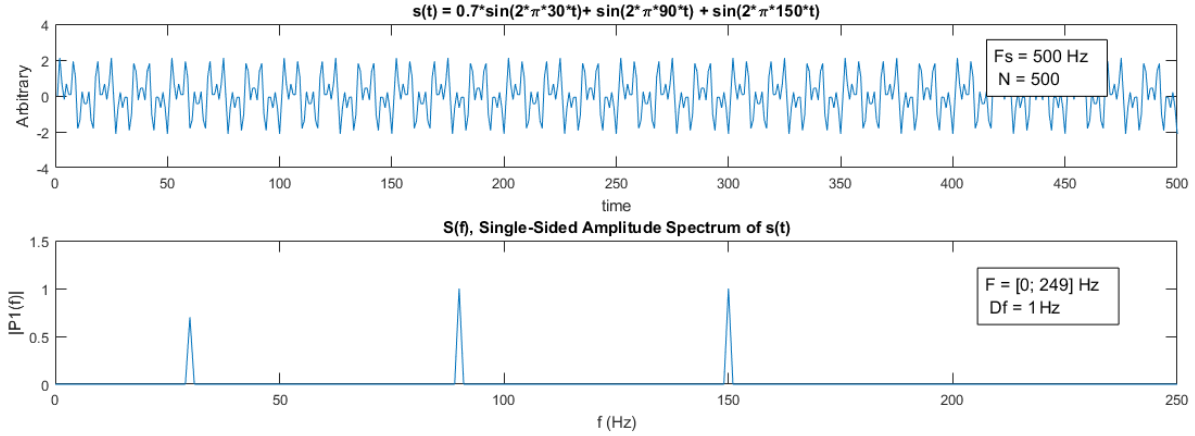

Figure 4.1: ***Simulation of Fourier Analysis****. The simulation represents a clean signal $s(t)$ composed on three sinusoidal components. The sampling rate of the signal is $F_s = 500\,Hz$ and the number of data point is $N = 500$. Also, the bandwidth and the frequency resolution of the spectrum are evaluated. The Fourier analysis of the signal returns the frequency of the components chosen to compose the signal.*

are dependent upon the *bandwidth* (or frequency range, $\mathbb{F}$) and the *frequency resolution* (Δf) of the $S(f)$, which are respectively:

$$\mathbb{F} = \left[0; \frac{F_s}{2} - \frac{F_s}{N}\right] \qquad \Delta f = \frac{F_s}{N} \tag{4.2}$$

In conclusion, the sampling frequency of the instrument and the number of data points are important to produce a high resolution in the Fourier analysis. A simulation of Fourier analysis is shown in Figure 4.1.

A real signal frequency spectrum is not clear as the simulation shows in Figure 4.1 because there are a lot of sources of noise. An example of a real signal analysed in this thesis is reported on page 50 (Figure 3.9). It is the Fourier analysis of the physiological parameters of one of the volunteers.

In this work, we use the Fourier Analysis method for various goals. For the physiological measurement (PPU, RESP), it gives us the frequency of the respiratory and the cardiac cycles of the subject. That frequency could be identify from the Fourier Analysis of the CCH probes because of the field changes produced by the respiration [1]. The movement dataset are analysed to characterize the breathing activity. We also measured the movements of the bed to look for its vibration during the measurement, which could be a source of noise.

4.1.2 Principal Component Analysis (PCA)

Principal component analysis (PCA) is a multivariate analysis [1] method widely used. The PCA reduces the dimensionality of the space that represent the data to highlight the similarity and organize the observations in to meaningful groups. The approach to reduce the dimensionality of the original space (or mapping the original space) is combining the features that describes the data to create a new sub set of features on lower-dimensional space called *Principal Component*. This approach is called *Features Extraction* and the new features must preserve the informations of the original features. The information preserved on PCA is the variance [2] of the dataset. The dimensionality reduction is the mapping of the original space into a lower dimension space: the transformation could be linear or not, PCA methods is based on linear transforms. If $\vec{x}$ are the features in the original space ($\mathbb{R}^N$), the $\vec{y}$ ($\mathbb{R}^M$, $M < N$) new features are given by: $\vec{y} = \mathbf{C}\vec{x}$, where $\mathbf{C}$ is the $M - by - N$ matrix of the coefficient of the transformation. The PCA uses the *covariance matrix* [3] ($\mathbf{\Sigma}$) as the matrix of the coefficient. The eigenvectors of the $\mathbf{\Sigma}$ are orthonormal vectors [4] that represent the *Principal Component* (or *loadings*): each original feature is represented as a linear combination of principal components, the orthonormal basis vectors of the lower-dimension space. The variances of the original features in to the lower-dimensional space are the eigenvalues of the $\mathbf{\Sigma}$. Hence, the first principal component is the most important because it describes most of the variance of the data. The others component are less important and they are orthogonal to the first.

In this work, PCA will help to characterize the signals from the magnetic field probes and the relationship of the directions (translations and rotations along x, y, z axis) of the movements recorded. In this section, the analysis of the directions is used to explain the general method.

The data analysed are a matrix of 6-by-100 data. The columns correspond to the features, translations ($T_x,\ T_y,\ T_z$) and rotations ($R_x,\ R_y,\ R_z$) around the axes and the rows correspond to the time series of the measurements. The Plot of the data and the results of the PCA are shown in Figure 4.2. The data are plotted on the "Movements" plot. The "Loadings" plot shows the values of the loading coefficient in the gray scale.

[1] **Multivariate Analysis**. Multivariate analysis is used to analyse observations that have more than one single statistical outcome variable.

[2] **Variance**. The variance of a dataset is a measurement of the spread of the data point respect their average value. For a continuous variable (X), it is defined as the square of the standard deviation (σ_x) of the variable: $Var(X) = \sigma_x^2$.

[3] **Covariance and Covariance Matrix**. The *Covariance* is defined as a measure of the correlation between two variables, $cov(X, Y) = E[X, Y] - E[X]E[Y]$, where $E[\star]$ is the *expectation value* (or mean) of the variable. Consider X is a vector, $X = [x_1, \ldots, x_N]$. The *Covariance Matrix* ($\mathbf{\Sigma}$) is a matrix whose the elements are the covariance between each element of the vector: $\mathbf{\Sigma}_{i,j;i\neq j} = cov(x_i, x_j) = E[(x_i - \mu_{x_i})(x_j - \mu_{x_j})]$, $\mathbf{\Sigma}_{i,j;i=j} = 1$, where $\mu_{\star_i} = E[\star_i]$ is the mean value of the element considered.

[4] **Orthonormal vectors.** Two vectors (p_i, p_j) are orthonormal if for $i \neq j$ their scalar product is $p_i^T \cdot p_j = 0$ and $p_i^T \cdot p_j = 1$ for $i = j$.

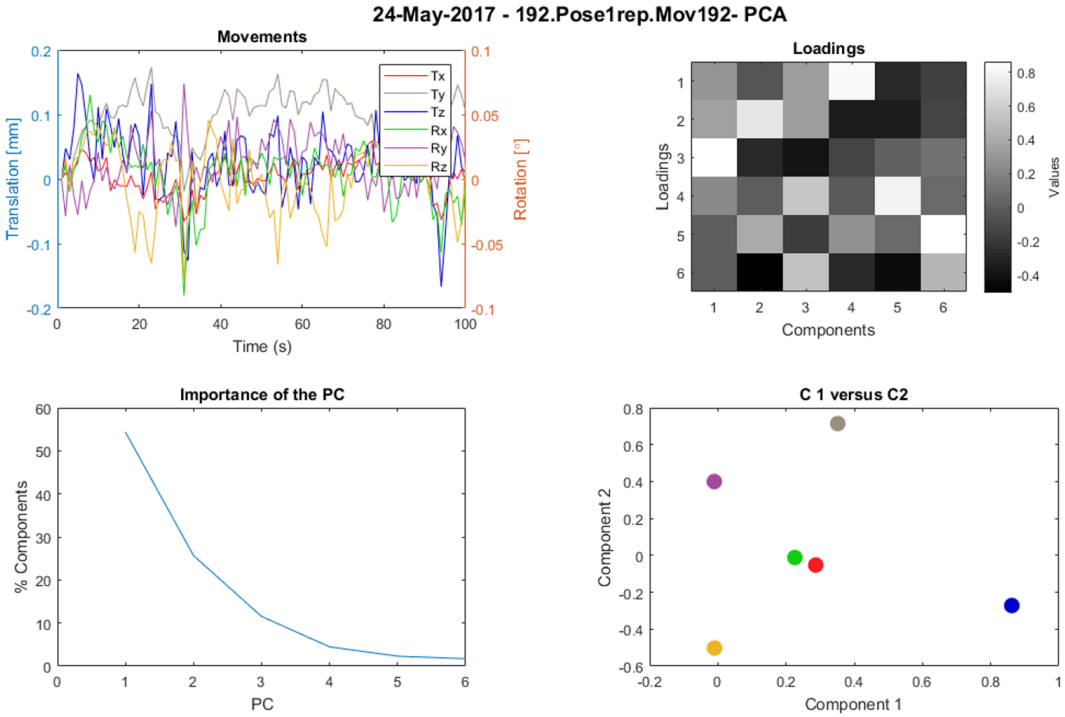

Figure 4.2: ***Example of PCA computes on the movements data.***

These coefficients represents the weight of each original feature that is used to obtain the principal components. The "Importance of PC" plot represent the percentage of the variance described by each principal component. It is clear that, in this case, the first and second components are sufficient: together, they describes more than the 90% of the variance. The most important are the first two components, so they are used in the "C 1 versus C 2" plot that represents one of the planes of the space formed by the principal component. In that plot, the position of the filled circle carry on the information about the correlation of the measurements that appears divided in clusters. For example, the rotation and translation around x axes are closely related, hence probably they are strongly correlated. Since it is a unsupervised clustering method, it is necessary validate the clustering with another method.

4.1.3 Hierarchical Clustering Analysis (HCA)

Hierarchical Clustering Analysis (HCA) is a methodology used to group similar data of a dataset in to a *cluster* (or groups). Our dataset is formed by the first two or three principal component of PCA, it depends on the analysis. The approach of the analysis could be "bottom up" or *agglomerative*, when it grouped the cluster formed by one single data point into a big cluster, or "top down" or *divisive*, when it splits a huge cluster formed by all the data in to a small cluster. The MatLab function used computes the agglomerative analysis: it starts with N singleton cluster, the features; the nearest pair of features are the first n-clusters ($n < N$), they are the most similar; the nearest clusters are agglomerate into k-clusters ($k < n < N$) and so on until one cluster is left ($1 < \cdots < k < n < N$). The issue is how defined the distance between two data point and between two clusters. First, we have to define the metric of the space. The choice of the *distance* defines the similarity between the data points: we use the *Euclidean distance*. [5]. The distance between two clusters is defined by the *linkage* function: we use the *Ward's method* [6] The dendrogram (Figure 4.3) is the plot used to represent

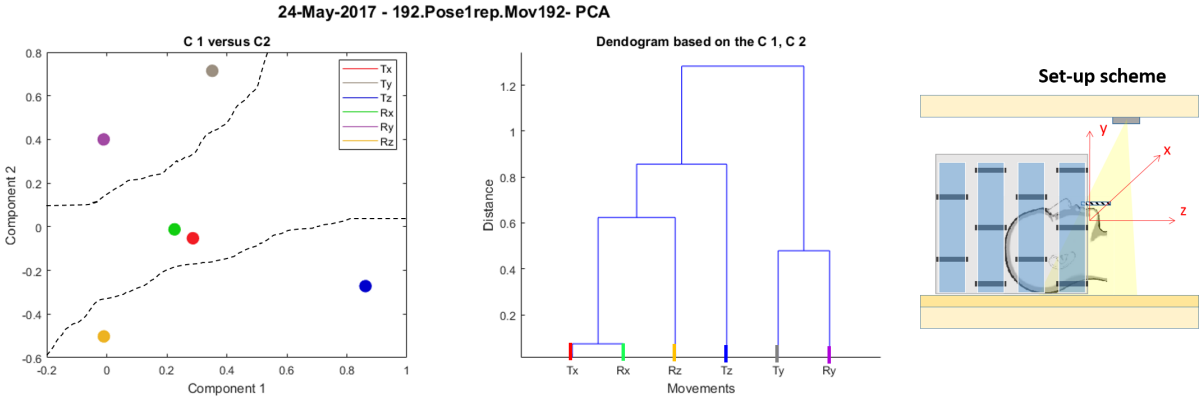

Figure 4.3: ***Example of dendrogram of the movements data compute with the first two compoment found by PCA analisys.*** *The set-up scheme shows the reference frame of that mesurements. The clusters emerged are highlighted drawing a dashes black line by hand.*

the results of HCA. Thus example is based on the results of the PCA analysis of the movement data described on the previous section. The dendrogram consist in a series of squared lines that connect the features, in this case the movements, in a hierarchical tree. They values represent the distance between the features, hence the height of the squared

[5] **Euclidean Distance**. The Euclidean distance is the length of the segment that connects two points ($\mathbf{a} = (a_1, a_2, a_3, \dots)$, $\mathbf{b} = (b_1, b_2, b_3), \dots$) in the Euclidean space. The distance is defined as: $d(\mathbf{a}, \mathbf{b}) = \sqrt{\sum_{i=1}^{2}(b_i - a_i)^2}$.

[6] **Ward's method**. The linkage function determines the distance between clusters. Ward's Method establish the criterion to link: two cluster are merged if the variance of the clusters decrease.

lines is the distance between the connected data points in the principal component space. The results of this analysis is quite obvious: translations and the rotations around the same axes are correlated. The dashed black line on the "C 1 vs C 2" plot are drawn by hand to show the clusters. The other result that emerge from the dendrogram is that the movements around the x and z axes are connected, the reason is the set-up configuration: the movements around the y axes aren't accessible movements during the MR scan. In this thesis the hierarchical clustering is used to validate the results of the principal component analysis.

4.2 Preliminary analysis

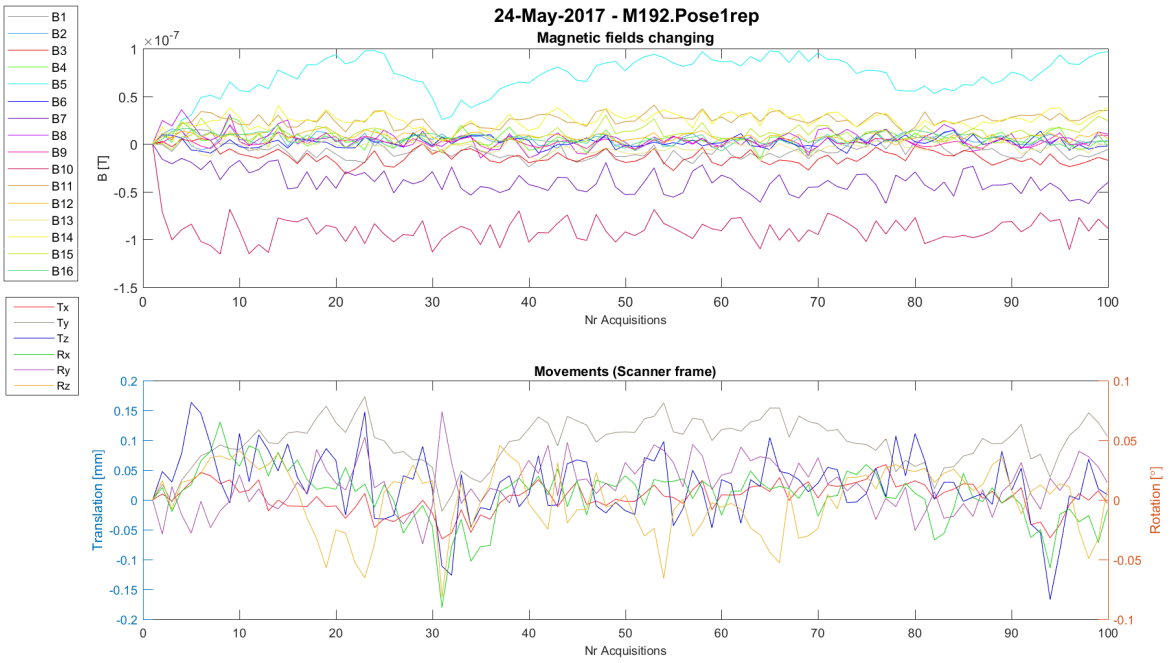

Figure 4.4: ***Pose 1 rep****. Magnetic field variation and movement measurements for the Volunteer 1 (M192) during the activity Pose 1 rep. The pose corresponds to the shake one position of the head on Figure 3.1 (page 40)*

During the experiment of 24th May, we noticed that the signal of the magnetic field probe B10 wasn't highly stable. Hence, we decided to analyse an activity set composed of the static activity. For this analysis, we have chosen the volunteer M192 because the head shape is quasi-spherical, really close to the phantom shape. The upper part of the head finish between the second and the third plastic rings. The signals of the magnetic field probes and the measurement of the MPT camera for the Volunteer 1 (M192) during

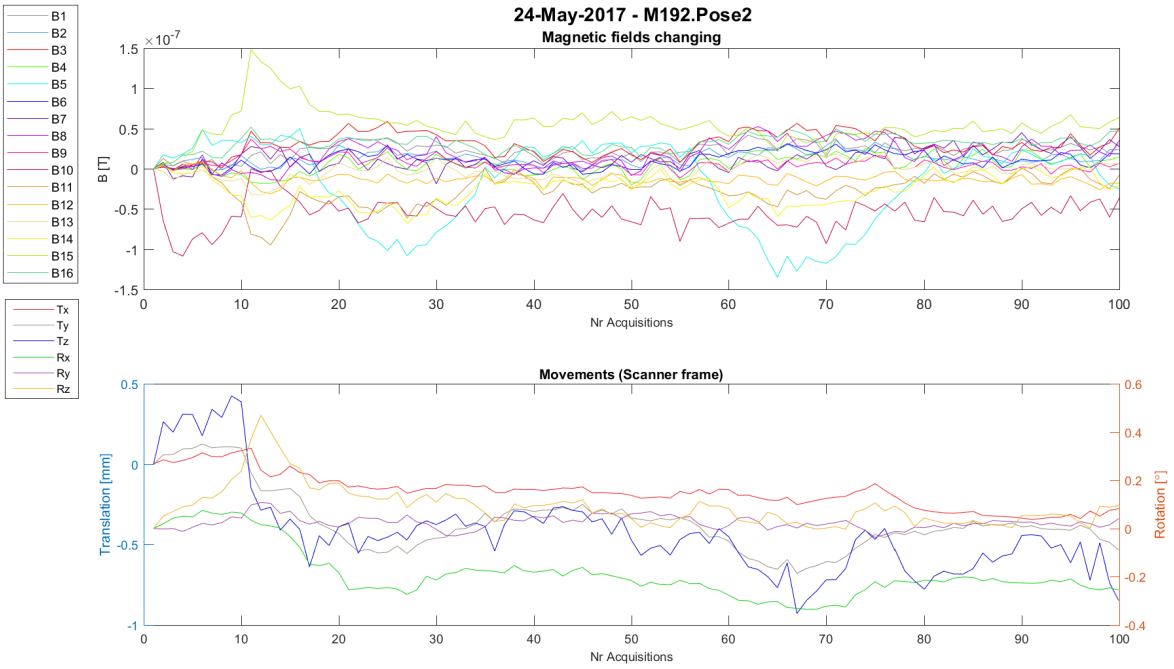

Figure 4.5: ***Pose 2.*** *Magnetic field variation and movement measurements for the Volunteer 1 (M192) during the activity Pose 2. The pose corresponds to the nod one position of the head on figure 3.1 (page 40)*

the activity Pose 1 rep, Pose 2, Pose 3 are respectively showing on Figure 4.4, 4.5, 4.6. The magnetic fields changes are referred to the scanner frame, the movements dataset is down sampled and it is referred to the MPT camera frame.

The plots of the changing magnetic fields lead to a couple of conclusion. First, the signal of the probe B10 on the plots of Pose 1 rep and Pose 3 is an outlier from the other signals, it isn't on the plot of Pose 2. Second, the signals of the probes follows the breathing and particulars the probe B5. We will check that hypothesis by principal component analysis (PCA) and with a hierarchical classification analysis (HCA).

The plots of the measurements of the movements are really noisy. For the Pose 1 rep, the movements that follow the respiration are the translation along the x axis and the rotation around the x axes. For the Pose 2 and 3, we know that the marker is tilted respect to the CLU camera, so it maybe the movements in that positions are not well characterized in the scanner reference frame.

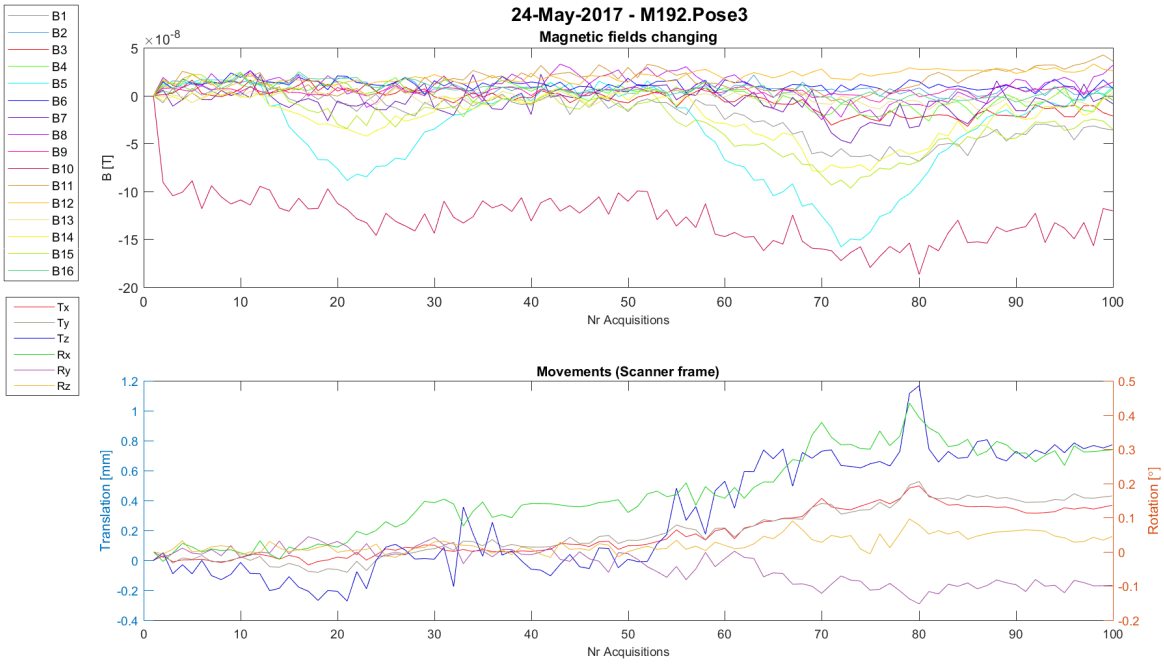

Figure 4.6: ***Pose 3.*** *Magnetic field variation and movement measurements for the Volunteer 1 (M192) during the activity Pose 3. The pose corresponds to the nod five position of the head on Figure 3.1 (page 40)*

4.2.1 Protocol of analysis I

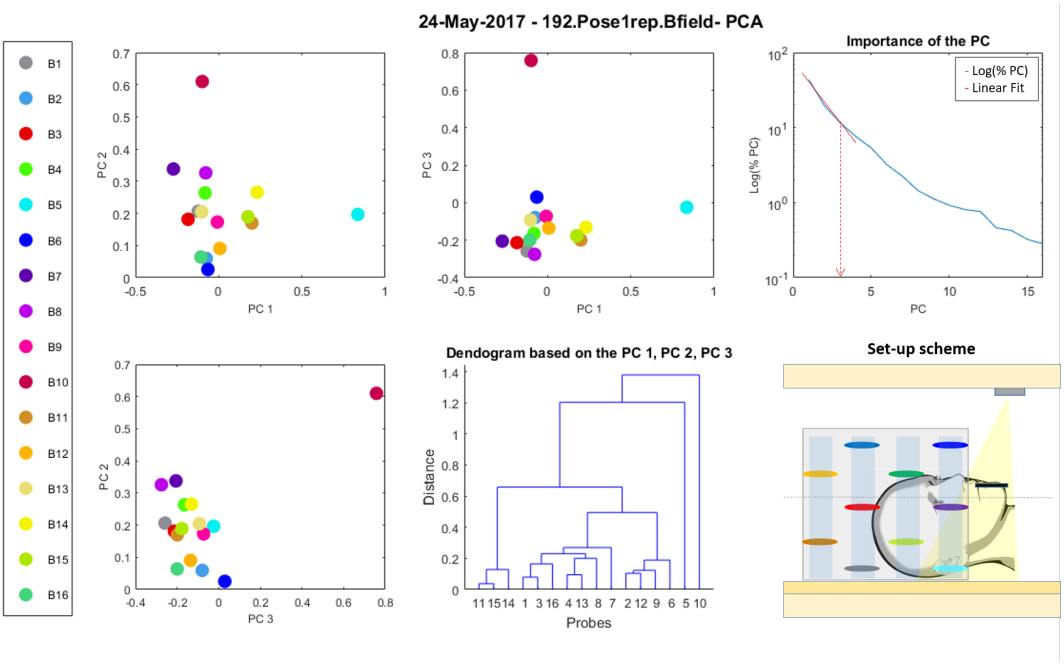

Figure 4.7: ***Pose 1 rep.*** *Principal Component Analysis of the fields probes for the Volunteer 1 (M192) during the activity Pose 1 rep. The pose corresponds to the shake one position of the head on Figure 3.1 (page 40).*

The PCA analysis of the signals from the magnetic field probes for the volunteer M192 during the activity Pose 1 rep, Pose 2, Pose 3 are shown on Figure 4.7, 4.8 and 4.9. Each figure is divided into 3 parts. The first concerns the principal component (PC): three plots show the first three principal components combined to visualize the groups of the probes that shows a similar behaviour and the last plot shows the percentage of the importance of the principal components. This plot is used to establish how many PC are considered for the hierarchical classification. The linear fit (red line) ends at the beginning of the dashed red line that indicates the number of PC chosen. The second part of the Figure is the dendrogram that subdivides clearly the groups of the probes and it is based on the first three PC. The last part is a schematic picture of the set-up that shows the position of the head were respect to the instruments. The hypothesis about the probes B10 and B5 identified from the Figure 4.4, 4.5, 4.6 (from page 70) is confirmed by the PCA analysis. The probe B10 on the plots of Pose 1 rep and Pose 3 is an outlier from the other probes, it isn't on the plot of Pose 2. That is shown clearly on the plot of the PC 2 versus PC 3 on the Figure 4.9. Also the probe B5 is an outlier, but the reason is that the signals of that probes follows the breathing better than the other, as is shown on Figure 4.4, 4.5, 4.6.

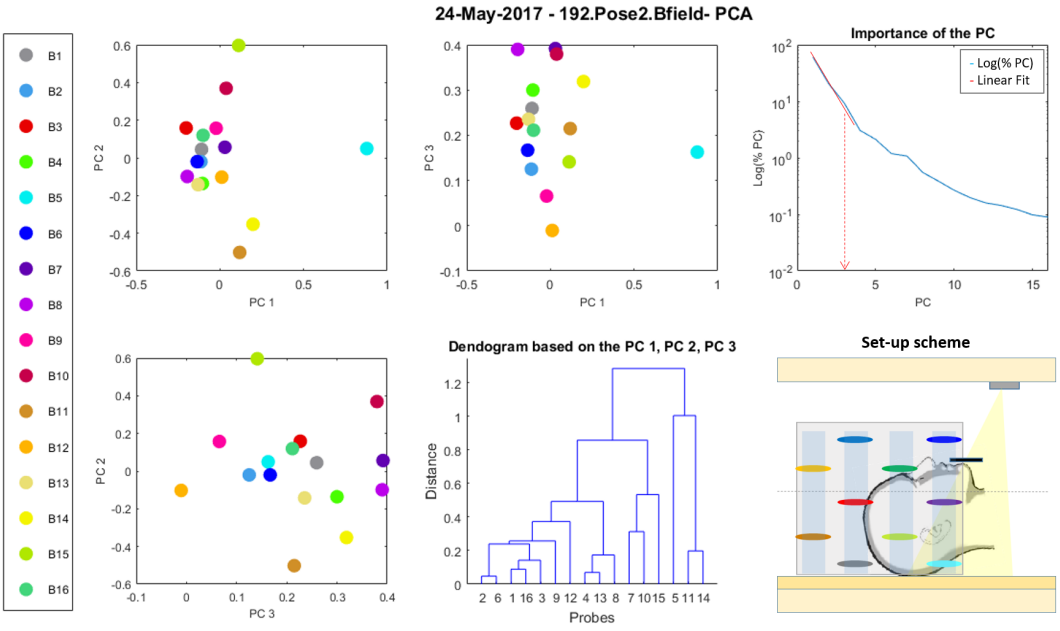

Figure 4.8: ***Pose 2****. Principal Component Analysis of the signals of the fields probes for the Volunteer 1 (M192) during the activity Pose 2. The pose corresponds to the nod one position of the head on Figure 3.1 (page 40).*

The dendrograms obtained for the activities are different, but, in general, they describe well the plot obtained by the PC 1 versus PC 3. The probes included in the same cluster have a similar positions in the ring. To visualize better the clusters, the PCA is computed again without the probes B5 and B10 to remove its variance on the data set.

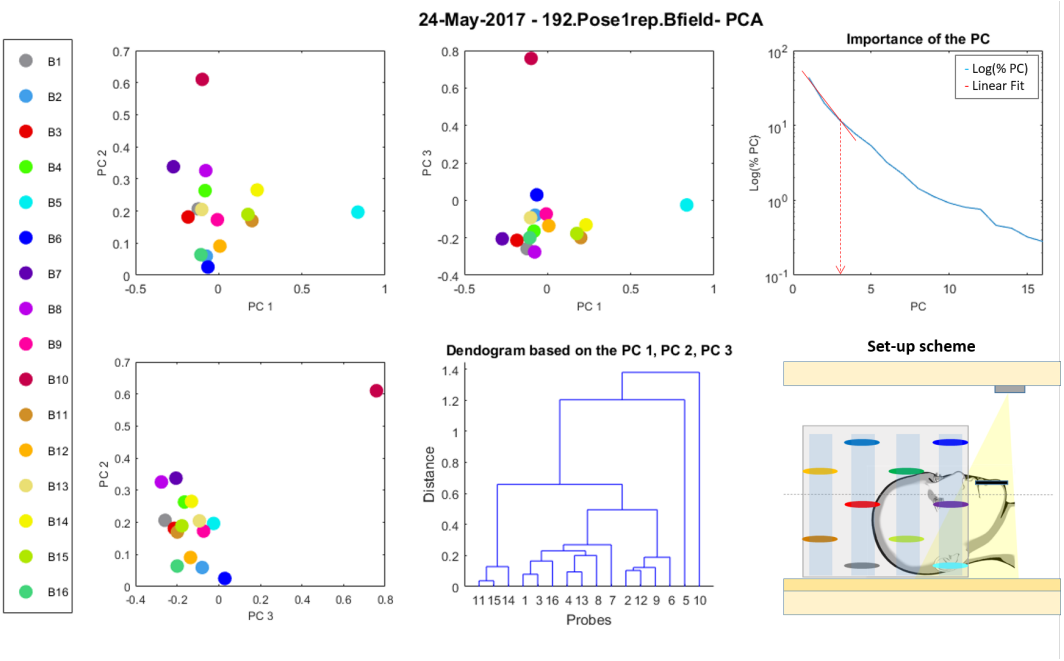

Figure 4.9: ***Pose 3****. Principal Component Analisis of the signals of the fields probes for the Volunteer 1 (M192) during the activity Pose 3. The pose corresponds to the nod five position of the head on Figure 3.1 (page 40).*

4.2.2 Protocol of analysis II

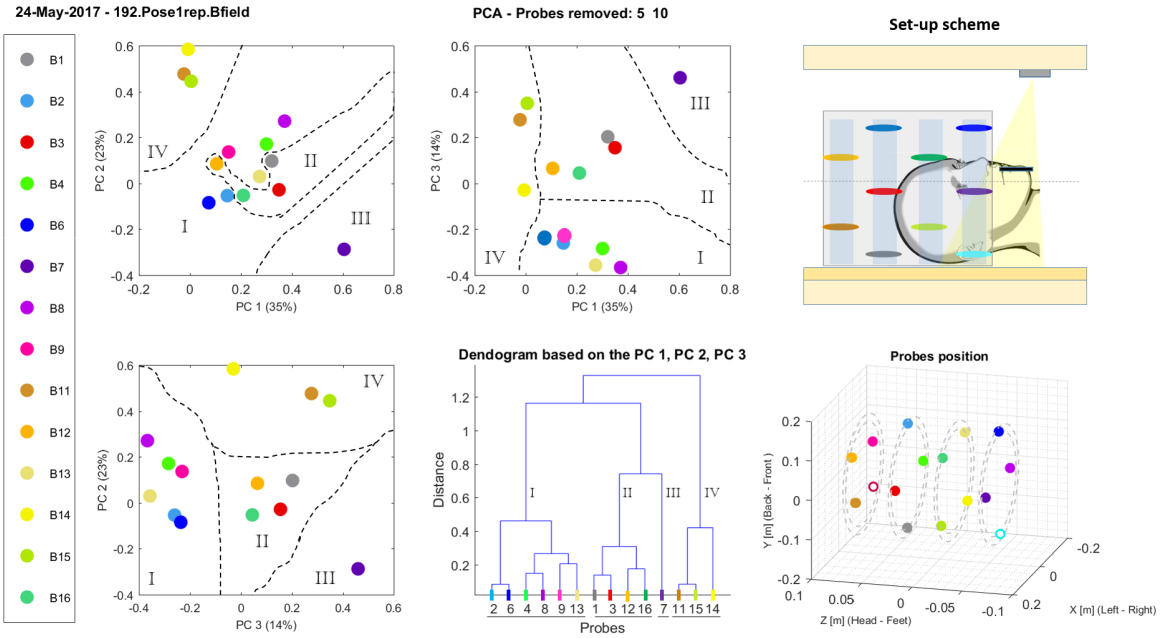

Figure 4.10: ***Principal Component Analysis of the signals of the field probes signal for the volunteer M192 during the activity Pose 1 rep, without the signal of the probes B5 and B10.*** *The clusters (I, II, III, IV) emerged are highlighted drawing a dashes black line by hand.*

The PCA analysis of the signals of the magnetic fields probes without the data of the probes B5 and B10, for the volunteer M192, during the activity Pose 1 rep, Pose 2, Pose 3 are shown on Figures 4.10, 4.11, 4.12 respectively. The figures are divided in 3 parts. The first shows the principal component (PC): three plots show the first three principal components combined to visualize the groups of the probes that shows similar behaviour. The dashed lines are drawn by hand to visualize the groups. The second part of the figure is the dendrogram, it is based on the first three PC and it subdivides clearly the groups of the probes. The Latin numbers and the line under the Arabic number are added on the dendrogram to tag the groups. The last part is a schematic picture of the set-up that shows the position of the head respect to the instruments and the 3D view of the position of the probes, the excluded probes (B5 and B10) appear white. The results are summarized in table 4.1. The clusters found for the different activities are similar: there are several probes that appear in the same groups for all the activities. They comprise a fixed subset of probes that could be customised for each volunteer, thus we will verify this usual on the next analysis. The probes excluded from the subset could be inherent to with the type of activity.

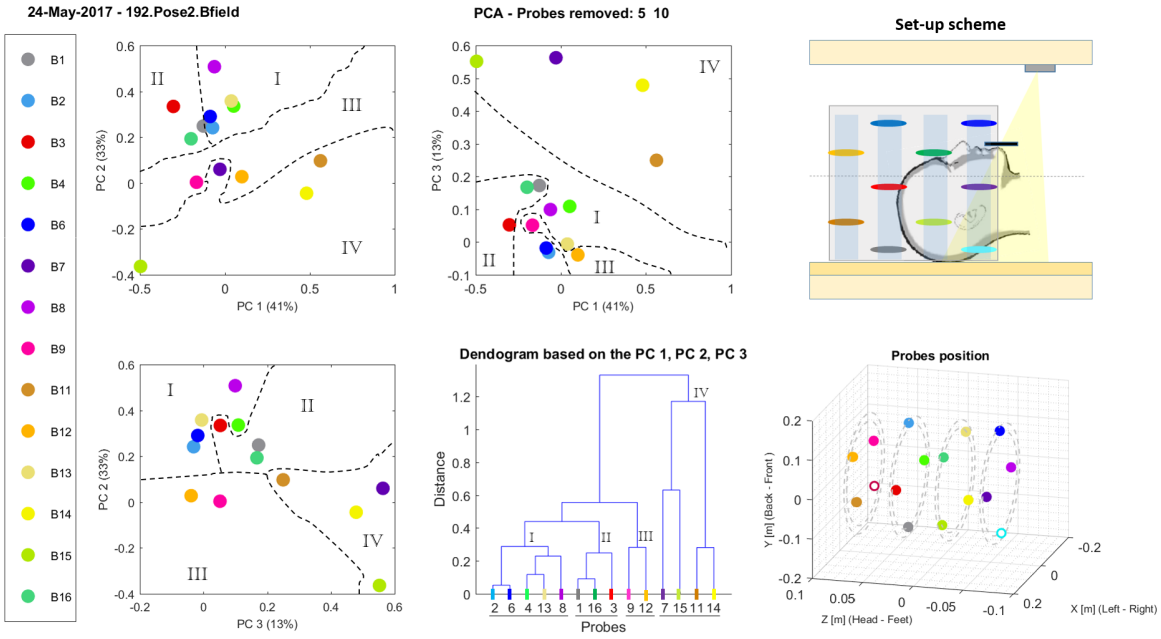

Figure 4.11: ***Principal Component Analysis of the signals of the field probes signal for the volunteer M192 during the activity Pose 2, without the signal of the probes B5 and B10.*** *The clusters (I, II, III, IV) emerged are highlighted drawing a dashes black line by hand.*

	Cluster I	Cluster II	Cluster III	Cluster IV	Excluded
Pose 1 rep	2, 4, 6, 8, 9, 13	1, 3, 12, 16	7	11, 14, 15	5, 10
Pose 2	2, 4, 6, 8, 9, 13	1, 3, 7, 12, 16	7	11, 15, 14	5, 10
Pose 3	2, 4, 6, 9 ,13	1, 3, 16	7, 11, 12, 15	8, 14	5, 10

Table 4.1: ***Results.*** *Groups emerged from the PCA of the signal from the fields probes for the volunteer M192 during the activity Pose 1 rep, Pose 2, Pose 3, without the signal of the probes B5 and B10.*

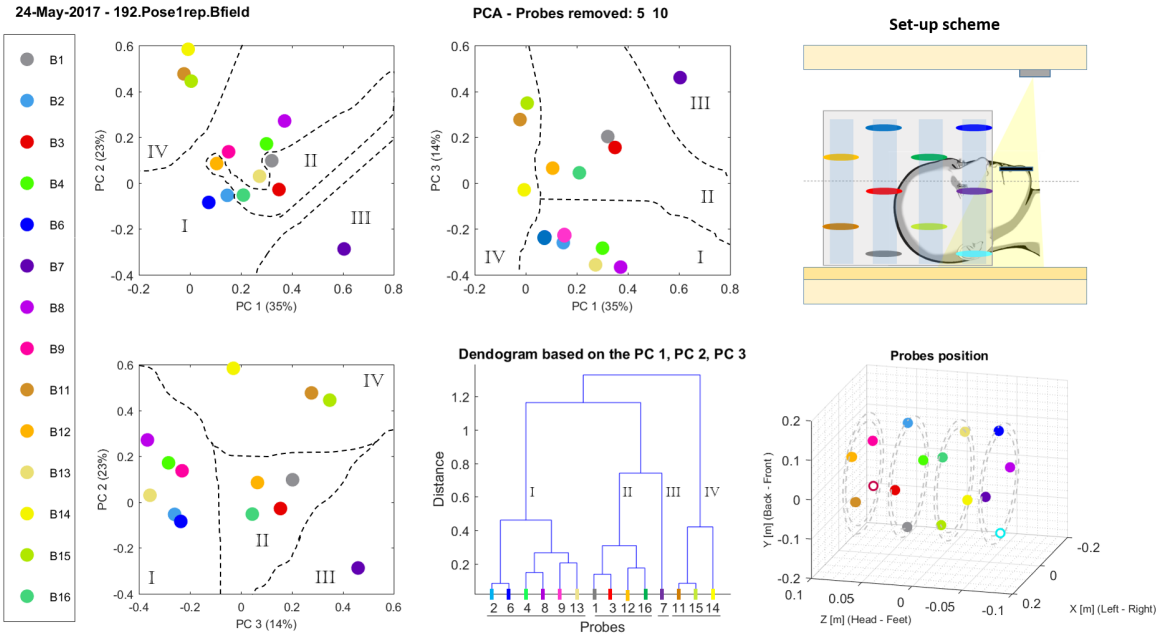

Figure 4.12: ***Principal Component Analisis of the signals of field probes signal for the volunteer M192 during the activity Pose 3, without the signal of the probes B5 and B10.*** *The clusters (I, II, III, IV) emerged are highlighted drawing a dashes black line by hand.*

4.2.3 Results

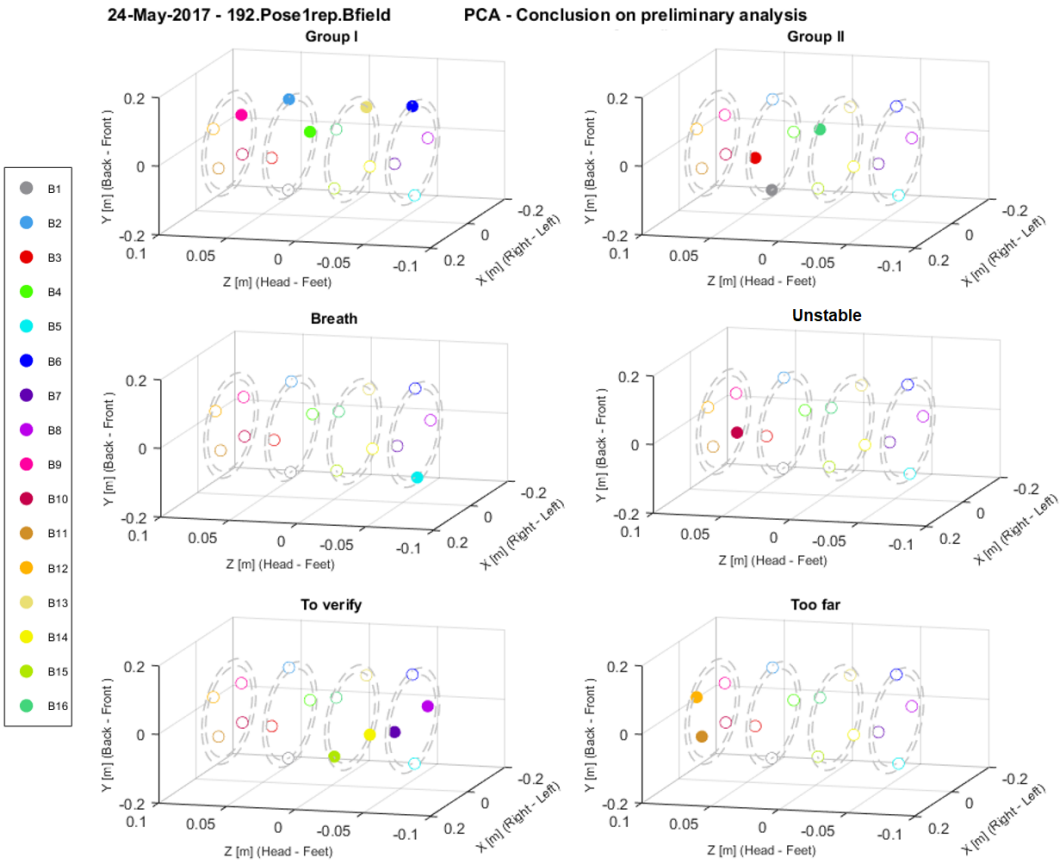

Figure 4.13: ***Classification of the probes based on the data of the static activity of the volunteer M192 during the experiment of the 24th May 2017.*** *The groups are based on the cluster that emerged from consecutive PCA and HCA analysis did on the magnetic fields changing datasets.*

The Figure 4.13 helps us to understand if the subset of the cluster is inherent with the position of the probes around the head. The order of the rings is from neck to the top part of the head, in that plot from right to left along z axes (tagged "Head - Feet" axes), the protection ring is excluded from the scheme. There are six plots that summarize the conclusions emerging from both the PCA analysis. All the probes are drawn on each plot, but only the probes that represent the groups (Groups I, II, III, IV) are represented by a filled circle.

The groups I, "Unstable" and 'Too far" are formed by the probes on the top part and on the last rings. The head of that volunteer is small and the probes aren't close enough to measure the magnetic field changing during the activities. The Group III, "Breath" and "To verify" represent the bottom part of the rings and are divided in front-bottom

part (group "Breath and "To verify") and the center-bottom part. The probes are the probes closer to the head on each activities. The division between center and front part could be due to the movements made during the respiration.

In conclusion, the groups match with the position of the probes around the head and the activity did.

4.3 Background

The background is measured only for the experiment of 19th of June. It consists on the measure of a magnetic field change without the volunteers present, but with the phantom. It consist also on the measure of the vibration of the bed, because it isn't strictly joint with the magnet bore (the description of the reference frame is on page 33): it can't rotate in any direction, but it can translate because the system that permits its movements isn't strictly integrate to the magnet bore. It is possible that the vibrations of the pump of the magnet influences the movements of the bed, hence the measure of the movements.

4.3.1 Magnetic field variations

The measurements of the changing magnetic field and the movements for the phantom is on Figure 4.14. The plot shows clearly that the phantom, that was covered with small pillows to integrate it with the plastic ring, doesn't move. Hence, the magnetic field change is smaller than the change observed for the previous analysis. However, there are two probes, the B7 and the B10 again, that show got a singular behaviour.

With the PCA we checked if that behaviour will compromise the measurement. The result is reported on Figure 4.15. It shows that only the probe B7 is an outlier for that experiment, hence that probe will be excluded from the next PCA and it will be considered as a cluster. Also the probes B2 and B6 seem to be separate to the other, but the distance (evaluated on the dendrogram) is half than distance of probes B7: they won't be excluded.

The results of the PCA analysis without the probe B7 is on Figure 4.16. The probes are divided on three groups, the fourth is constituted of probe B7 only. The probes B6 is alone on the Group III. The Groups I and II represent the bottom and the top part of the ring respectively. That division on group will be consider as a background division of the probes. The range of the varying magnetic fields is really small ($10^{-8}T$) and probably won't influence the measure with the volunteers.

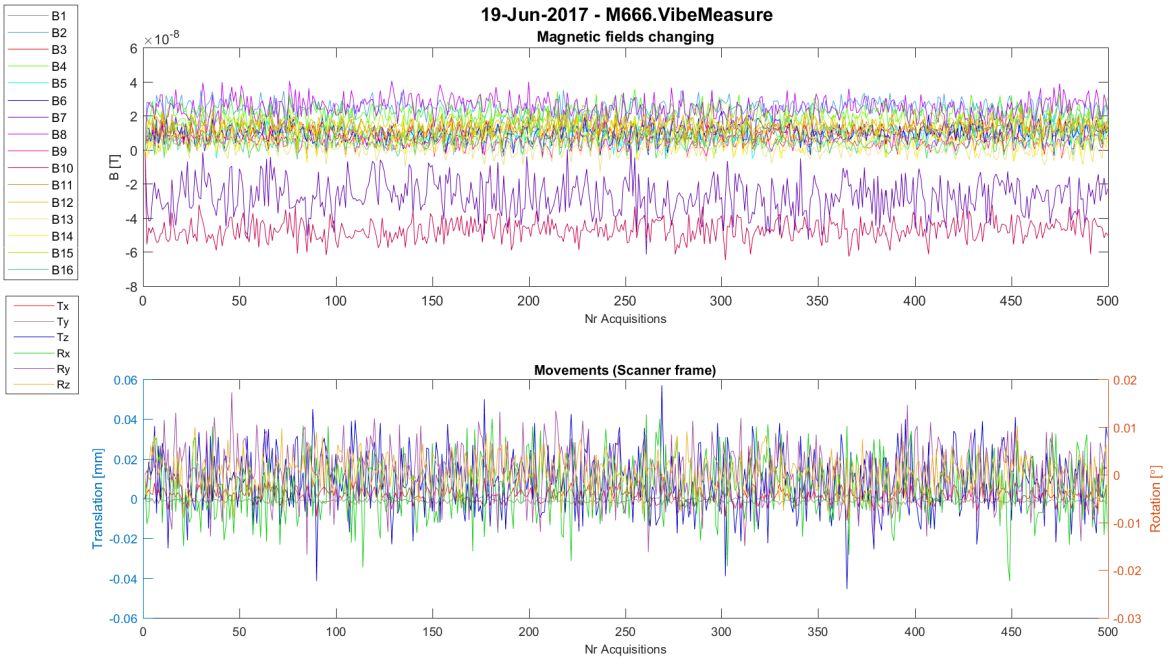

Figure 4.14: ***Magnetic fields changing and movements for M666 (phantom).*** *Only the first 500 acquisitions are plotted. The range of the changing magnetic field ($\pm 6 \times 10^{-8}\,T$) is consistent whit the stability of the magnetic field generated to the scanner (order of magnitude of $10^{-6}\,T$). The range of the movements is less than the error of the MPT (± 0.1 $[mm]$ and ± 0.1 $[°]$), in fact we know that it doesn't move. Hence, the magnetic field changes is small.*

4.3.2 Movements of the bed

The second background measurement to evaluate is the vibration of the bed. The measurements of the movements of the marker 206, fixed on the bed, for the subject M666 (phantom), M192 (volunteer 1) and M193 (volunteer 2) are on Figure 4.17. As we expected, the bed didn't rotate in the magnet bore during the experiment: the values are are 10 times less than the error of the instruments (evaluated as $\pm 0.1\,°$). Instead, we expected that the bed translations are less when the volunteer on, but the plots show the opposite results. However, the range of the translations on both plot is comparable with the error of the instruments (evaluated as $\pm 0.1\,mm$), also that values aren't significant and it means that the bed didn't vibe a lot. To evaluate which directions could be the more influenced of the vibration of the bed, the data are analysed with the FFT (Figure 4.18). The frequency used to compute the analysis is the one set on the MPT ($80\,Hz$) considered as the average value of the sampling rate of the instruments. As we expected, the translation along the direction of the movements of the bed (T_z) is the one that has the highest frequency spectrum. There is also a small peak, for each movements, at

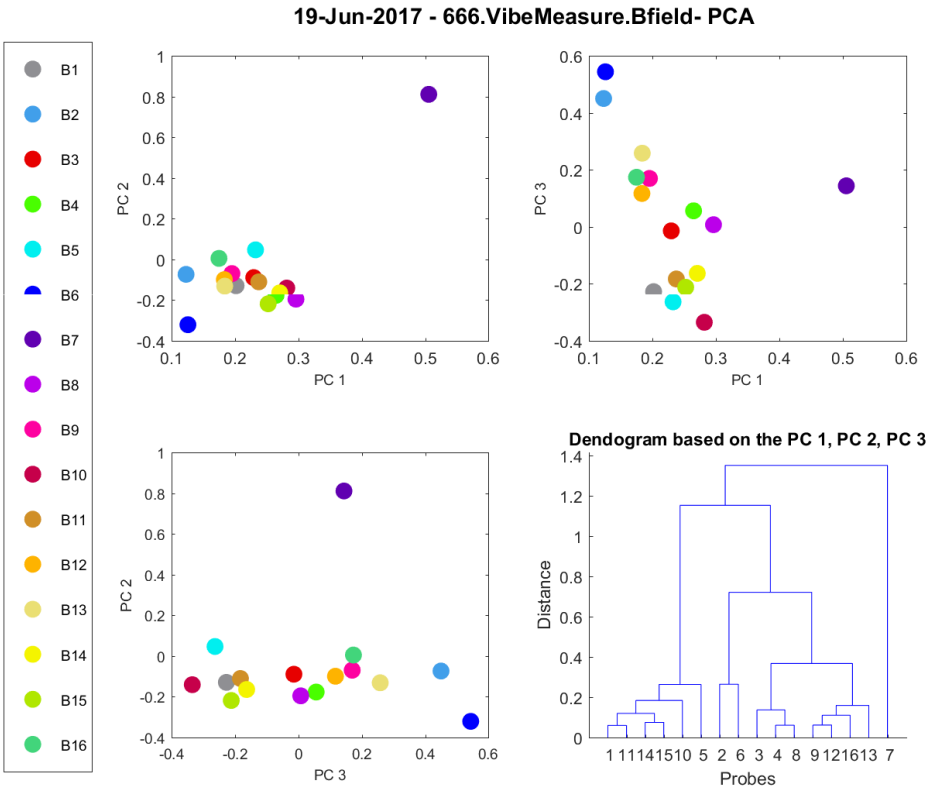

Figure 4.15: ***Classification of the probes for M666 (phantom).*** *The groups are based on the cluster that emerged from consecutive PCA and HCA analysis.*

the frequency that correspond to the frequency of the cooling pump that generates the magnetic fields (approximately 2 Hz).

In conclusion, the coupling with the bed and the magnet bore could slightly influence the measurement on the movements values. That conclusion is based on two volunteers out of three.

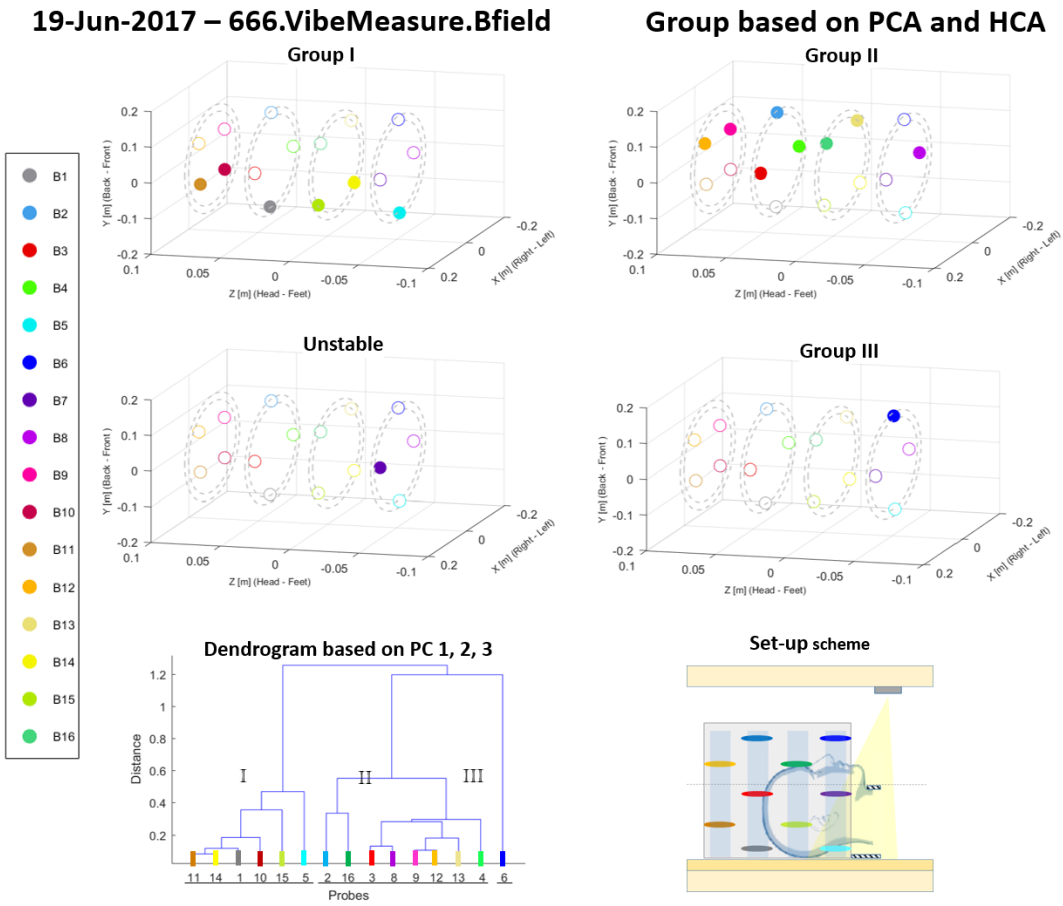

Figure 4.16: ***Classification of the probes for M666 (phantom).*** *The groups are based on the cluster that emerged from consecutive PCA and HCA analysiswithout the probe B7. The "Unstable" reports the resutls of the first analysis: B7 shows a different behaviour to the other.*

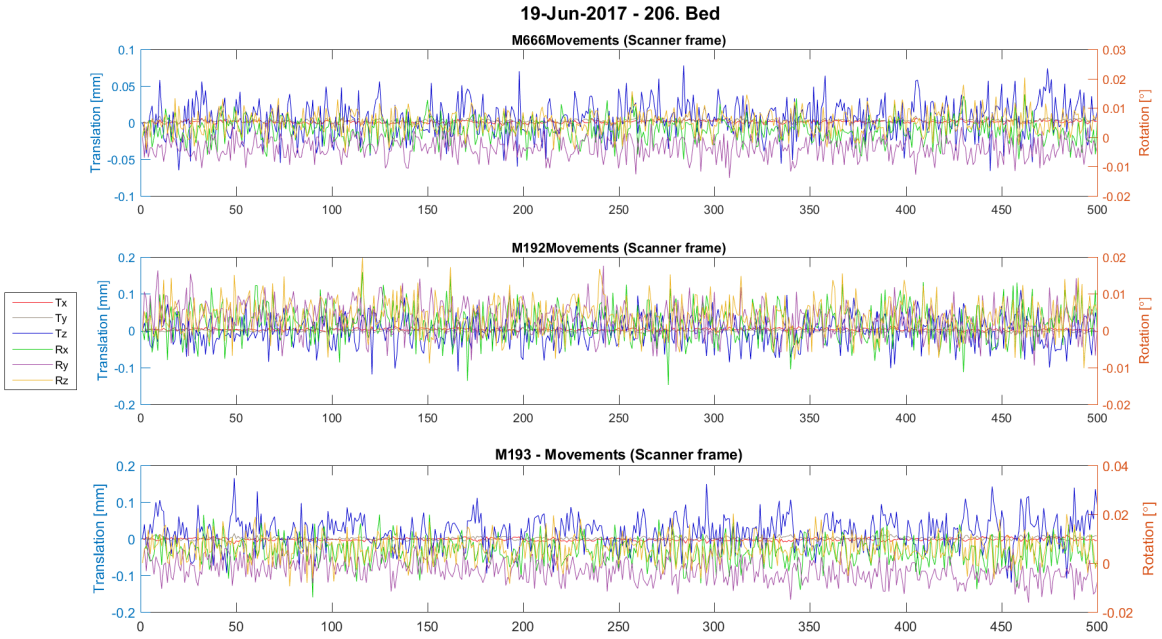

Figure 4.17: ***Movements of the bed during the experiment of 19th June.*** *The dataset used isn't down sampled and is transformed to the scanner frame with the approximations described. The plot shows the movements of the bed during Vibe Measure activity for the subject M666 (phantom), during the breathing activity for the subject M192 (volunteer 1) and for the subject M193 (volunteer 2) respectively.*

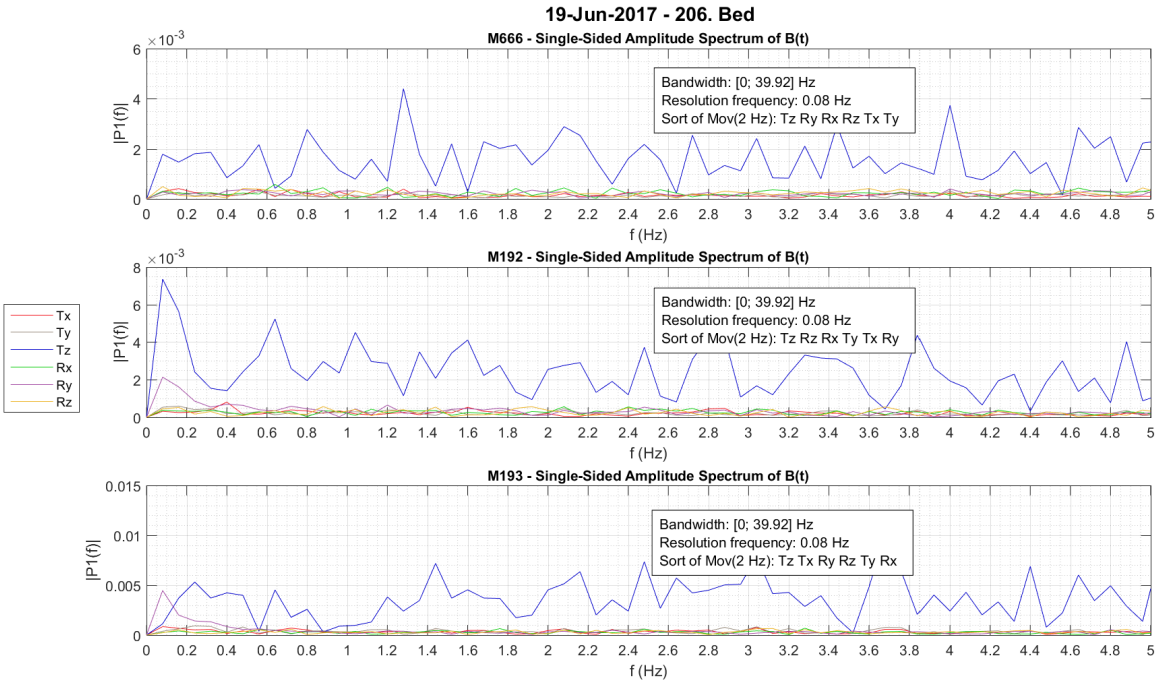

Figure 4.18: ***Fourier Analysis of the signal on Figure 4.17.*** *Only the first part of the spectrum is plotted. The bandwidth and the resolution frequency are evaluated. The various movements are sorted in descendent order according to their amplitude in the Fourier spectrum evaluated at frequency of the cooling pump that generate the magnetic fields.*

4.4 Resting state

During the MRI scanning, the patient rest in the scanner. The Breathing dataset represents the resting state situation. Understanding the behaviour of the probes during that activity could be crucial for the future step of the project, finding a function that fits the magnetic fields changing and the movements of the head.

The sequences of the analysis done on section 4.2 works and define a protocol. Hence, we will follow the same protocol to analyse the Breathing dataset and it will be report only the the dendrogram and the graphic representation of the groups. The analysis excludes the probe B7 as a conclusion of the background measurement.

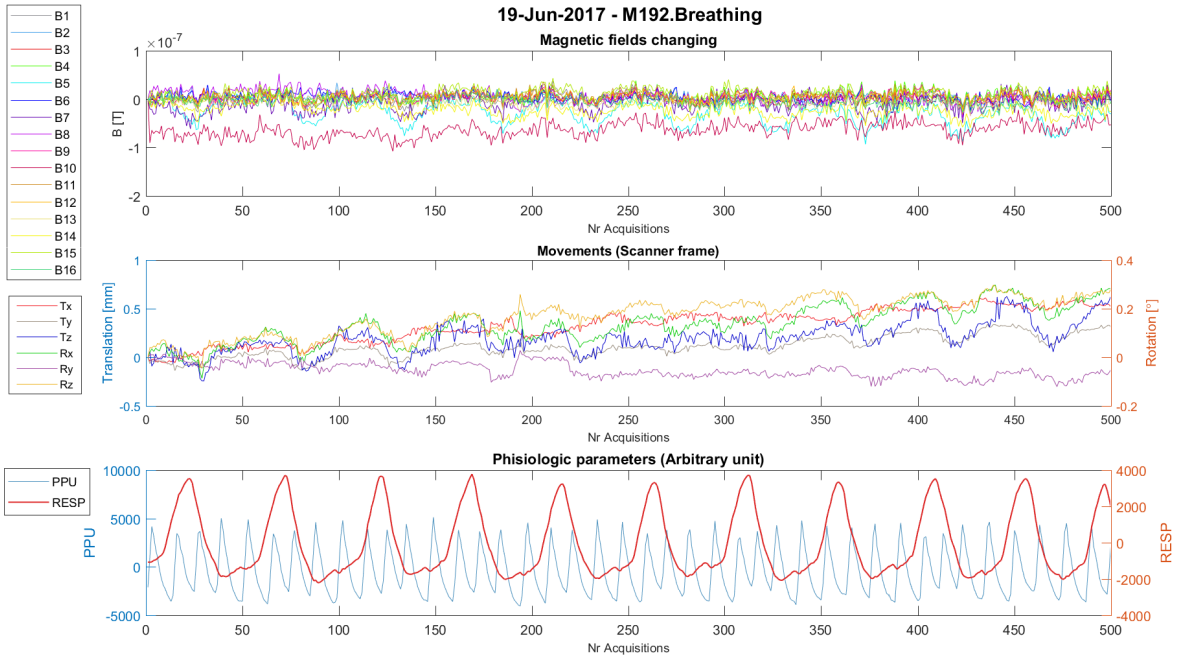

Figure 4.19: ***Magnetic fields changing, movements measurements and physiological parameters for the volunteer M192 during the resting state (Breathing).*** *Only the first 500 acquisitions are plotted.*

Volunteer 1 (M192). The measurements of the changing magnetic field, the movements and the physiological parameters for the volunteer M192 (volunteer 1) are on Figure 4.19. The plot shows clearly the correlation between the respiration and the changes of the magnetic field, the changes are ten times the changes of the background measurement. Also the movements follow the same behaviour and the general trend is upward. The rotation values are small, the maximum relative error is

$\approx 0.1°/0.4° = 25\%$. The translations values are small as well, the maximum relative error is $\approx 0.1\,mm/1\,mm = 10\%$.

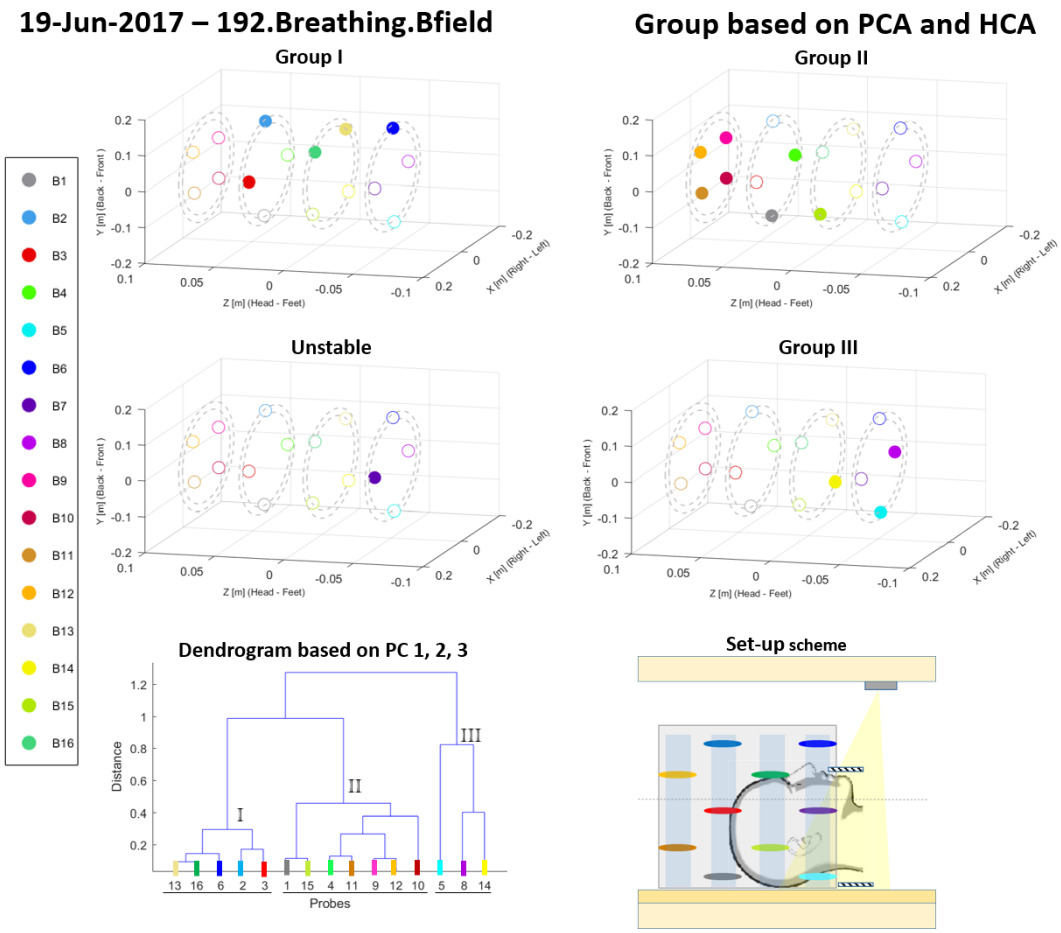

Figure 4.20: ***Classification of the probes based on the data of the static activity of the volunteer M192 during the activity Breathing.*** *The groups are based on the cluster that emerged from consecutive PCA and HCA analysis.*

The results of the PCA analysis (without the probe B7) is shows on Figure 4.20. The probes are divided into three groups, the fourth is constituted of probe B7 only, as the background measurement. However, the division of the top and bottom part of the ring is less clear. The Group I represents mainly the top part. The Group II includes the probes that change less, but for different reasons. From the MRI and B field map analysis, we know that the head of this volunteer ended on the second ring. Hence, the head still near the probes B15, the probes B1 and B4 are enough close to measure a small changing field, but the probes of the latest ring aren't. The Group I also grouped probes that aren't close to the front of the head. Based on the analysis of the Pose 1

rep, Pose 2, Pose 3 of that volunteer, we know that the probe B5 is the one that feels the field changes due to the respiration most. Therefore, the Group II could represent the probes with similar behaviour to B5 for that activity. For symmetry reasons, the probe B7 could be included in that group.

That group set is a kind of combination of the groups found for the same volunteer in the preliminary analysis (Figure 4.13).In that analysis the volunteer didn't hold a pose "symmetric" as the resting state in the space between the probes. That prove that the distance of the head to the probe counts to individuate the pose of the head, it could be a parameters that helps to develop the fitting model in the future.

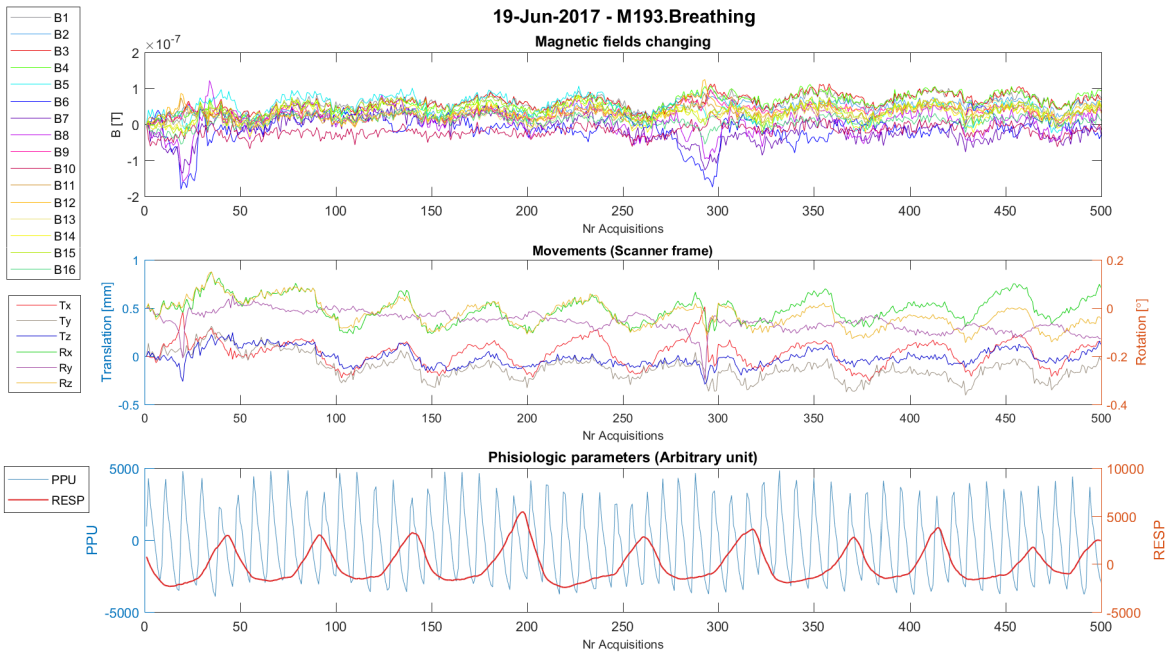

Figure 4.21: ***Magnetic fields changing, movements measurements and physiological parameters for the volunteer M193 during the resting state (Breathing).*** *Only the first 500 acquisitions are plotted.*

Volunteer 2 (M193). The measurements of the magnetic field changes, the movements and the physiological parameters for the volunteer M193 (volunteer 2) are show on Figure 4.21. The observations are similar to those made for the volunteer 1. The range of the magnetic fields changes is more than the volunteer 1. The reason could be that the volunteer hasn't got such a symmetric head as the volunteer 1. Furthermore, the first and the second plots reveals that the volunteer has got two ticks, at the beginning and around the acquisition number 300. The movements doesn't follow well the

respiration, in particular at the beginning of the measurement: it is possible that the coupling between the bite and the upper teeth isn't good.

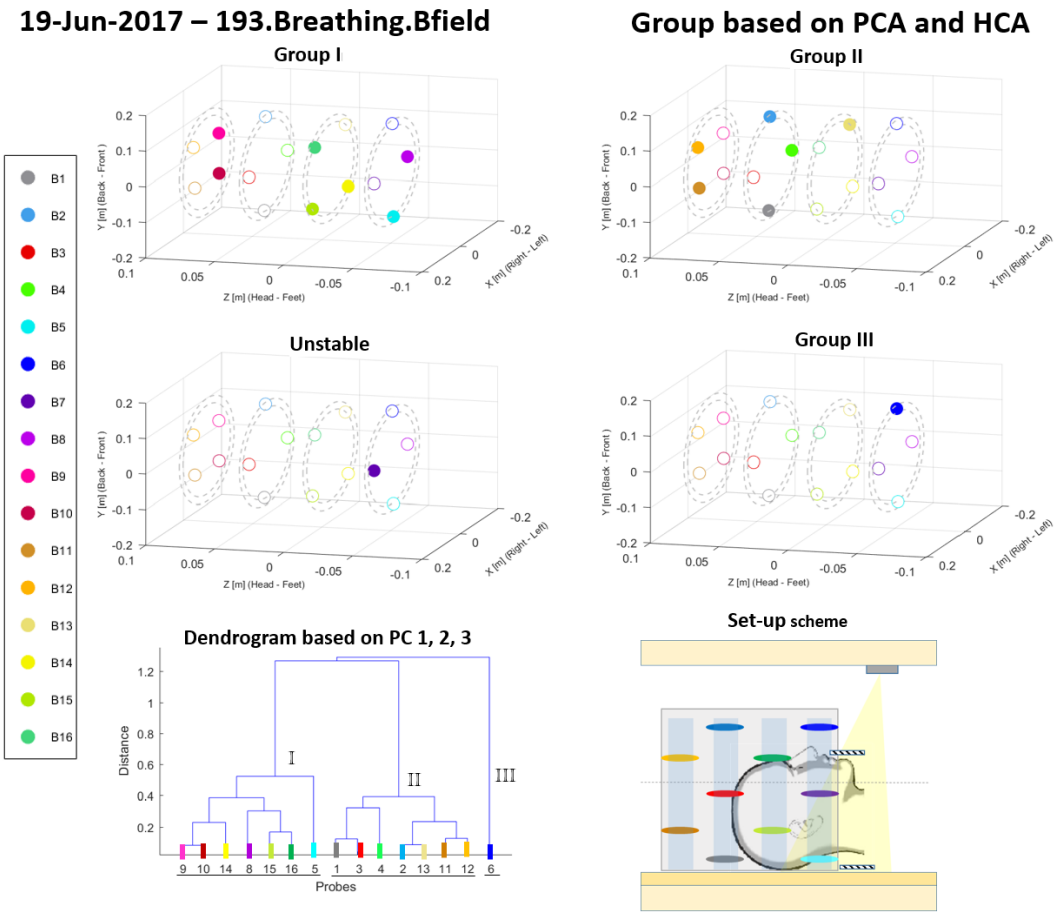

Figure 4.22: ***Classification of the probes based on the data of the static activity of the volunteer M193 during the activity Breathing.*** *The groups are based on the cluster that emerged from consecutive PCA and HCA analysis.*

The results of the PCA analysis (without the probe B7) are show on Figure 4.22. The probes are divided into three groups more similar to the background groups than the for volunteer 1. The main difference is on the last ring, that is too far to the head to record well the changing magnetic field. Both these probes are connected to a subgroup on the dendrogram. The other differences are due to the shape of the head and to the movements, that the phantom doesn't show. From the MRI and B field map analysis, we know that the head of this volunteer ended between the second and the third rings, close to the second. In fact, the probes on the bottom part of the ring are all grouped on the Group I, except for the probes B1 where the head still. That probe is grouped

with the probes on the top part of the rings, that are far from the head.

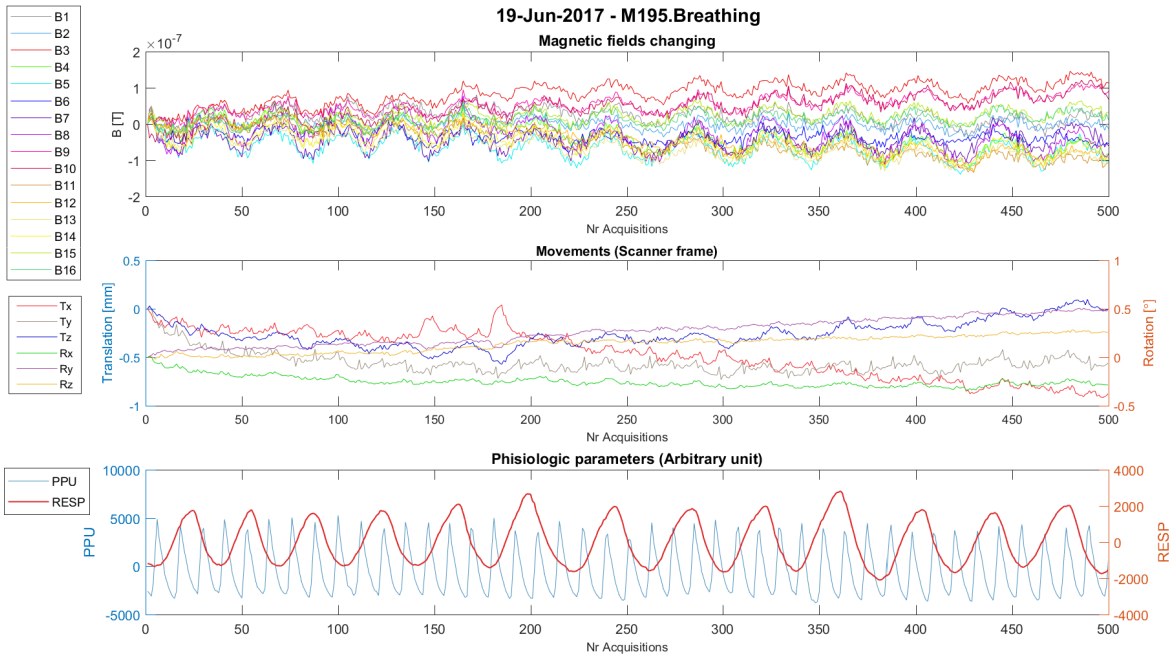

Figure 4.23: ***Magnetic field changes and movement measurements for the volunteer M195 during the activity Breathing.*** *Only the first 500 acquisitions are plotted.*

Volunteer 3 (M195). The measurements of the changing magnetic fields, the movements and the physiological parameters for the volunteer M195 (volunteer 3) are shows on Figure 4.23. The observations about these data is similar to the those made for the volunteers 1 and 2 except for the range of the translations and rotations. This volunteer has the biggest head of all the volunteers and it ends on the third ring. Therefore, the head lay on three rings instead two (volunteer 2) or one and half (volunteer 1) that means that it has got less degree to translate and rotate inside the rings. Also, it is clear that each person makes a specific movements during the breathing.

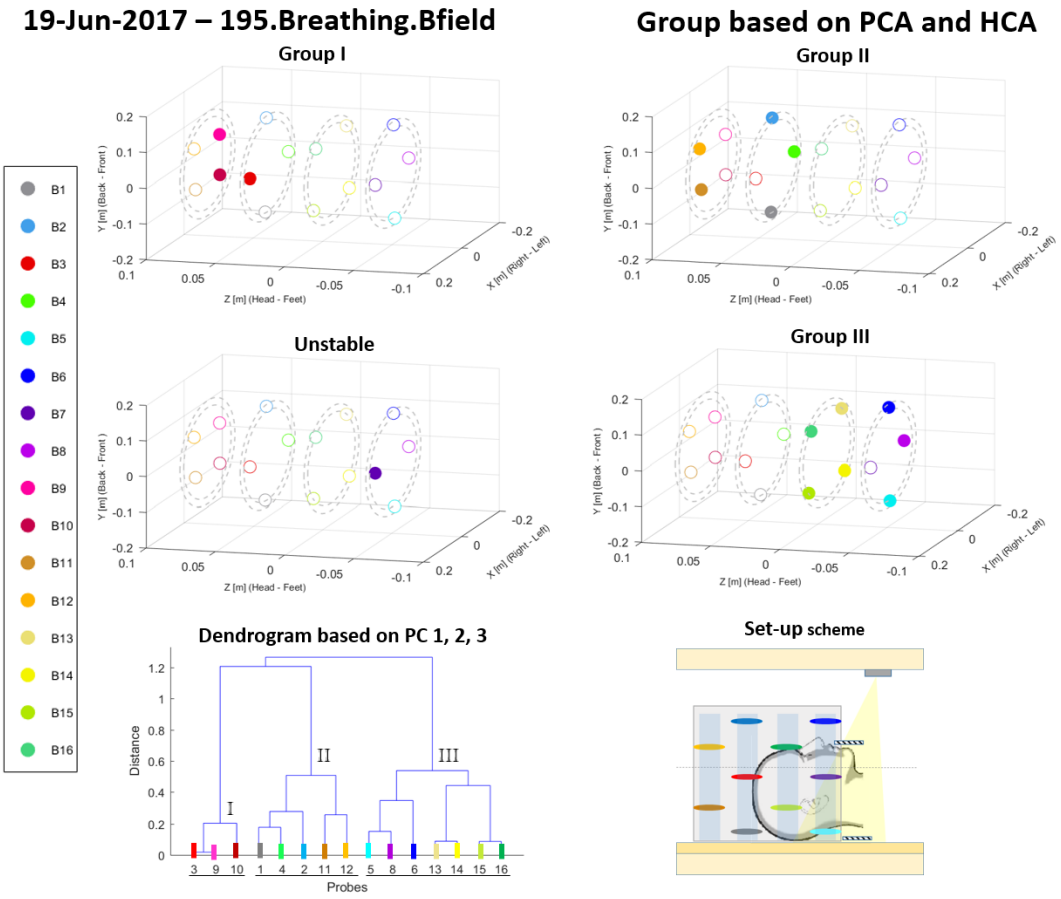

Figure 4.24: ***Classification of the probes based on the data of the volunteer M195 during the activity Breathing.*** *The groups are based on the cluster that emerged from consecutive PCA and HCA analysis.*

The results of the PCA analysis (without the probe B7) are on Figure 4.24. The probes are divided into three groups based on the front/back division shows, instead the top/bottom as the other analysis. The first two rings are on the Group III. From the MRI and B field map analysis, we know that the head of this volunteer ended at the third rings. The bottom part of the head, from the ears to the neck, are included on the first two ring. The neck is anatomically connected to the chest, that rise and fall during the respiration. Hence, the bottom part to the head could be the only one that follows the movements of the chest and change the magnetic field. The Group I and II represent the probes on the last two rings, in fact they are connected on the dendrogram.

4.4.1 Characterization of the Movements

The last analysis helps to explain better the difference and the similarity between the clusters found for the volunteers. It concerns the movements of the head during the respiration.

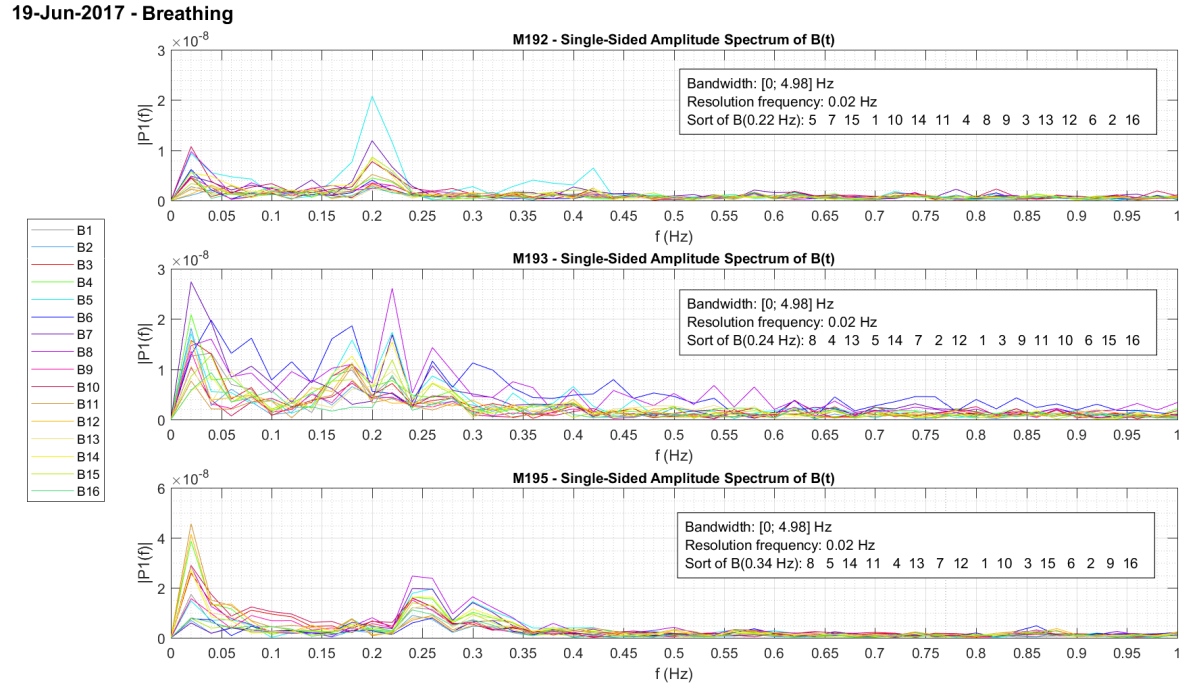

Figure 4.25: ***Fourier Analysis of the changing magnetic field.*** *Only the first part of the spectrum is plotted. The original data are show on Figure 4.19, 4.21, 4.23 respectively. The bandwidth and the resolution frequency are evaluated. The various probes are sorted in descendent order according to their amplitude in the Fourier spectrum evaluated at respiration frequency. The frequencies of the respiration evaluated on subsection 3.2.3 are adapted to the bandwidth of the analysis.*

We computed the Fourier Analysis of the signal of the magnetic fields to identify the probes that most feel the effect of the respiration. The results are shows on Figure 4.25. Each plot represents one volunteers, there is a low frequency component below the 0.1 Hz and a peak that correspond to the respiration frequency. The sort of amplitude of the spectrum of the probes at this frequency is different for each volunteer, the groups of probes that emerge from the PCA analysis are similar. For example, for volunteer 3, the group of probes that most feels the field change due to the respiration is the Group III. The probes are: B5, B6, B8, B13, B14, B15, B16. The first half of the sort of the probes found for that volunteers is: B8, B5, B14, B11, B4, B13, B7, B12. Four of the probes of the Group III are in that list. Similar results are obtained for the others volunteers.

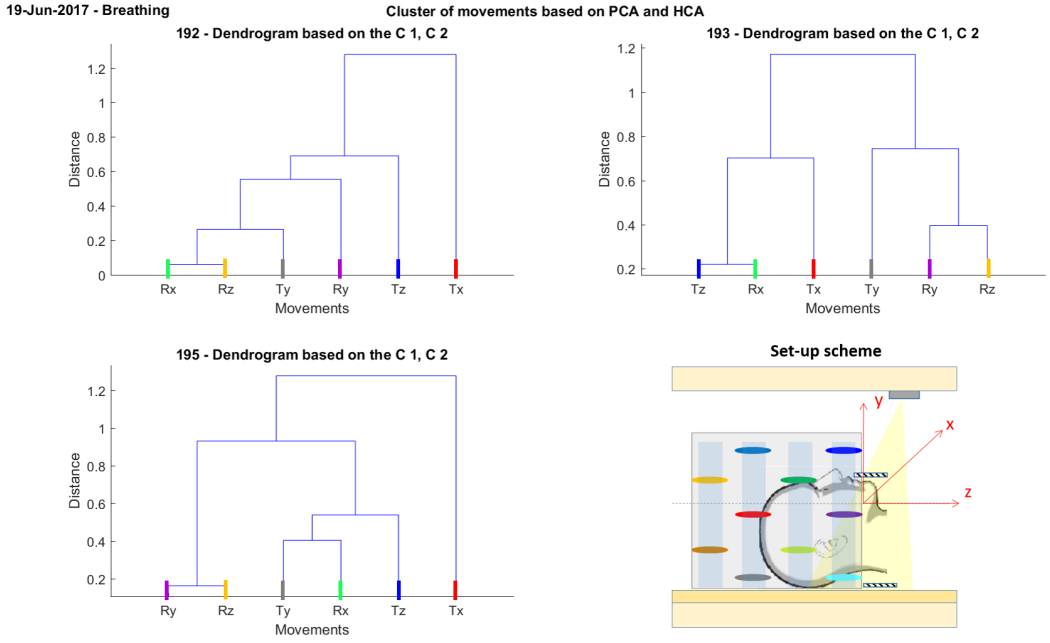

Figure 4.26: ***Classification of the movements during the activity Breathing.*** *The groups are based on the cluster that emerged from consecutive PCA and HCA analysis. The original data are on Figure 4.19, 4.21, 4.23. The three dendrogram represents the involuntary movements due to the breathing that the three volunteers did. Based on the background measurement, we know that the T_z could be the most influenced by the vibrations of the bed. Based on the movements data of the volunteers M193, we know that the coupling between the skull and the bite bar isn't rigdly for that volunteer. Altough, it is clear that the mechanic of the breathing is unique for each volunteers.*

The second analysis is to understand the head movements that the volunteers made during breathing. The results of the HCA (coupled with PCA as before) computed on the movements dataset is show on Figure 4.26. The dendrograms of the volunteers are completely different: the kinetic of the respiration is unique for each volunteer and could influence in a different way the changing magnetic field.

M666	*Group I:*1, 5, 10, 11, 14, 15	*Group II:* 2, 3, 4, 8, 9, 12, 13, 16	*Group III:* 6
M192	*Group III:* 5, 8, 14	*Group I:* 2, 3, 6, 13, 16	*Group II:* 1, 4, 9, 10, 11, 12, 15
M193	*Group I:* 5, 8, 9, 10, 14, 15, 16	*Group II:* 1, 2, 3, 4, 11, 12, 13	*Group III:* 6
M195	*Group III:* 5, 6, 8, 13, 14, 15, 16	*Group II:* 1, 2, 4, 11, 15	*Group I:* 3, 9, 10
Results	*Results I:* 5, 7, 8, 14, 15, 16	*Results II:* 2, 3, 13, 4, 11	*Outlier:* 1, 6, 9, 10, 12

Table 4.2: ***Results.*** *Groups emerged from the PCA of the signal from the fields probes for all the volunteers during the resting state, without the signal of the probes B7. The probes B7 are included in the first results group for symmetry reasons.*

4.5 Results

The clusters found during the background and resting state analysis are detailed in table 4.2. The rows of the table are the subjects. The first corresponds to the background measure, from the second to the fourth correspond to the volunteers and the last one reports the results. The groups aren't the same for each column. The probes that better shows the breathing are on the first, the worst one on the last column. The results group are evaluated on the groups found for the volunteers. The probes that appear in the column for two or more volunteers are inserted in the corresponding results group. The

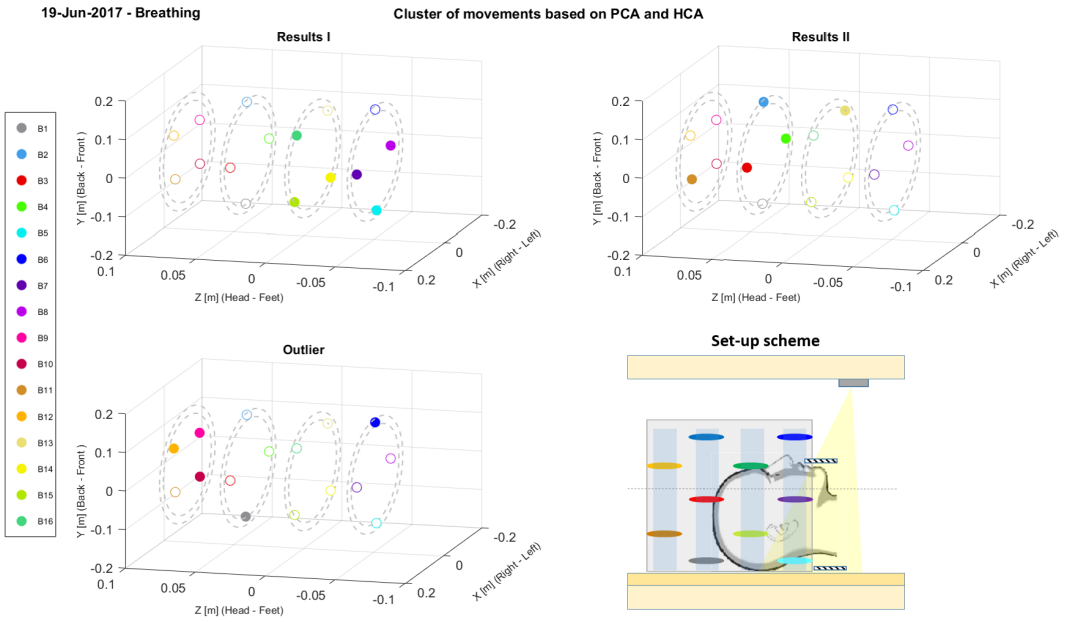

Figure 4.27: ***Classification of the probes based on the data of the resting state of all the volunteers.*** *The groups are based on the cluster that emerged from consecutive PCA and HCA analysis.*

results group are represented in the rings on Figure 4.27. They show that the division via the front/back part of the rings is the most reasonable. It means that the most of the information about the movements are carried by six out of sixteen probes and those probes are located on the first two rings.

We could try to change the position of the probes to sampled better the changing magnetic fields in that zone of the head.

Chapter 5

Conclusion

My thesis is a part of a project whose aim is to find better regression method to predict the movement of the patient by the perturbation of magnetic field. My thesis is focused on improving the actual set-up of the experiment to obtain a more suitable datasets to begin the regression analysis. In the future, this approach will be used in Retrospective Motion Correction and ultimately in Prospective Motion Correction.

Improvement on the set-up and on the line-up of the data sets. The experimental set-up is formed by three instruments placed into the magnet bore of a 7 T MRI Scanner to quantify the magnetic fields perturbations and the movements. The instruments are: the *Clip on Camera head* (CCH), a set of 16 fields probes arranged around the head, the *Moire Phase Tracking* (MPT), a optical camera that measure the movements of a holographic marker fixed on the top of a bite bar, and the tool of the 7 T Scanner to measure the physiological parameters *Physlog*.

The instruments aren't built to work together: the start of the acquisitions is not synchronized a priori, their sampling rate is different, and they don't acquire the data in the same reference frame. The only way to connect the three instruments is to send a common TTL signal during the experiment. The improvement on the set-up of the instruments made with this thesis was to develop a software procedure for an automatic coupling. The signals are recorded on the log file of the instruments and the data stream is elaborated in post processing.

Set-up characterization. We have performed measurements to verify the improvement of the set-up, and to characterize the behaviour of the probes to describe the movements of the head related to breathing and vibrations. We performed two experiments with three volunteers and one anthropological phantom.

Preliminary analysis. We used PCA (Principal Component Analysis) to identify groups of probes with the same behaviour on three datasets of the same volunteers

during three static activities. The first three PCA components were used to compute the HCA (Hierarchical Cluster Analysis). From this analysis it emerged that is possible to subdivide the probes into specific clusters. The clusters represent: probes that are more sensible to the breathing, probes that are close or far to the head and probes showing a unreliable behaviour during the experiments.

Background analysis. The second analysis aimed to characterize the background of the instruments, with and without the volunteers, and the resting state of the volunteer, the static activity called "Breathing". The background measurements on the magnetic field probes reveal that the probes are subdivided in two "background cluster's' and a cluster composed by one probe with unreliable behaviour (not the same probes found on the preliminary analysis). The "background clusters" represent the bottom and the top part of the four rings. The background measurements on the bed movements reveals that the coupling with the bed and the magnet bore could slightly influence the measurements on the movements value. The most important movements are translations along the z axis: the values measured with the volunteers are bigger than the values measured with the phantom, a result opposite to what we would have expected.

Resting state analysis. Thanks to the background measurements we excluded the probes with unstable behaviour from the analysis. The dataset analysed represents the resting state of the three volunteers. The aim is to characterize individual involuntary movements due to the relative position between the head and the probes. Our analysis shows that the probes are mainly divided by the front/back part of the mounting system. By Fourier analysis of the probe time series we could identify the probes that better respond to involuntary movements due to breathing, characterized by specific periodicities at low frequencies.

In conclusion, the thesis allowed improvements on the set-up and on the line-up process work and, despite anatomical and mechanic differences between the sampled volunteers, we identified common groups of magnetic field probes able to characterize involuntary movements on all measured volunteers.

Bibliography

[1] Laura Bischoff, James Smith, Olivier Mougin, Glyn Spencer, Kingkarn Aphiwatthanasumet, Penny Gowland, Richard Bowtell. *"Relating external magnetic field changes to head movement using motion and field cameras"*, ISMR (International Society for Magnetic Resonance in Medicine) 2017;

[2] J.P. Marques, R.Bowtell. *"Application of a Fourier-based method for rapid calculation of field inhomogeneity due to spatial variation of magnetic susceptibility"*, First published: 13 April 2005;

[3] Skope Magnetic Resonance Technologies, *"Clip-on Camera Head Manual"*

[4] Metria Innovation, Inc. *"Moiré Phase Tracking System User Manual"*, Model MT 384ib

[5] Philips, *User manual of 7 T Scanner*

[6] Yolanda Duerst, Bertram J. Wilm, Benjamin E. Dietrich, S. Johanna Vannesjo, Christoph Barmet, Thomas Schmid, David O. Brunner, and Klaas P. Pruessmann. *"Real-time feedback for spatiotemporal field stabilization in MR system"*, Magnetic Resonance in Medicine 73: 884893, 2015;

[7] Barmet C, De Zanche N, Pruessmann KP. *"Spatiotemporal magnetic monitoring for MR"*, Magnetic Resonance in Medicine 60(1): 187-97, 2008 July;

[8] Maclaren J, Herbst M, Speck O, Zaitsev M. *"Prospective motion correction in brain imaging: a review"*, Magnetic Resonance in Medicine 69(3): 621 36, 2013 March;

[9] F.Bloch. *"Nuclear Induction"*, Physical Review (70), 1946;

[10] F.Bloch, W. W. Hansen, M. Packard. *"The Nuclear Induction Experiment"*, Physical Review (70), 1946;

[11] Stig Ljunggren. *"A simple graphical representation of Fourier-based imaging methods"*, Journal of Magnetic Resonance(54): 338 343, 1983;

[12] Ben Kenwright. *"A Beginners Guide to Dual-Quaternions: What They Are, How They Work, and How to Use Them for 3D Character Hierarchies"*, School of Computing Science, Newcastle University, 2012;

[13] Pierre LeVan, Julian Maclaren, Michael Herbst, Rebecca Sostheim, Maxim Zaitsev, Jurgen Hennig. *"Ballistocardiographic artifact removal from simultaneous EEG-fMRI using an optical motion-tracking system"*, NeuroImage (70): 1 11, 2013;

[14] Joel Mispelter, Mihaela Lupu, Andre Briguet. *"NMR PROBEHEADS for biophysical and biomedical experiments - Theorical Principles and Practical Guidelines"*, Imperial College Press: 1 21, 2006;

[15] J.H. Duyn. *"The future of ultra-high field MRI and fMRI for study of the human brain"*, NeuroImage 26(2): 1241 1248, August 2012;

[16] Domenico Formica, Sergio Silvestri. *"Biological effects of exposure to magnetic resonance imaging: an overview"*, BioMedical Engineering OnLine, 2004;

[17] Valentina Hartwig, Giulio Giovannetti, Nicola Vanello, Massimo Lombardi, Luigi Landini, Silvana Simi. *"Biological Effects and Safety in Magnetic Resonance Imaging: A Review"*, International Journal of Environmental Research and Public Health, 2009;

[18] De Zanche N, Barmet C, Nordmeyer-Massner JA, Pruessmann KP. *"NMR probes for measuring magnetic fields and field dynamics in MR systems"*, Magnetic Resonance Medicine 60(1), 2008;

[19] C.M.Collins et al. *"Numerical calculations of the static magnetic field in three dimensional multi-tissue models of the human head"*, Magnetic Resonance Imaging 20(5), June 2002;

[20] Joep Wezel , Andrew G. Webb , and Matthias J. van Osch. *"Effect of head motion on B_0 shimming based on magnetic Field probes"*, ISMR (International Society for Magnetic Resonance in Medicine) 2017;

[21] Karl Pearson. *"On lines and planes of closest fit to systems of points in space"*, University College, London, 1901;

[22] William H. Press, Saul A. Teukolsky, William T. Vetterling, Brian P. Flannery. *"Numerical Recipes 3rd Edition: The Art of Scientific Computing"*;

[23] Donald W. McRobbie, Elizabeth A. Moore, Martin J. Graves and Martin R. Prince. *"MRI From Picture to Proton"*, Cambridge University Press, Second Edition;

Ringraziamenti

Grazie agli affetti,
Grazie all'amore,
Grazie alla passione
e Grazie all'ardore.
Grazie alla Mamma che sempre mi aiuterà.
Grazie al Papà che mi ha spinta più in là.
Grazie alla Nonna e la sua capacità
di farmi sorridere con la sincerità.
Grazie Paolo e Grazie Silvia
mi avete accolta come una figlia.
Grazie alle Amiche e agli Amici,
Grazie ai sorrisi che, anche se in foto,
vengono condivisi.
Sorrisi che sanno di distanza,
fino a che non siamo nella stessa stanza.
Grazie alle mie Mamme, alla nostra Luce,
è Grazie a noi che ora ha una voce!
Grazie a chi, in quel bosco in disparte,
sta accogliendo la mia arte.
Grazie alle mie Sorelle:
otto ruote,
un solo cuore... che batte,
nel petto,
intenso e lento…
come quando il momento arriva,
e la pista è piena … di Noi.
Grazie agli Allenatori,
per avermi cresciuta,
di avermi spronato a rialzarmi dopo ogni caduta,
per aver condiviso le gioie della vittoria
e quelle di ogni occasione perduta.
Grazie ai Dirigenti sempre presenti,
Grazie alle Mamme sempre sull'attenti!
Grazie ai Professori, Grazie perché
La lezione più importante sui libri non c'è!
Grazie ai pranzi in facoltà,
Dove abbiamo lasciato la dignità?
Grazie all'amica, quella migliore,
a cui, tanto tempo fa!, donai un pezzo di cuore.
Ma il pezzo più grande l'ho donato a te,
che la mattina ti svegli accanto a me.
Mi guardi, mi abbracci e mi dici:
"Il mondo è cattivo,
ma insieme, siamo felici".
Ogni giorno di Noi è una scoperta,
Se riesci a tirarmi fuori dalla coperta!
Ma c'è una persona che devo ringraziare,
non la conosco da tanto e me ne stavo per dimenticare.
E' sempre stata con me, dentro di me.
Finalmente ha risposto al mio invito.
Non sapevo come amarla, ma ora l'ho capito:
Grazie. .. anche a me.

In the end, Thanks to all those who made possible and wonderful my internship!
Thanks to Prof. Fantazzini and Dott. Brizi for helping me during the choice.
Thanks to Prof. Remondini and Dott. Giampieri for guiding me during the thesis and, hopefully, to carry on with the project.
Thanks to Professor Bowtell for his kindness and for giving me an important chance for my future.
Thanks to Jim for never denying my help requests.
Thank to Glyn that helped me to build the most colorful OR gate of the world: with a pony everything is better!
Thanks to the SPMIC family and all my new friends: I am up to have the most tasty beer in JA, followed by dancei-dancei night soon!!